NTNU
Norwegian University of
Science and Technology

Kinetics of Alumina Carbochlorination

Executing and modelling the carbochlorination of alumina.

Kristiane Melingen

A thesis presented for the degree of Master of Science and Technology

Materials Science and Engineering (MTKJ)

Submission date: July 2020

Supervisor: Christian Rosenkilde, Norsk Hydro, NTNU IMA

Co-Supervisor: Christian Rosenkilde, Norsk Hydro, NTNU IMA

Norwegian University of Science and Technology

Department of Materials Science and Engineering

Abstract

The kinetics of various grades of alumina, Al_2O_3, have been studied in reaction with CO and Cl_2, and a reactor was designed and produced for this purpose. Temperature and gas flow have been varied for smelter grade (SMG)-Al_2O_3. Calcined aluminum trihydrate (ATH) at 800, 900 and 1000 °C, producing γ-, δ- and θ-Al_2O_3, have been reacted at 700°C. In addition, a Python script was developed to fit the experimental data, confirming that the reaction may, indeed, follow the shrinking-core model (SCM). However, the model should be adjusted with respect to particle size distribution in the future. Results and previous publications have given reason to believe mass transfer/diffusion is rate determining at temperatures 650 - 800 °C. Furthermore, it is believed that within the temperature range 550 - 600 °C, there is mixed rate control from both diffusion and reaction. As for alumina quality, using 800 - 1000 °C-calcined forms has proven to be the leading option in comparison to SMG-Al_2O_3 due to less complications with the reactor, resulting from slower reaction rate. However, a high reaction rate is desired, and may not cause the same issues in a large-scale reactor. This lead to the conclusion that for the system used in this work, calcined ATH at 800 - 1000 °C is the recommended Al-source, but SMG-Al_2O_3 may be superior in a different set-up due to its higher reaction rate.
All in all, most experiments provided high conversion, but should be further studied with respect to varying gas flow in the future. Furthermore, particle size distribution should be experimentally determined prior to carbochlorination and the SCM script should be adjusted accordingly. In addition, it should be confirmed that diffusion and/or reaction are rate-controlling in the stated temperature ranges through testing with a catalyst and adjustments to pressure.

Sammendrag

Kinetikken av varierende kvaliteter av alumina, Al_2O_3, har blitt undersøkt i reaksjon med CO og Cl_2. En reaktor har blitt designet og produsert av denne grunn. Temperatur og gasstrøm har blitt variert for smelter grade (SMG)-alumina. Kalsinert aluminium trihydrat (ATH) ved 800, 900 og 1000 °C, som produserte blandinger av γ-, δ- og θ-Al_2O_3, har blitt reagert ved 700 °C. I tillegg har et Python script blitt utviklet for å tilpasse eksperimentelle data, som bekrefter at reaksjonen kan følge shrinking-core model (SCM). Likevel burde modellen bli justert med hensyn til distrubisjon av partikkelstørrelse i fremtiden. Resultater fra dette arbeidet og tidligere publikasjoner har gitt grunn til å påstå at massetrasport/diffusjon er ratekontrollerende ved temeperaturene 650 - 800 °C. I tillegg, er det grunn til å påstå at både diffusjon og reaksjon er ratekontrollerende ved 550 - 600 °C.[12] [19] Med tanke på alumina kvalitet har 800 - 1000 °C-kalsinerte prøver vist seg å være fortrukket i sammenligning med SMG-alumina på grunn av færre komplikasjoner med reaktoren, som kom fra lavere reaksjonsrate. Likevel er en høy reaksjonsrate ønskelig, og det er mulig en høy rate ikke forårsaker de samme komplikasjonene i en reaktor på større skala. Dette førte til konklusjonen at for systemet presentert her, burde kalsinert ATH ved 800-1000 °C brukes, og SMG-alumina kan være anbefalt for et annet system på grunn av dens høyere reaksjonsrate.

Alt i alt, ga de fleste eksperimentene høy omsetning for Al_2O_3, men burde bli videre undersøkt for variernde gasstrøm i fremtiden. I tillegg, burde distribusjon av partikkelstørrelse eksperimentelt bestemmes på førhånd av karboklorinering, og SCM-scriptet burde endres likedan. Det burde også bli bekreftet at diffusion og/eller reaksjon er ratekontrollerende ved de oppgitte temperaturene, ved å utføre forsøk med katalysator og variasjoner ved trykk.

Preface

The following thesis was conducted for Norwegian University of Science and Technology, at the Department of Materials Science and Engineering. The work is produced as a partial requirement to obtain a degree of Master of Science and Technology. It should be noted that experiments in the following thesis were conducted by Bjørnar Gjesdal of Norsk Hydro, which was not initially intended. This work was planned to surround these experiments only, but due to restrictions surrounding the covid-19 pandemic, this was not possible, and Gjesdal had to conduct the experiments instead. The thesis objective was then adjusted to include the modelling of the reaction kinetics and comparing them with the experimental results from Gjesdal.
A specialization project and a literature study were conducted prior to the following thesis, providing information on kinetics and experimental data of Al_2O_3. Parts of the experimental data are included in Chapter 3, and were obtained through BET, XRD, TGA and ICP analyses.

Objectives

The main objectives of the following thesis are

- Design a reactor that allows for performing carbochlorination experiments on Al_2O_3, and have it produced.
- Determine which quality of alumina is best suited for carbochlorination.
- Produce a Python script that represents the shrinking-core model, in order to observe whether the carbochlorination of Al_2O_3 follows the shrinking-core kinetic model or not.
- Obtain kinetic parameters that may represent the carbochlorination of Al_2O_3, and determine what accounts for diffusion- and/or reaction-controlled rate.

Structure of Report

The following report is structured into six chapters, which are briefly described below.

Chapter 1: Introduction is divided into two parts. The first part is Background and Motivation, which provides the reasoning behind the project, and what has been done so far. The second part is Aim and Scope of the Work, which gives an overview of the topics that will be discussed.

Chapter 2: Theory is devoted to the theoretical framework of the study and will include information about the experimental methods that have been, and will be, used. In addition, this section will provide a thorough understanding of the reaction at hand, and the thought behind the kinetic modelling.

Chapter 3: Experimental Methods is devoted to describe how all experiments were performed. The first subchapter covers the analytical methods and results of the specialization project, whereas the remaining subchapters explain the use of the reactor for carbochlorination of Al_2O_3 and the model fitting.

Chapter 4: Results covers all output of carbochlorination and model fitting.

Chapter 5: Discussion presents a critical view and comparison of the results.

Chapter 6: Conclusion and Recommendations presents a final view of the thesis with suggestions for the future.

Acknowledgements

First of all, I would like to thank my supervisor, Christian Rosenkilde, for your support, patience and input throughout these two semesters. I am very thankful to have been a part of such an interesting project.
I would also like to thank Bjørnar Gjesdal for being so helpful, and always taking the time to share your views and discuss with me.
Furthermore, I would like to thank my friends and family for being so supportive throughout my years at NTNU, especially this last semester. Last, but not least, I want to thank Markedsføringsgjengen at Studentersamfundet i Trondhjem for making my time as a student the best anyone could ask for.

Contents

1 Chapther 1

Introduction **1**

1.1 Background and Motivation 1

1.2 Aim and Scope of the Work 4

2 Chapter 2

Theory **6**

2.1 Alumina Qualities 6

2.1.1 α-Alumina 6

2.1.2 γ-Alumina 7

2.1.3 δ- and θ-Alumina 7

2.1.4 Bayer/SMG Alumina 8

2.2 Calcination 9

2.3 Analytical Methods from Specialization Project 9

2.3.1 XRD 10

2.3.2 ICP 10

2.3.3 TGA 10

2.3.4 BET 11

2.4 Carbochlorination of Alumina 11

2.5 Reaction Kinetics 14

2.5.1 Shrinking Core Model 14

2.5.2 Gas Analysis 17

2.6 Pearson Product Moment Correlation 17

2.7 Arrhenius Equation 18

2.8 Gas Diffusion 18

3 Chapter 3

Experimental Methods **19**

3.1 Calcination and Analytics 19

3.1.1 BET 19

3.1.2 XRD 20

3.1.3 TGA 21

3.1.4 ICP . . . 23
3.1.5 Calcination . . . 24
3.2 Carbochlorination . . . 25
3.2.1 Reactor . . . 25
3.2.2 Experimental Matrix . . . 27
3.2.3 Gas Analysis . . . 28
3.3 Model Fitting . . . 29

4 Chapter 4

Results **31**

4.1 Carbochlorination and Model Fitting . . . 31
4.1.1 Experiment 1 . . . 31
4.1.2 Experiment 2 . . . 34
4.1.3 Experiment 3 . . . 36
4.1.4 Experiment 4 . . . 38
4.1.5 Experiment 5 . . . 40
4.1.6 Experiment 6 . . . 42
4.1.7 Experiment 7 . . . 44
4.1.8 Experiment 8 . . . 46
4.1.9 Experiment 9 . . . 48
4.1.10 Arrhenius Plot . . . 50
4.1.11 Quantification . . . 52

5 Chapter 5

Discussion **55**

5.1 Gas Analysis . . . 55
5.2 Kinetics . . . 55
5.3 Model Fitting . . . 58
5.4 Quantification . . . 59

6 Chapter 6

Conclusion and Recommendations **61**

Appendix A A: SCM Script **67**

Appendix B B: XRD **73**

Appendix C C: Chlorine, Pressure and Flow Plots **77**

Appendix D D: Experimental Conversion Values **89**

List of Figures

1 Simplified visualization of the Hall-Héroult cell.[5] . . . 2
2 Flow sheet of the Hall-Héroult process.[5] . . . 3
3 Visualization of Alcoa's cell.[23] . . . 3
4 Flow sheet of Alcoa's smelter process.[5] . . . 4
5 Representation of α-alumina's crystal structure with respective lattice parameters. . . . 6
6 Representation of γ-alumina's crystal structure with respective lattice parameters. . . . 7
7 Representation of δ-alumina's crystal structure with respective lattice parameters. . . . 8
8 Representation of θ-alumina's crystal structure with respective lattice parameters. . . . 8
9 Transformations of Alumina Hydrates[11]. . . . 9
10 Conversion of γ-alumina from the reaction with a $CO-Cl_2$ mixture. (1) 649 K (2) 674 K (3) 698 K (4) 723 K (5) 775 K (6) 830 K (7) 878 K (8) 922 K (9) 973 K (10) 1023 K (11) 1064K (12) 1123 K.[20] 12
11 Schematic of different mechanisms of the shrinking core model. The grey areas represent unreacted parts of a particle, whereas the white areas in (b) and (c) represent solid products.[22] . . . 14
12 Diffractograms of calcined samples with respective calcination temperatures.[16] . . . 20
13 Diffractograms of ATH (black) in comparison to calcined samples with respective calcination temperatures.[16] . . . 21
14 TGA results of SMG sample. The red curve represents changes in temperature, the green curve represents changes in wt% and the blue curve is the DSC curve. The gas flow of N_2 is constant at 30 ml/min.[16] . . . 22
15 TGA results of ATH. The red curve represents changes in temperature, the green curve represents changes in wt% and the blue curve is the DSC curve. The N_2 gas flow is constant at 30 ml/min.[16] . 23
16 Temperature dependence of LOI. . . . 25
17 Sketched design of quartz reactor used for carbochlorination of Alumina. . . . 26
18 Adjusted set-up for the carbochlorination reactor due to complications with clogging. Figure is constructed by Bjørnar Gjesdal. . . . 27
19 Conversion of SMG Al_2O_3 carbochlorinated at 550°C, together with plots of SCM's adjusted to fit the experiment with respect to k_r and D. The experimental conversion points are calculated from the titrations performed throughout the carcochlorination experiment, as presented in subchapter 3.2.3. . . 32
20 Resulting parameters from the SCM-script for adjusted diffusion coefficient, with respect to time and distance into bed for carbochlorination of SMG-alumina at 550°C. . . . 33
21 Resulting parameters from the SCM-script for adjusted reaction constant, with respect to time and distance into bed for carbochlorination of SMG-alumina at 550°C. . . . 33

22 Conversion of SMG Al_2O_3 carbochlorinated at 600°C, together with plots of SCM's adjusted to fit the experiment with respect to k_r and D. The experimental conversion points are calculated from the titrations performed throughout the carcochlorination experiment, as presented in subchapter 3.2.3. . . 34
23 Resulting parameters from the SCM-script for adjusted diffusion coefficient, with respect to time and distance into bed for carbochlorination of SMG-alumina at 600°C. 35
24 Resulting parameters from the SCM-script for adjusted reaction constant, with respect to time and distance into bed for carbochlorination of SMG-alumina at 600°C. 35
25 Conversion of SMG Al_2O_3 carbochlorinated at 650°C, together with plots of SCM's adjusted to fit the experiment with respect to k_r and D. The experimental conversion points are calculated from the titrations performed throughout the carcochlorination experiment, as presented in subchapter 3.2.3. . . 36
26 Resulting parameters from the SCM-script for adjusted diffusion coefficient, with respect to time and distance into bed for carbochlorination of SMG-alumina at 650°C. 37
27 Resulting parameters from the SCM-script for adjusted reaction constant, with respect to time and distance into bed for carbochlorination of SMG-alumina at 650°C. 37
28 Conversion of SMG Al_2O_3 carbochlorinated at 700°C, together with plots of SCM's adjusted to fit the experiment with respect to k_r and D. The experimental conversion points are calculated from the titrations performed throughout the carcochlorination experiment, as presented in subchapter 3.2.3. . . 38
29 Resulting parameters from the SCM-script for adjusted diffusion coefficient, with respect to time and distance into bed for carbochlorination of SMG-alumina at 700°C. 39
30 Resulting parameters from the SCM-script for adjusted reaction constant, with respect to time and distance into bed for carbochlorination of SMG-alumina at 700°C. 39
31 Conversion of SMG Al_2O_3 carbochlorinated at 800°C, together with plots of SCM's adjusted to fit the experiment with respect to k_r and D. The experimental conversion points are calculated from the titrations performed throughout the carcochlorination experiment, as presented in subchapter 3.2.3. . . 40
32 Resulting parameters from the SCM-script for adjusted diffusion coefficient, with respect to time and distance into bed for carbochlorination of SMG-alumina at 800°C. 41
33 Resulting parameters from the SCM-script for adjusted reaction constant, with respect to time and distance into bed for carbochlorination of SMG-alumina at 800°C. 41
34 Conversion of SMG Al_2O_3 carbochlorinated at 700°C, with gas flows of 40 and 60 ml/min of Cl_2 and CO, respectively. Plotted together with plots of SCM's adjusted to fit the experiment with respect to k_r and D. The experimental conversion points are calculated from the titrations performed throughout the carcochlorination experiment, as presented in subchapter 3.2.3. 42

35 Resulting parameters from the SCM-script for adjusted diffusion coefficient, with respect to time and distance into bed for carbochlorination of SMG-alumina at 700°C. 43
36 Resulting parameters from the SCM-script for adjusted reaction constant, with respect to time and distance into bed for carbochlorination of SMG-alumina at 700°C. 43
37 Conversion of $\gamma-$, $\delta-$ and $\theta-Al_3O_3$ carbochlorinated at 700°C, together with plots of SCM's adjusted to fit the experiment with respect to k_r and D. The experimental conversion points are calculated from the titrations performed throughout the carcochlorination experiment, as presented in subchapter 3.2.3. 44
38 Resulting parameters from the SCM-script for adjusted diffusion coefficient, with respect to time and distance into bed for carbochlorination of 1000°C-calcined alumina at 700°C. 45
39 Resulting parameters from the SCM-script for adjusted reaction constant, with respect to time and distance into bed for carbochlorination of 1000°C-calcined alumina at 700°C. 45
40 Conversion of $\gamma-$ and $\delta-$-Al_3O_3 carbochlorinated at 700°C, together with plots of SCM's adjusted to fit the experiment with respect to k_r and D. The experimental conversion points are calculated from the titrations performed throughout the carcochlorination experiment, as presented in subchapter 3.2.3. 46
41 Resulting parameters from the SCM-script for adjusted diffusion coefficient, with respect to time and distance into bed for carbochlorination of 900°C-calcined alumina at 700°C. 47
42 Resulting parameters from the SCM-script for adjusted reaction constant, with respect to time and distance into bed for carbochlorination of 900°C-calcined alumina at 700°C. 47
43 Conversion of $\gamma-$-Al_3O_3 carbochlorinated at 700°C, together with plots of SCM's adjusted to fit the experiment with respect to k_r and D. The experimental conversion points are calculated from the titrations performed throughout the carcochlorination experiment, as presented in subchapter 3.2.3. . . 48
44 Resulting parameters from the SCM-script for adjusted diffusion coefficient, with respect to time and distance into bed for carbochlorination of 800°C-calcined alumina at 700°C. 49
45 Resulting parameters from the SCM-script for adjusted reaction constant, with respect to time and distance into bed for carbochlorination of 800°C-calcined alumina at 700°C. 49
46 Arrhenius plot for respective values of k_r 50
47 Arrhenius plot for respective values of D 51
48 Comparison of conversion with respect to temperature. Here, the plots have been produced with estimated D-values for their respective temperature, from the Arrhenius equation regression line for D (Equation 36 53
49 Comparison of conversion with respect to diffusion coefficient. Here, the basis D is $2.53{\cdot}10^{-10}$, as this is the Arrhenius value at T = 700 °C (Table 29), and it is increased/decreased by 50%. 53

50 Comparison of conversion with respect to radius. Here, the basis radius is 50 μm and it is increased/decreased by 50%. 54
51 Comparison of conversion with respect to gas flow. The green plot is from the SCM script, adjusted to Experiment 6, whereas the blue plot is from the SCM script at 700 °C with adjusted gasflow and D adjusted for the diffusion of Cl_2 as shown in Equation 35. The orange plot is also from the script, with D = $2.53 \cdot 10^{-10}$ 54
52 Diffractogram of SMG-alumia. Blue corresponds to alpha and red corresponds to gamma. 73
53 Diffractogram of sample 800. Blue corresponds to gamma. 74
54 Diffractogram of sample 900. Blue corresponds to delta and green corresponds to gamma. 75
55 Diffractogram of sample 1000. Blue corresponds to delta and green corresponds to theta. 75
56 Diffractogram of sample ATH. Red corresponds gibbsite. 76
57 Pressure and flow plot for Experiment 1. 77
58 Cl_2 levels during carbochlorination of SMG Al_2O_3 at 550°C. Calculated Cl_2 is the total amount of Cl_2 that enters the inlet, whereas the absorbed Cl_2 is the Cl_2 that exits the outlet and has not reacted with Al_2O_3. 78
59 Pressure and flow plot for Experiment 2. 79
60 Cl_2 levels during carbochlorination of SMG Al_2O_3 at 600°C. Calculated Cl_2 is the total amount of Cl_2 that enters the inlet, whereas the absorbed Cl_2 is the Cl_2 that exits the outlet and has not reacted with Al_2O_3. 80
61 Pressure and flow plot for Experiment 3. 81
62 Cl_2 levels during carbochlorination of SMG Al_2O_3 at 650°C. Calculated Cl_2 is the total amount of Cl_2 that enters the inlet, whereas the absorbed Cl_2 is the Cl_2 that exits the outlet and has not reacted with Al_2O_3. 82
63 Pressure and flow plot for Experiment 4. 82
64 Cl_2 levels during carbochlorination of SMG Al_2O_3 at 700°C. Calculated Cl_2 is the total amount of Cl_2 that enters the inlet, whereas the absorbed Cl_2 is the Cl_2 that exits the outlet and has not reacted with Al_2O_3. 83
65 Pressure and flow plot for Experiment 5. 83
66 Cl_2 levels during carbochlorination of SMG Al_2O_3 at 800°C. Calculated Cl_2 is the total amount of Cl_2 that enters the inlet, whereas the absorbed Cl_2 is the Cl_2 that exits the outlet and has not reacted with Al_2O_3. 84
67 Pressure and flow plot for Experiment 6. 84

68 Cl_2 levels during carbochlorination of SMG Al_2O_3 at 700°C, with gas flows of 40 and 60 ml/min of Cl_2 and CO, respectively.. Calculated Cl_2 is the total amount of Cl_2 that enters the inlet, whereas the absorbed Cl_2 is the Cl_2 that exits the outlet and has not reacted with Al_2O_3. 85
69 Pressure and flow plot for Experiment 7. 85
70 Cl_2 levels during carbochlorination of $\gamma-, \delta-$ and $\theta-Al_3O_3$ at 700°C. Calculated Cl_2 is the total amount of Cl_2 that enters the inlet, whereas the absorbed Cl_2 is the Cl_2 that exits the outlet and has not reacted with Al_2O_3. 86
71 Pressure and flow plot for Experiment 8. 86
72 Cl_2 levels during carbochlorination of $\gamma-$ and $\delta-$-Al_3O_3 at 700°C. Calculated Cl_2 is the total amount of Cl_2 that enters the inlet, whereas the absorbed Cl_2 is the Cl_2 that exits the outlet and has not reacted with Al_2O_3. 87
73 Pressure and flow plot for Experiment 9. 87
74 Cl_2 levels during carbochlorination of $\gamma-$-Al_3O_3 at 700°C. Calculated Cl_2 is the total amount of Cl_2 that enters the inlet, whereas the absorbed Cl_2 is the Cl_2 that exits the outlet and has not reacted with Al_2O_3. 88
75 Conversion values from titration for each carbochlorination experiment. 89

List of Tables

1 Measured and given surface areas of respective samples. The calcined samples are given names according to their respective calcination temperatures (sample 800 is calcined at 800 °C, and so on).[16] 20
2 Phases observed in the samples. These results are based on the diffractograms in Appendix B. The calcined samples are given names according to their respective calcination temperatures (sample 800 is calcined at 800 °C, and so on).[16] 21
3 Heating procedure of TGA analysis 22
4 Decomposition program of samples in the microwave prior to ICP analysis. 23
5 Results obtained from ICP analysis. ICP values are presented in ppm and RSD in % .[16] 24
6 Weight changes of calcined samples after calcination.[16] 24
7 LOI of the calcined samples.[16] 25
8 Experimental matrix for carbochlorination of Alumina. 28
9 Summary of experimental results. 31
10 Results of weighing before and after carbochlorination of SMG Al_2O_3 at 550°C 32
11 Fitted values for diffusion coefficient and reaction constant for carbochlorination of SMG-alumina at 550°C, with respective R^2-values for SCM model vs. experimental values. 33

12 Results of weighing before and after carbochlorination of SMG-Al_2O_3 at 600°C 34
13 Fitted values for diffusion coefficient and reaction constant for carbochlorination of SMG-alumina at 600°C, with respective R^2-values for SCM model vs. experimental values. 35
14 Results of weighing before and after carbochlorination of SMG Al_2O_3 at 650°C 36
15 Fitted values for diffusion coefficient and reaction constant for carbochlorination of SMG-alumina at 650°C, with respective R^2-values for SCM model vs. experimental values. 37
16 Results of weighing before and after carbochlorination of SMG Al_2O_3 at 700°C 38
17 Fitted values for diffusion coefficient and reaction constant for carbochlorination of SMG-alumina at 700°C, with respective R^2-values for SCM model vs. experimental values. 39
18 Results of weighing before and after carbochlorination of SMG Al_2O_3 at 800°C 40
19 Fitted values for diffusion coefficient and reaction constant for carbochlorination of SMG-alumina at 800°C, with respective R^2-values for SCM model vs. experimental values. 41
20 Results of weighing before and after carbochlorination of SMG Al_2O_3 at 700°C. The flow rates of Cl_2 and CO were 40 and 60 ml/min, respectively. 42
21 Fitted values for diffusion coefficient and reaction constant for carbochlorination of SMG-alumina at 700°C, with respective R^2-values for SCM model vs. experimental values. 43
22 Results of weighing before and after carbochlorination of $\gamma-$, $\delta-$ and $\theta-Al_3O_3$ at 700°C 44
23 Fitted values for diffusion coefficient and reaction constant for carbochlorination of 1000°C-calcined alumina at 700°C, with respective R^2-values for SCM model vs. experimental values. 45
24 Results of weighing before and after carbochlorination of $\gamma-$ and $\delta-$-Al_3O_3 at 700°C. 46
25 Fitted values for diffusion coefficient and reaction constant for carbochlorination of 900°C-calcined alumina at 700°C, with respective R^2-values for SCM model vs. experimental values. 47
26 Results of weighing before and after carbochlorination of $\gamma-$-Al_3O_3 at 700°C. 48
27 Fitted values for diffusion coefficient and reaction constant for carbochlorination of 800°C-calcined alumina at 700°C, with respective R^2-values for SCM model vs. experimental values. 49
28 Values used to produce Arrhenius plot. 50
29 Values for reaction coefficient at various temperatures, k_r, and diffusion coefficient, D, calculated from the Arrhenius equations. 52

Chapther 1

Introduction

1.1 Background and Motivation

In this subchapter, some text is extracted and/or rewritten extracts from the previously mentioned specialization thesis, written in relation to this project.[16]

The work presented in this thesis is part of a project initiated by Norsk Hydro, in order to reduce emissions related to the production of aluminum. The project as a whole entails enhancing a process, previously used by Alcoa. The production method currently used by Norsk Hydro is the Hall-Héroult process, and releases approximately 1.5 kg CO_2 for each kg of aluminum produced. The Hall-Héroult process is an industrially utilized method of producing aluminum, whereas the Alcoa process was only utilized at one factory that operated for about 10 years before it was terminated in the 1980's. Though the Hall-Héroult process is significantly optimized and well-established, it also has high energy demands, with an operation temperature of typically 960 °C. In comparison, Alcoa's electrolysis process operated at 700 °C. More specifically, aluminum was produced at a rate of 13,000 kg/day per cell with an electrolysis energy consumption of 9.6 kWh/kg. Whereas the Hall-Héroult process consumes about 13.4 kWh/kg, and the largest cells produce close to 5,000 kg/day.[23] [18] [15]

Following are brief descriptions and further comparison of the two processes.

During electrolysis in the Hall-Héroult process, alumina is dissolved in cryolite, Na_3AlF_6, with additions of AlF_3 and CaF_2. Followingly, the overall cell reaction that occurs is:

$$2\,Al_2O_3 + 3\,C \rightleftharpoons 4\,Al + 3\,CO_2 \tag{1}$$

The cell anode consists of solid carbon, which is oxidized and released to the atmosphere as CO_2, while Al^{3+} is reduced to Al at the cathode (see Figure 1). As the anode is consumed through electrolysis, it must replaced on a regular basis.[23] [5]

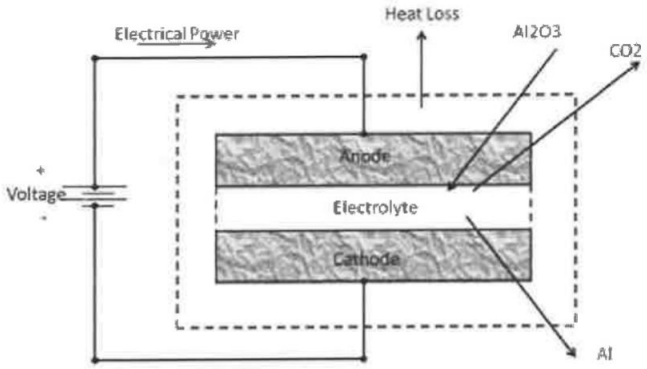

Figure 1: Simplified visualization of the Hall-Héroult cell.[5]

A flow sheet of the Hall-Héroult process is presented in Figure 2 below.

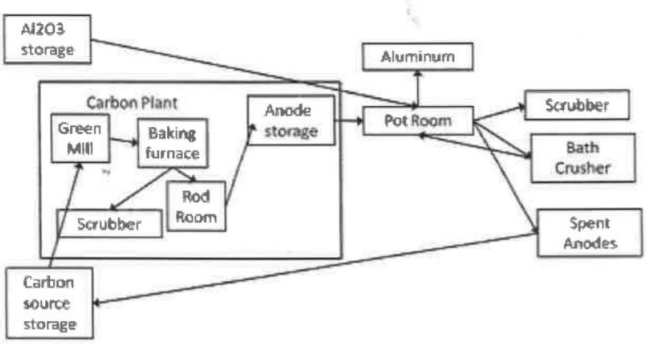

Figure 2: Flow sheet of the Hall-Héroult process.[5]

Though there is limited access to information about the Alcoa project, it is known that the source of aluminum was alumina obtained through the Bayer process (mainly γ-alumina). This is the same grade alumina used in the Hall-Héroult process. Alumina was carbochlorinated through the following reaction, using solid C as the reductant, prior to electrolysis:

$$2\,Al_2O_3 + 3\,C + 6\,Cl_2 \rightleftharpoons 4\,AlCl_3 + 3\,CO_2 \tag{2}$$

Following chlorination, aluminum was produced through electrolysis of $AlCl_3$ in a molten salt bath (NaCl/LiCl), with an overall cell reaction of:

$$2\,AlCl_3 \rightleftharpoons 2\,Al + 3\,Cl_2 \tag{3}$$

Alcoa's cell design differs to the design of the Hall-Héroult cells, by having additional bipolar plates between the cathode and anode. This cell design enabled high energy efficiency.

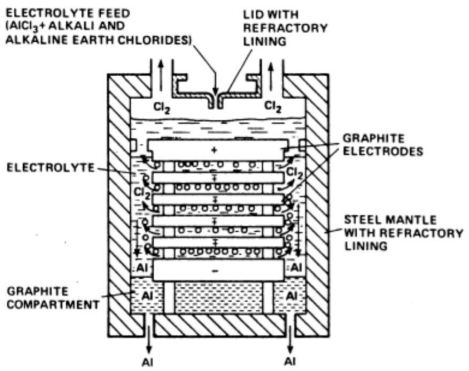

Figure 3: Visualization of Alcoa's cell.[23]

Furthermore, as aluminum was collected at the cathode, it drained down to a sump, where it could be removed at convenience. In addition, the bipolar design allowed for shorter distances between cathodes and anodes, reducing resistance within the cell.[5] A flow sheet of the process is presented in Figure 4 below.

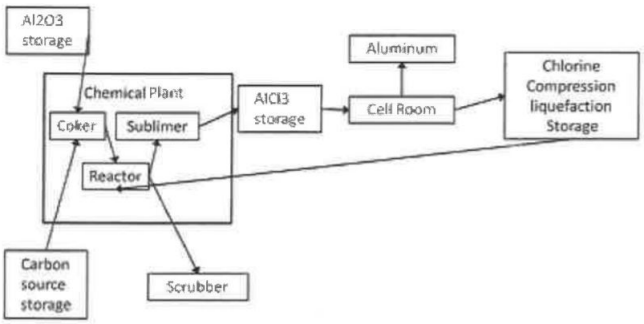

Figure 4: Flow sheet of Alcoa's smelter process.[5]

However, there were several issues regarding the chlorination reactor. Ultimately, it more of less exploded and the factory was shut down. There were also found large amounts of solidified $NaAlCl_4$, $LiAlCl_4$ and $AlCl_3$ in the reactor. As Na is a very common pollutant in alumina, especially Bayer alumina, this is a potential challenge.[23] In addition, as carbon was used as the reductant, highly toxic chlorinated hydrocarbons (CHCs) were produced. CHCs stem from C_6-rings reacting with Cl_2. A proposed solution to this issue is to use CO as a reactant in this project, as opposed to solid carbon, as CO does not contain any C_6-rings. The carbochlorination reaction will therefore be:

$$Al_2O_3 + 3\,CO + 3\,Cl_2 \rightleftharpoons 2\,AlCl_3 + 3\,CO_2 \tag{4}$$

Though the ratio of moles Al produced to moles CO_2 released is half to that of the Hall-Héroult process, the CO_2 off-gas is nearly pure.[18] This makes it easier to handle, compared to the off-gas from the Hall-Héroult process, which is quite dilute as it contains below 1% CO_2.

A separate study will examine the CO_2-handling in regards to this project. Most likely, the CO_2 will either be put to storage, or potentially recycled to CO for use in the chlorination reactor.[18] [15]

1.2 Aim and Scope of the Work

In the previously mentioned specialization thesis, different grades of alumina were produced and analyzed, as the quality of alumina may be vital in relation to the carbochlorination reaction.[16] This owes to the fact that the alumina quality can significantly affect the outcome of the process, especially in terms of impurities and reactivity. Therefore, some of the grades of alumina that were produced and characterized were carbochlorinated in the work described here. Thus, one can determine which Al_2O_3-phase is more suited for carbochlorination.

In order to conduct the carbochlorination reaction of alumina (Reaction 7) a reactor was produced. The experiments were on a small scale as the work aimed to obtain information on the reaction kinetics. This was obtained through adjusting parameters, such as temperature and alumina quality. In addition, a Python script to represent the reaction outcome was produced. The script provides a proposed kinetic model with parameters that were adjusted in order to fit the experimental results of the reactions. The proposed kinetic model is the shrinking-core model (SCM). It is important to note that the SCM remains a suggestion, and the reaction's kinetics may or may not be suitable. Therefore, the thesis also aimed to conclude whether the reaction follows the SCM or not. Furthermore, previous studies on the same reaction suggest diffusion is more influential on the reaction rate at higher temperatures, whereas the reaction itself is more influential at lower temperatures.[12] Therefore, this work aimed to, hopefully, determine which is more influential on reaction rate and conversion, and obtain values for the reaction rate constant, k_r, and diffusion coefficient, D. If successful, the script will be able to predict the results of the reaction under specific conditions.

Chapter 2

Theory

2.1 Alumina Qualities

This subchapter is extracted from the specialization thesis.[16]

Alumina, in its many configurations, is extensively studied. Research on alumina has uncovered significant variations within classification of alumina qualities and properties. Phases of alumina are one such property. These phases vary in a magnitude of aspects, such as grain size, crystal structure, surface area, reactivity, etc. Following are descriptions of some selected alumina phases/qualities that are in relation to the aluminas that will be studied in this work.[16]

2.1.1 α-Alumina

α-alumina differs from other polymorphs by being stable at all temperatures, except at its melting point of 2051°C. Its stability and low reactivity makes it suitable for many high-temperature applications. It can be achieved from other phases of alumina or aluminum hydroxide by exposing them to high temperatures, starting at approximately 1100 °C, as viewed in Figure 9. It belongs to the space group R-$\bar{3}$c with a trigonal crystal system, as see in Figure 5, with ABAB-stacked (hcp) oxygen atoms.[14] [16]

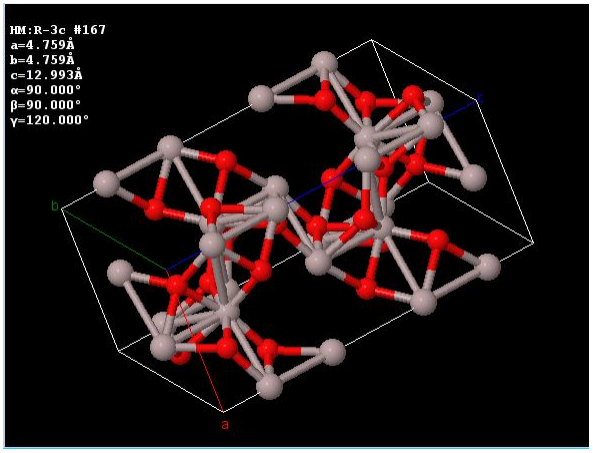

Figure 5: Representation of α-alumina's crystal structure with respective lattice parameters.

2.1.2 γ-Alumina

γ-alumina is considered the most investigated transition phase of alumina. It has a high surface area compared to other phases, and is quite sensitive to temperature changes.[3] With a space group of $Fd\bar{3}m$, it exhibits a face centered cubic (fcc) system.[14] As seen in figure 6, γ-alumina has a cubic unit cell with a = 7.9Å.

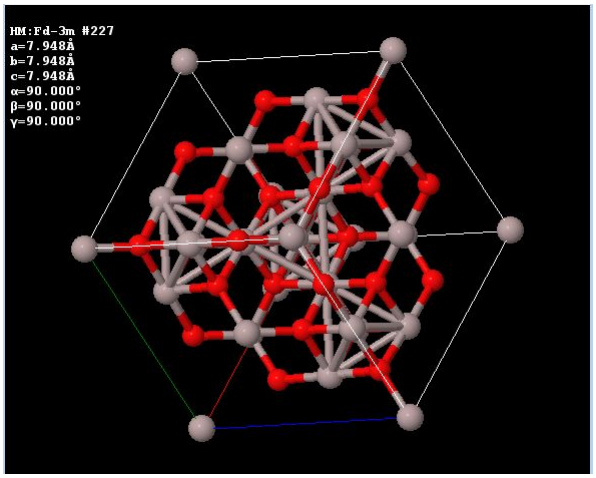

Figure 6: Representation of γ-alumina's crystal structure with respective lattice parameters.

As for formation, γ-alumina occurs through calcination of boehmite within the temperature range 500-750 °C. γ-Alumina's transition to α-alumina can be significantly impacted by mechanical grinding. It has been demonstrated that α-alumina forms at 1000 °C with ground γ-alumina as the starting point, while an unground sample demands for 1200 °C to convert. Even high-energy mechanical milling alone can convert γ-alumina to α-alumina.[3] This proves that there is a co-relation between aggregate size and convertion of γ-alumina.[16]

2.1.3 δ- and θ-Alumina

δ-Alumina emerges during calcination of boehmite around the temperature range 800-950 °C. It will keep the ABC-stacking of oxygen planes already present in γ-alumina, however, a much higher degree of order is observed in the cations.[3] The crystal structures of δ- and θ-Alumina can be seen in Figures 7 and 8, respectively.

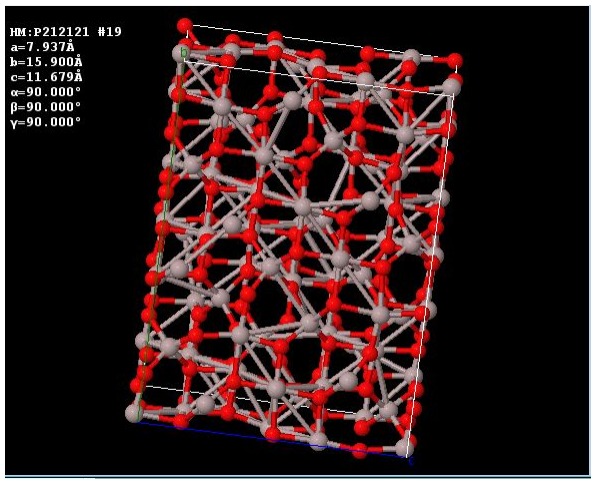

Figure 7: Representation of δ-alumina's crystal structure with respective lattice parameters.

Followingly, as the temperature is increased, θ-alumina will appear. As with its precursor, ABC-stacking is observed in the oxygen planes, and order of the cations increases. Its symmetry is monoclinic with a C2/m space group. Synthesising pure θ-phase from boehmite or bayerite is quite rare. As δ-alumina has similar enthalpies, it is a regular side-product at calcination temperatures up to 950 °C. In addition, α-alumina could also appear in small amounts, even at temperatures below 1000 °C.[3] [16]

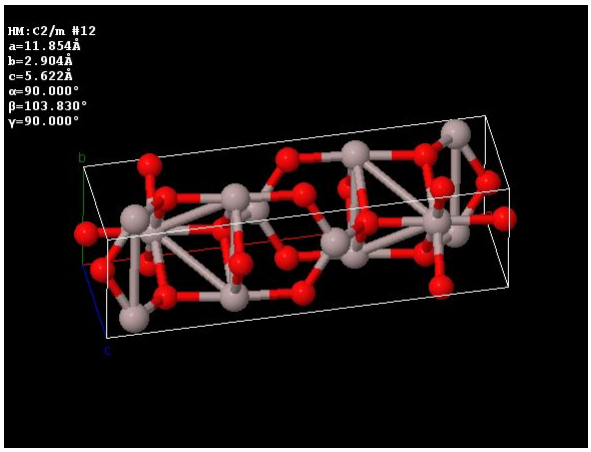

Figure 8: Representation of θ-alumina's crystal structure with respective lattice parameters.

2.1.4 Bayer/SMG Alumina

The alumina produced by Hydro is considered "Bayer-alumina" or smelter grade-alumina (SMG), as it is produced through the Bayer process, and while it is mainly γ-phase, it is a mixture of γ- and α-alumina. As previously men-

tioned, this is the alumina quality that is used during the Hall Héroult process, and was also used in the Alcoa process. The raw material of Bayer alumina is bauxite. It requires about 2-3.5 kg bauxite to produce 1 kg Al_2O_3, along with an energy consumption of about 2.2 kWh/kg. Furthermore, Bayer alumina usually contains impurities like Fe_2O_3 TiO_2, Na_2O and SiO_2. In regards to the chlorination process, these substances may be of concern, as impurities were part of the reason that lead to the shutdown of Alcoa's plant.[23] [5] [16]

2.2 Calcination

The following subchapter is extracted from the specialization project.[16] By heating aluminum hydroxides, they pass through several phase transitions, eventually converting to α-alumina as seen in Figure 9. This occurs due to densification and loss of water, which both increase with calcination temperature. Followingly, a lowering in surface area will occur. The structural hydroxyl groups are irreversibly removed.[3]

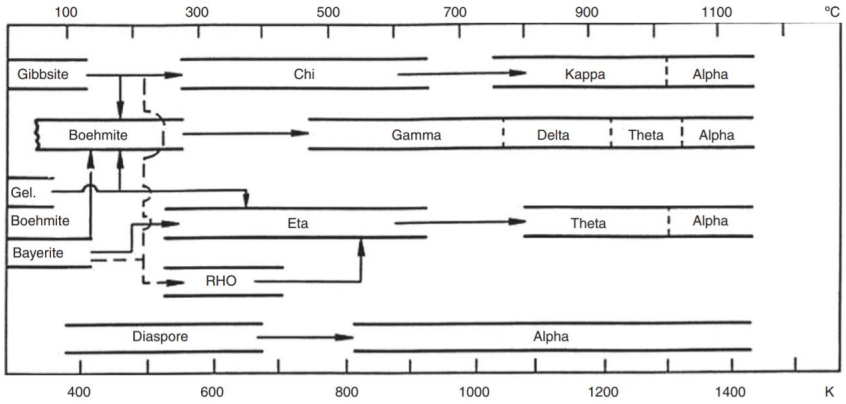

Figure 9: Transformations of Alumina Hydrates[11].

Furthermore, the environment in which alumina hydroxides are calcined will affect the outcome. If, for example, gibbsite (α-$Al(OH)_3$) were heated (60-300°C) while exposed to water vapor, it transforms to boehmite (α-AlO(OH)). In comparison, gibbsite will transform to χ-alumina (300-500 °C) and κ-alumina (800-1150 °C) in dry air.[3] [16]

2.3 Analytical Methods from Specialization Project

Following are descriptions of analytical methods performed in relation to the different aluminas and ATH studied in this report. Each analysis has been performed in order to obtain specific properties characterizing the samples. These analyses were performed in relation to the specialization project. The text in this subchapter is therefore extracted from the previously written speicialization thesis.[16]

2.3.1 XRD

X-Ray Powder Diffraction, XRD, is a method of analysis for crystalline materials, used for phase identification. It works by exposing a sample to an X-ray beam, then measuring the diffraction pattern as a function of outgoing direction. The X-rays are generated through heating a filament within a cathode ray tube, producing electrons. By applying voltage the electrons are accelerated towards the target material. If these electrons have the energy to displace electrons within the inner shells of the material, X-ray spectra characteristic to the material are produced. This is detected by an X-ray detector as it rotates with the sample. The intensity of the reflected X-rays that satisfy Bragg's equation ($n\lambda=2d\sin\theta$) are then converted to a count rate and plotted with respect to 2θ. This enables the user to not only identify the phases present, but also gives information about unit cell dimensions.[7] [16]

2.3.2 ICP

Inductively coupled plasma, ICP, is an analysis method used for identification of elements within a sample. ICP enables recognition of elements at very low concentrations. Prior to analysis, samples must be liquefied, and during analysis the sample is exposed to a sample torch that vaporizes sample droplets. The sample torch usually consists of argon as hot plasma. The argon is charged with an electromagnetic coil, then lit in order to produce a quick discharge that dissociates the sample into its component ions and/or atoms. Followingly, either atomic emission or ion mass is then used to detect elements that are present. In this work, mass spectroscopy (MS) was used to determine species, meaning elements were separated with respect to ion mass. While ICP-MS has the advantage of detecting elements at extremely low concentrations, even isotope compositions, a disadvantage is that spectral and non-spectral interferences may occur.[6] [21] [16]

2.3.3 TGA

A thermogravimetric analyser, TGA, is a device used for measuring the mass of a sample as a function of time and temperature. This enables the user to observe a sample's thermal stability. If a loss in weight occurs this will be due to decomposition, evaporation, reduction or desorption. However, if a weight gain is observed this is caused by oxidation, absorption or adsorption. When studying alumina, for example, TGA enables the user to observe the temperatures at which water detaches from the sample. Furthermore, differential scanning calorimetry (DSC) is a measure of difference in heat flow rate between an inert reference and a sample during TGA. The DSC curve will demonstrate either heat released or heat absorbed by a sample, corresponding to exothermic or endothermic responses, respectively. Endothermic response will result from processes such as evaporation and melting. Exothermic responses, on the other hand, can come from crystallization and oxidation.[2] [16]

2.3.4 BET

BET analysis is a method used to determine the specific surface area of a sample by measuring the adhesion of gas molecules to a sample surface. Usually, N_2 gas is used as it its inert and easily obtained with high purity. As the adhesion will depend on temperature, the system is cooled using liquid N_2. Followingly, the sample is exposed to known amounts of gas, and partial vacuum conditions are induced. If no more adsorption occurs through increasing the pressure, the saturation pressure is obtained. After analysis the data is plotted as amount of gas adsorbed with respect to the relative pressure. The BET surface area can then be determined by finding X_m through the following equation:

$$\frac{1}{X[(P_0/P)]-1} = \frac{1}{X_m C} + \frac{C-1}{X_m C}(\frac{P}{P_0}) \tag{5}$$

X corresponds to the weight of adsorbed N_2, $\frac{P}{P_0}$ is the relative pressure, X_m is the volume of gas adsorbed at standard conditions and C is a constant. At least 3 data points within a $\frac{P}{P_0}$-range of 0.025 to 0.03 are necessary to sufficiently determine the surface area. However, if complications occur single point surface area can be an option, though the result will not be as accurate. Single point BET is obtained through ignoring the constant C.[10] [16]

2.4 Carbochlorination of Alumina

The following subchapter is extracted from the specialization thesis.[16]
Following are some details surrounding carbochlorination of alumina. As previously mentioned, the carbochlorination of alumina occurs through the reaction between Al_2O_3, Cl_2 and C or CO:

$$\mathrm{Al_2O_3} + \frac{3}{2}\mathrm{C} + 3\,\mathrm{Cl_2} \rightleftharpoons 2\,\mathrm{AlCl_3} + \frac{3}{2}\mathrm{CO_2} \tag{6}$$

$$\mathrm{Al_2O_3} + 3\,\mathrm{CO} + 3\,\mathrm{Cl_2} \rightleftharpoons 2\,\mathrm{AlCl_3} + 3\,\mathrm{CO_2} \tag{7}$$

Whereas the reaction with CO produces the double amount of CO_2, it avoids the production of CHC's and is, therefore, the reaction that will be studied further in this work.

As $AlCl_3$ has a boiling point of 180 °C, it will be gaseous after formation, and must therefore be separated from CO_2 before electrolysis.[1] CO_2 will then be sent to storage or recycled as CO to be used in the carbochlorination reaction again.

The vast majority of literature on carbochlorination of alumina has either been on γ-alumina or α-alumina. Unsurprisingly, γ-alumina has been more successfully chlorinated. However, some α-alumina has reacted in previous experiments.[12] In 1981 A. Toth performed carbochlorination experiments on γ-alumina with a $CO-Cl_2$-mixture at

various temperatures, and achieved nearly 100% conversion (Figure 10). The samples were pre-calcined at 1123 K for 30 minutes, achieving a standard state with low residual OH content.[20]

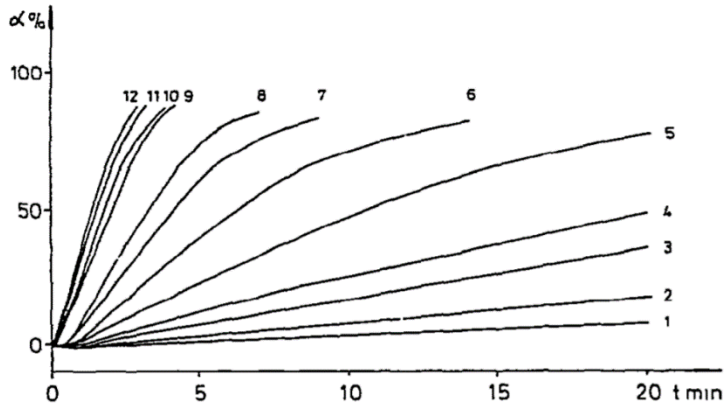

Figure 10: Conversion of γ-alumina from the reaction with a $CO-Cl_2$ mixture. (1) 649 K (2) 674 K (3) 698 K (4) 723 K (5) 775 K (6) 830 K (7) 878 K (8) 922 K (9) 973 K (10) 1023 K (11) 1064K (12) 1123 K.[20]

The following text is extracted from the literature study on carbochlorination, written in relation to this project[15]: "Though several papers have concluded the γ-$Al_2O_3 - Cl_2 - CO$ reaction rate as temperature independent above 873 – 973 K, Toth found it to be steadily increasing up to 1123 K. This could come from the fact that Toth preheated the alumina samples before the reaction. In turn, impairments of the reactivity due to structural changes are avoided. Furthermore, for the $CO - Cl_2$ reaction a chemical control region with a temperature limit of 700 K was determined and displayed first order kinetics with activation energy, E, equal to 106 kJ/mole. For the temperature range of 775 – 878 K E = 56 kJ/mole, demonstrating the region controlled by pore diffusion and chemical reaction. As for the temperature range of 920 – 1123 K E = 23 kJ/mole. This implies that the process proceeds under the control of external mass transfer. Toth assumed a Langmuir-Hinshelwood mechanism for the reaction, providing reaction constants ranging from 0.14 to 0.18 s^-1.[20]

The activation energies correspond well with work by Milne and Mueller. They do, however, not correspond with Landsberg's values.[12] There is reason to believe this is due to his samples being pre-calcined, causing the structure, surface area and chemical behavior to be different. It could also be due to $COCl_2$ forming in the system, because his value is closer to the activation energy calculated for the reaction with phosgene.[23] As for reaction rate, an increase was observed for the $CO - Cl_2$ reaction while using a small excess of Cl_2. Furthermore, it is known that formation of phosgene is accelerated photocatalytically.[20]" [15] Formation of phosgene was also observed for the carbochlorination reaction, however, this decreased with increasing temperature and is unreasonable to put in effect above 900 K as phosgene will dissociate to CO and Cl_2." [20] [15] The carbochlorination reaction itself is exothermic, as is the formation of phosgene.[16]

Though it has been reported that some α-alumina has reacted in a carbochlorination process, it is undesirable due to its low reactivity. Furthermore, the low reactivity has lead to residues of α-alumina in the reactor, which was quite damaging. Wayne Cotten, who worked at the Alcoa plant, has stated: "if the alumina had even a small amount of α-alumina in it, it would accumulate and eventually severely reduce the reaction efficiency to the point the reactor would have to be shut down and drained. The spent bed would be a waste product, and the down time reduces the production efficiency and increases the production cost. Obtaining alumina containing no α-phase is difficult, especially if the sample has been calcined. Most calcined aluminas will contain some α-alumina from the heat exposure." [5] [15]

Furthermore, it is known that the purity of the $AlCl_3$ will be notable for electrolysis. The purity of the alumina will, therefore, affect the outcome of the electrolysis in addition to the chlorination reactor.[5] It is also desirable for the $AlCl_3$ to be as anhydrous as possible, owing to the fact that water in the chlorination reactor will produce HCl through the following reaction:[23]

$$H_2O + Cl_2 + CO \rightleftharpoons 2\,HCl + CO_2 \tag{8}$$

Not only will production of HCl consume Cl_2, but it will also contaminate the CO_2.[16]

2.5 Reaction Kinetics

Kinetics is an essential part to discuss in order to optimize the reaction rate and conversion. With regards to this, the reaction rate constant, k_r, and the diffusion coefficient, D, must be determined. In addition, it is important to discover which of them is the rate limiting factor. For example, if k_r is rate limiting, is can be raised through catalysis, increased surface area, etc. However, if D is rate limiting, the rate must be adjusted otherwise, i. e. by increasing the gas flow.

2.5.1 Shrinking Core Model

The shrinking-core model (SCM) is a method of describing situations in which solid particles are consumed through reaction or dissolution. This results in the particles shrinking in size as the reaction or dissolution continues. The model applies to a wide range of situations, such as the burning of a coal particle or the dissolution of a pill in the stomach. SCM is commonly applied to gas-solid reactions in which the products are solid and/or gaseous. Within the SCM, one can separate between mechanisms, depending on the reaction outcome (Figure 11).[22]

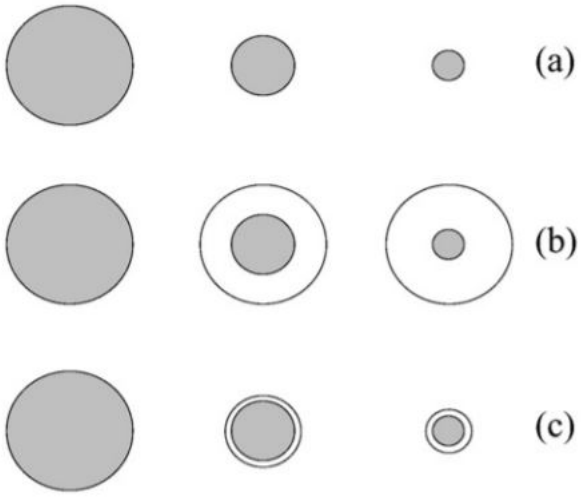

Figure 11: Schematic of different mechanisms of the shrinking core model. The grey areas represent unreacted parts of a particle, whereas the white areas in (b) and (c) represent solid products.[22]

In this case, Reaction 7, the products are gaseous, thus (a) in Figure 11 is the suggested mechanism. The SCM has been applied as a suggested kinetic model for Reaction 7 as it is mathematically quite simple and allows for assuming uniform particle shape and shrinkage. Thus, the particles will keep their spherical shape until complete consumption.

Furthermore, gas diffusion is a vital part when considering gas-solid reactions in porous media. In this case the porous medium is Al_2O_3, into which both CO and Cl_2 will need to diffuse, at the same time as $AlCl_3$ and CO_2 are exiting the particle.

In this case it is known that the equilibrium is largely shifted towards the products. In addition, it has been previously determined by Toth that the reaction is of first order with respect to Cl_2. Though this will not be confirmed in this work, a model for a different order of reaction is recommended to be studied in the future. The reaction constant is presumed to be dependent on Cl_2 and Al_2O_3 through the following rate expression:[13]

$$\frac{d}{dt}n_{\mathrm{Al_2O_3}} = \frac{1}{3}k \cdot c_{\mathrm{Cl_2}} \tag{9}$$

From Reaction 7 the mole balance becomes:

$$\frac{d}{dt}n_{\mathrm{CO}} = \frac{d}{dt}n_{\mathrm{Cl_2}} = 3 \cdot \frac{d}{dt}n_{\mathrm{Al_2O_3}} = -1.5 \cdot \frac{d}{dt}n_{\mathrm{AlCl_3}} = -\frac{d}{dt}n_{\mathrm{CO_2}} \tag{10}$$

In looking at the case where the chemical reaction is rate determining an expression that includes particle radius, r, is produced. In this case it is assumed that the gas concentration is the same on the surface of the particle as the surrounding gas. Firstly, the particle volume is defined with the assumption of spherical particles.

$$V_p = \frac{4\pi r^3}{3} \tag{11}$$

Moles of Al_2O_3 per particle is defined as:

$$n_{\mathrm{Al_2O_3}} = \frac{\rho V_p}{M_{\mathrm{Al_2O_3}}} \tag{12}$$

Where $M_{\mathrm{Al_2O_3}}$ is the molar weight of Al_2O_3 and ρ is the density. Differentially, the expression becomes:

$$dn_{\mathrm{Al_2O_3}} = \frac{\rho}{M_{\mathrm{Al_2O_3}}}dV = \frac{\rho \cdot 4\pi r^2}{M_{\mathrm{Al_2O_3}}}dr \tag{13}$$

By combining Equations 13, 10 and 9 a rate expression with respect to radius is produced:

$$\frac{3}{4\pi r^2}(\frac{d}{dt}n_{\mathrm{Al_2O_3}}) = \frac{3}{4\pi r^2}\frac{\rho \cdot 4\pi r^2}{M_{\mathrm{Al_2O_3}}}\frac{d}{dt}r = \frac{\rho}{M_{\mathrm{Al_2O_3}}}\frac{d}{dt}r = -\frac{1}{3}k \cdot c_{\mathrm{Cl_2}} \tag{14}$$

Followingly:

$$\frac{\rho}{M_{\mathrm{Al_2O_3}}}dr = -\frac{1}{3}k \cdot c_{\mathrm{Cl_2}}dt \tag{15}$$

The expression is then integrated from initial radius r_0 to $r(t)$ on the left side, and from 0 to t on the right side:

$$\frac{\rho}{M_{\mathrm{Al_2O_3}}}\int_{r_0}^{r(t)} dr = -\frac{1}{3}k \cdot c_{\mathrm{Cl_2}}\int_0^t dt \tag{16}$$

Followingly, an expression for radius with respect to time is obtained:

$$r(t) = r_0 - \frac{M_{Al2O3}kc_{\mathrm{Cl_2}}t}{3\rho} \tag{17}$$

This expression is then used to express conversion, X:

$$X = 1 - \frac{V}{V_0} = 1 - \frac{r^3}{r_0^3} = 1 - \frac{1}{r_0^3}(r_0 - \frac{M_{Al2O3} k c_{\mathrm{Cl_2}} t}{3\rho})^3 \tag{18}$$

As previously mentioned, k is unknown in this experiment, and will be approximated in the script to match the reaction results. Though the calculations above assume the chemical reaction is rate determining, there is reason to believe diffusion will play a notable part, therefore, the rate constant, k, will be a combination of the mechanisms:

$$k = \frac{1}{\frac{1}{k_r} + \frac{1}{k_m}} \tag{19}$$

Where k_m is the mass transfer coefficient and k_r is the rate constant. For a falling particle k_m is calculated followingly:[13]

$$\frac{k_m 2r}{D} = 2 + 0.6(Sc)^{1/3}(Re)^{1/2} = 2 + 0.6(\frac{\mu}{\rho_g D})^{1/3}(\frac{2ru\rho_g}{\mu})^{1/2} \tag{20}$$

$$k_m = \frac{D}{r} + 0.6(\frac{\mu D^2}{\rho_g})^{1/3}(\frac{u\rho_g}{2r\mu})^{1/2} \tag{21}$$

Where, Sc is the Schmidt number, Re is the Reynold's number, μ is the dynamic viscosity, ρ_{gas} is the gas density and u is the gas velocity. Furthermore, it should be noted that if Cl_2 and CO diffuse through a fixed bed, their concentrations will differ along the bed. For example, if t = 0 is defined as the moment the reaction occurs, i.e. when the gas reaches the Al_2O_3, the gas concentration will be high at the beginning of the bed, whereas it will be much lower at the end. Therefore, the model should include the concentration profile of Cl_2, so that parameters may also be defined with respect to distance into bed. This is done by firstly looking at the mass balance, defining amounts of Cl_2-gas within a control volume ranging from z to Δz, where z is a length along the volume:

$$F\Big|_z - F\Big|_{z+\Delta z} + r'' a_c (A_r \Delta z) = 0 \tag{22}$$

Where, the left-hand term is the rate of gas entering the control volume, the second term is the rate of gas exiting the control volume and the third term is change in rate. A_r is the circumferential area of the gas travelling along the bed, r" is rate of generation and a_c is the external particle surface area of per volume of bed $[m^2/m^3]$. $\frac{dn_{\mathrm{Cl_2}}}{dt}$ [mol/s] is Cl_2 spent per particle, leading to the expression (neglecting diffusion):

$$u \cdot A_r \cdot c_{Cl2}\Big|_z - u \cdot A_r \cdot c_{Cl2}\Big|_{z+\Delta z} + c_p \cdot A_r \cdot \Delta z \frac{dn_{Cl2}}{dt} = 0 \tag{23}$$

Where, u is the gas velocity and c_p is the concentration of Al_2O_3 particles $[\#/m^3]$. The left-hand term represents Cl_2 [mol/s] within the control volume, the second term is Cl_2 [mol/s] leaving the control volume and the right-hand term is Cl_2 [mol/s] reacted in the control volume. Dividing the expression by $A_r \Delta z$ gives:

$$\frac{-(u \cdot c_{Cl2}\Big|_{z+\Delta z} - u \cdot c_{Cl2}\Big|_z)}{\Delta z} + c_p \frac{dn_{Cl2}}{dt} = 0 \tag{24}$$

$$lim_{\Delta z \to 0} = -u\frac{dc_{Cl2}}{dz} + c_p\frac{dn_{Cl2}}{dt} \tag{25}$$

Finally, the expression for concentration of Cl_2 with respect to time and distance into bed becomes:

$$\frac{dc_{Cl2}}{dz} = \frac{c_p}{u}\frac{dn_{Cl2}}{dt} \tag{26}$$

c_p can be approximated as follows, considering the concentration of particles is given by $\frac{\text{mass in} 1 cm^3 \text{ bulk alumina}}{\text{mass per particle of alumina}}$ [8]:

$$c_p = \frac{\rho_{bulk}}{\frac{4\pi r_0^3}{3}\rho_{\mathrm{Al_2O_3}}} \tag{27}$$

2.5.2 Gas Analysis

During reaction, CO and Cl_2 enter the reactor through two gas inlets before encountering Al_2O_3, which is placed on a porous filter (quartz frit). The filter will allow product gases, $AlCl_3$ and CO_2 to pass to the gas outlet. However, some CO and Cl_2 may also pass the filter, if they do not react. For results regarding conversion as a function of time, the gas exiting the reactor is exposed to a solution of lye, which absorbs chlorides. This way the amount of Cl_2 that passes through the reactor without reacting can be determined. This is also performed in order to enable multiple experiments without having to disassemble the reactor. Thus, the lye will absorb the unreacted Cl_2 gas, and as the amount of inlet Cl_2 gas is known, one can determine how much Cl_2 has been converted to $AlCl_3$. The lye consists of diluted NaOH and will therefore produce NaClO when exposed to Cl_2. The amount of chlorides absorbed is easily determined through titration. The titration is done by reacting chlorate ions with acidic potassium iodide, yielding elemental iodine. This produces a visible brown color. The iodine may in turn be titrated against a solution of sodium thiosulfate until the solution becomes clear. To aid determination of the endpoint, starch may be added as an indicator. This will turn the solution deep blue, before a sharp transition to a clear solution at the end point of the titration. The reactions are as follows:

$$\mathrm{ClO^- + 2\,I^- + 2\,H^+ \longrightarrow I_2 + Cl^- + H_2O} \tag{28}$$

$$\mathrm{I_2 + 2\,{S_2O_3}^{2-} \longrightarrow 2\,I^- + {S_4O_6}^{2-}} \tag{29}$$

The amount of Cl_2 is then determined through Equation 30.[9]

$$n_{\mathrm{Cl_2}} = \frac{n_{\mathrm{Na_2S_2O_3}}}{2} \tag{30}$$

2.6 Pearson Product Moment Correlation

Pearson product moment correlation coefficient, R, is used to determine the correlation of two sets of known data, x and y. The value of R^2 is thus interpreted as the proportion of variance in y with respect to x. This enables for

presenting a specific value for how much the SCM conversion deviates from the experimental conversion. R can be calculated as follows:

$$R = \frac{\sum(x - \bar{x})(y - \bar{y})}{\sqrt{\sum(x - \bar{x})^2 \sum(y - \bar{y})^2}} \tag{31}$$

Where, $\bar{x}$ and $\bar{y}$ refers to the average. The closer the value of R^2 is to 1 or -1, the less variance there is between the data sets.[17]

2.7 Arrhenius Equation

The Arrhenius equation is a mathematical term to represent the rate constant, k, with respect to temperature (T) and activation energy (E_a):

$$k = A \exp - \frac{E_a}{RT} \tag{32}$$

Where A is a pre-exponential constant and R is the gas constant. The diffusion coefficient can also be determined with the Arrhenius equation:

$$D = D_0 \exp - \frac{E_a}{RT} \tag{33}$$

Where D_0 is the maximum diffusion coefficient at infinite temperature. The equation can also be presented on the logarithmic form:

$$ln(k) = ln(A) - \frac{E_a}{RT} \tag{34}$$

On this form, ln(k) can be plotted with 1/T, and should produce a straight line with slope E_a and intercept ln(A).[4] This equation can be used to differ between temperature ranges in which the rate is diffusion- or reaction controlled.

2.8 Gas Diffusion

Gas diffusion is defined as *the gradual mixture of molecules of one gas with molecules of another by virtue of their kinetic porperties.* According to Graham's law of diffusion, *the rates of diffusion for two gases are inversely proportional to the square roots of their molar masses, under equal conditions of temperature and pressure.*:[4]

$$\frac{r_1}{r_2} = \sqrt{\frac{M_2}{M_1}} \tag{35}$$

In this case, that means that Cl_2's diffusion rate is x0.628 CO's diffusion rate at the same conditions. As for CO_2 and $AlCl_3$, the rate of diffusion for $AlCl_3$ should be x0.460 that of CO_2.[4]

Chapter 3

Experimental Methods

3.1 Calcination and Analytics

As previously mentioned, during the specialization project several analytical methods were conducted for varying grades of alumina. In addition, different phases of alumina were obtained through calcination.
Initially, four samples of different grade commercial Bayer aluminas were put through analyses, in addition to a sample of alumina trihydrate (ATH). The aluminas were from various refineries, but as only one of them was used in this thesis it will be referred to as SMG-alumina. This is because the aluminas' respective CoA's, provided by the refineries, are confidential. As previously mentioned, these samples were analyzed through BET, SEM, XRD, XRF, TGA and ICP. Furthermore, ATH was calcined within the temperature range 700 - 1000 °C, resulting in 4 new samples. In turn, these samples were characterized though BET, SEM and XRD.
However, only 3 of them (samples calcined at 800, 900 and 1000 °C) were carbochlorinated in this work, and only the analytical results that are relevant to the conclusive results of this thesis are provided. Following are descriptions and results from these respective analyses, extracted from the specialization project thesis.[16]

3.1.1 BET

The BET analysis was performed to provide the specific surface areas of the samples. Before the BET analysis the ATH was dried at 120 °C for 90 minutes to avoid moisture being released in the apparatus. In addition, all samples were degassed for at least 2 hours beforehand, using a Degas Smartprep machine.
The BET device used is a Tristar 3500. During the BET analysis all samples were put at an initial temperature of 30 °C, with a ramp rate of 10 °C/min.[16]

The given surface areas from the Certificate of Analysis (CoA) and the measured surface areas from the BET analysis with relative standard deviations (RSD) are presented in Table 1 below. RSD values are provided by standard measurements from the BET machine, relative to measured BET surface area.[16]

Table 1: Measured and given surface areas of respective samples. The calcined samples are given names according to their respective calcination temperatures (sample 800 is calcined at 800 °C, and so on).[16]

Sample	Single Point Surface Area [m^2/g]	BET Surface Area [m^2/g]	CoA Surface Area [m^2/g]	RSD [%]
SMG	74.93	77.22	76.50	3.70
ATH	68.95	70.78	-	3.74
800	84.01	85.95	-	3.66
900	66.47	67.65	-	3.75
1000	28.14	28.94	-	3.95

3.1.2 XRD

Using a D8-Focus powder diffractometer with CuKα radiation (i.e. a wavelength of 1.54 Å) XRD analyses were performed. The slit was put to 1 mm for 30 minutes for each sample. Samples were placed in 5 mm deep sample holders, with a maximum sample height of 4 mm prior to analysis. Afterwards, the results were plotted and used to determine which phases were present in all samples. In addition, calcined samples' diffractograms were plotted together to observe phase transition with regard to calcination temperature.[16]

The results from the XRD analyses of the calcined samples are presented in Figure 12, and in Figure 13 together with the ATH diffractogram.[16]

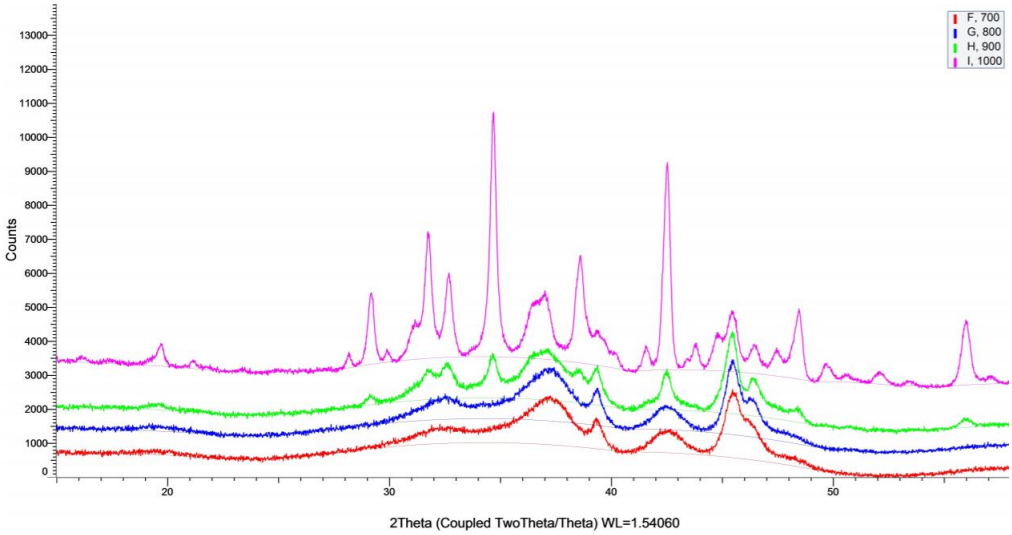

Figure 12: Diffractograms of calcined samples with respective calcination temperatures.[16]

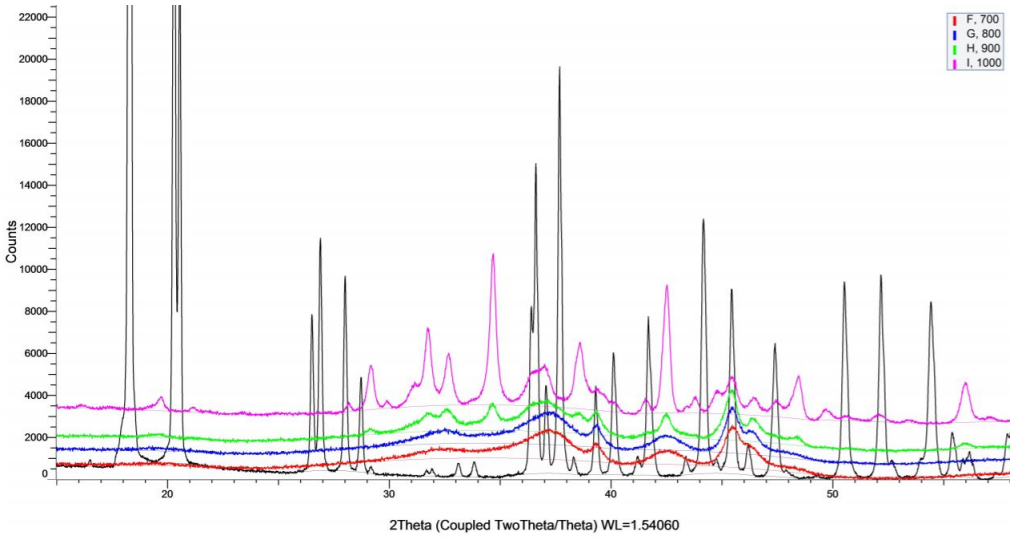

Figure 13: Diffractograms of ATH (black) in comparison to calcined samples with respective calcination temperatures.[16]

The phases found in the different samples are presented in Table 2 below.

Table 2: Phases observed in the samples. These results are based on the diffractograms in Appendix B. The calcined samples are given names according to their respective calcination temperatures (sample 800 is calcined at 800 °C, and so on).[16]

Phase	SMG	800	900	1000	ATH
α	X				
γ	X	X	X	X	
δ			X	X	
θ				X	
Gibbsite					X

These results are based on diffractograms of the respective samples, presented in Appendix B.[16]

3.1.3 TGA

For TGA analyses a TG-Hugin device was used, heating the samples to a final temperature of 1400 °C. Samples were placed in an alumina crucible combined with a lid, where the lid had a small hole in order for gaseous species to exit. The atmosphere consisted of N_2 as this is inert. Prior to each analysis, the system within the TG-Hugin was put

to vacuum and refilled with N_2-gas three times. Ensuring the system had no external contaminants. In addition, the samples, crucible and lid were weighed. The complete heating procedure is presented in Table 3 below:[16]

Table 3: Heating procedure of TGA analysis

Step. no.	T_{int} [°C]	Ramp [°C]	T_{end} [°C]	Dwell [min]	Atmosphere	Flow [ml/min]
1	24	20	300	5	N_2	30
2	300	5	1000	5	N_2	30
3	1000	5	1400	0	N_2	30
4	1400	-30	24	-	N_2	30

The TGA results are presented in Figure 14 and 15 below, and correspond to the procedure in Table 3.[16]

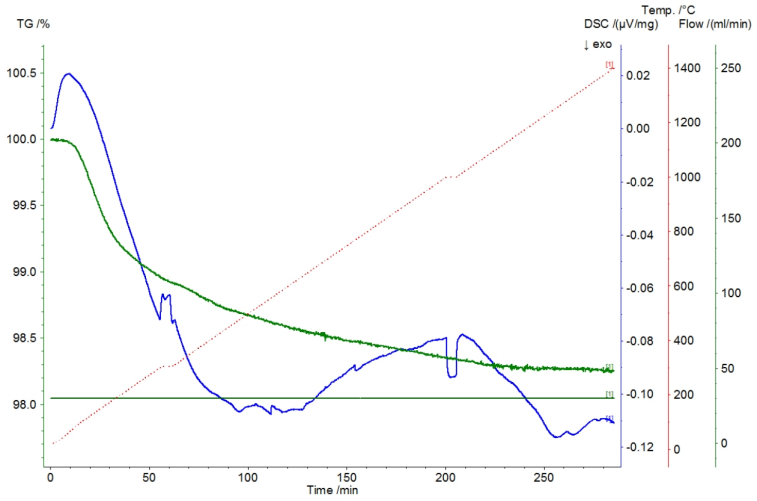

Figure 14: TGA results of SMG sample. The red curve represents changes in temperature, the green curve represents changes in wt% and the blue curve is the DSC curve. The gas flow of N_2 is constant at 30 ml/min.[16]

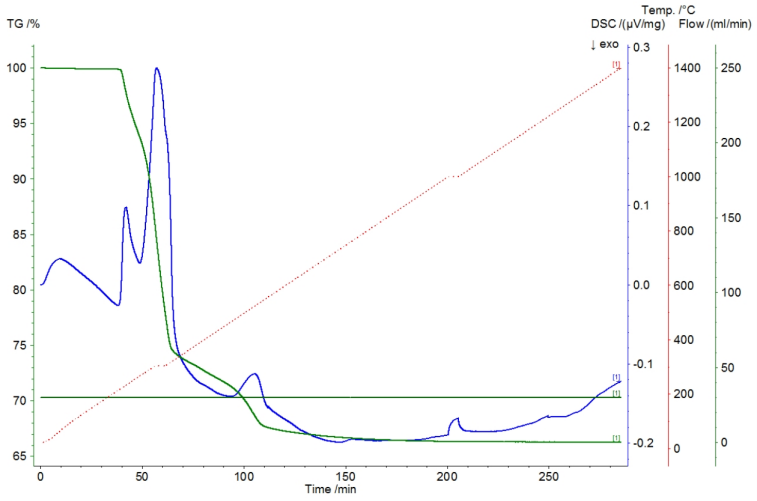

Figure 15: TGA results of ATH. The red curve represents changes in temperature, the green curve represents changes in wt% and the blue curve is the DSC curve. The N_2 gas flow is constant at 30 ml/min.[16]

3.1.4 ICP

Before ICP analyses the samples were dissolved in an acid mixture of H_2SO_4, HCl and HNO_3, followed by heat treatment by microwave. The decomposition program is presented in Table 4. The fractional relationship between acids in the solution was 6 parts H_2SO_4, 6 parts HCl to 1 part HNO_3. Like the XRF analysis, ICP provides information about composition of elements. However, ICP is more precise, and when considering the nature of the samples, more reliable. This is because XRF is commonly used on intact pieces of metal and not powders, such as alumina.[16]

Table 4: Decomposition program of samples in the microwave prior to ICP analysis.

Effect [W]	Time [min]
250	5
400	5
250	5
400	5
600	5
650	3
Vent	5

The results obtained from the ICP analysis are presented in Table 5 below, in ppm, with relative standard deviation,

(RSD), in %.[16]

Table 5: Results obtained from ICP analysis. ICP values are presented in ppm and RSD in % .[16]

	Pb	Na_2O	CaO	TiO_2	Fe_2O_3	CuO	ZnO	Ga_2O_3
SMG	1.8	4311	71.2	70.9	174.3	2.0	2.5	84.9
ATH	0.9	2884	69.4	40.2	99.8	1.0	1.4	54.9
RSD	58.5	28.6	72.5	100.9	56.3	129.1	91.5	39.9

3.1.5 Calcination

Samples of alumina trihydrate were calcined within the temperature range 700 - 1000 °C. As a margin of 100 °C between samples was used, four new samples were produced. Following Figure 9, it was attempted to achieve γ-, δ- and θ-phase.

The samples were all heated in the same calcination oven in an alumina crucible, with a heating rate of 200 °C/hr and kept at the elevated temperature for 2 hours. The samples in the crucible were partially covered during calcination. This was in order for the fine powder to stay in the crucible, while making sure water and other contaminants are able to evaporate out of the system. In addition, the samples and crucible were weighed before and after calcination. These results are presented in Table 6 below. The calcined samples are given names according to their respective calcination temperatures (sample 800 is calcined at 800 °C, and so on).[16]

Table 6: Weight changes of calcined samples after calcination.[16]

	Before calcination	**Weight [g]**	**After calcination**	**Weight [g]**
Sample 800	Crucible:	67.06	Crucible:	67.06
	Crucible and sample:	97.39	Crucible and sample:	86.26
Sample 900	Crucible:	67.05	Crucible:	67.05
	Crucible and sample:	97.34	Crucible and sample:	86.18
Sample 1000	Crucible:	67.05	Crucible:	67.05
	Crucible and sample:	97.59	Crucible and sample:	86.35

Furthermore, loss of ignition (LOI) was calculated for each sample, and plotted as a function of temperature in Graph

1 (also presented in Table 7).[16]

Table 7: LOI of the calcined samples.[16]

Sample	**LOI** [%]
800	36.69
900	36.84
1000	36.80

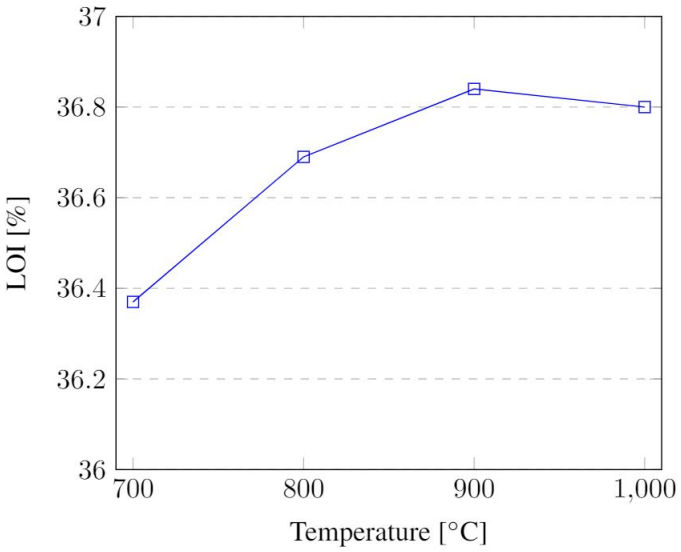

Figure 16: Temperature dependence of LOI.

3.2 Carbochlorination

As previously mentioned, the carbochlorination and gas analysis experiments could not be conducted as planned due to the covid-19 pandemic causing restrictions on presence in laboratories. The experiments described in the following subchapter were, therefore, conducted by Bjørnar Gjesdal of Norsk Hydro.

3.2.1 Reactor

A reactor was designed and constructed for the purpose of this thesis at NTNU Faculty of Natural Sciences Glasblowing Workshop. A sketch of the initial design is illustrated in Figure 17 below.

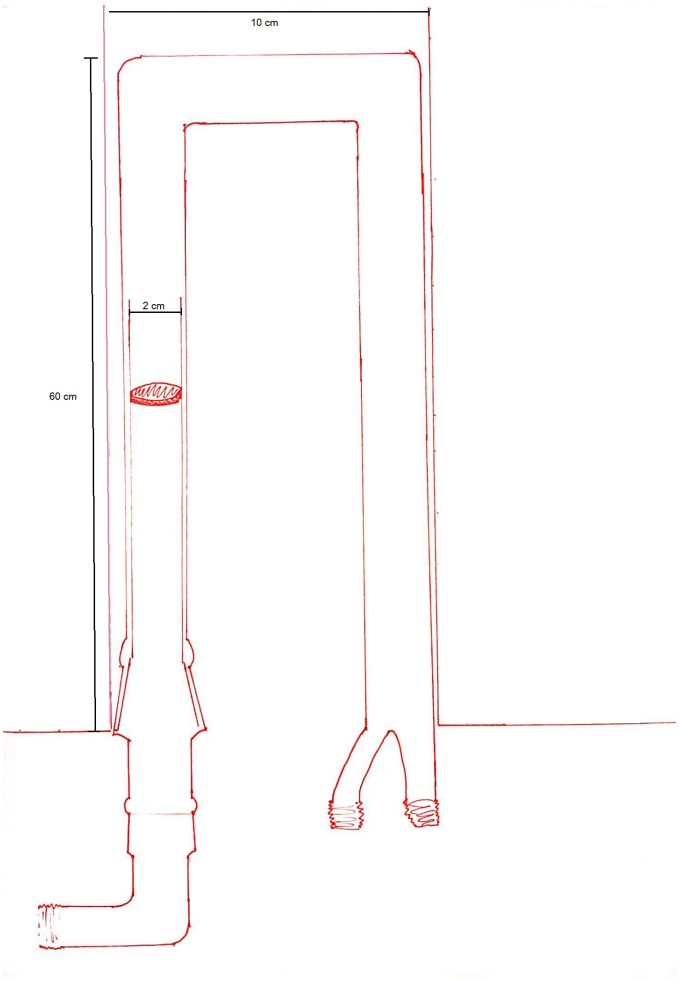

Figure 17: Sketched design of quartz reactor used for carbochlorination of Alumina.

Astrid Salvesen of NTNU constructed the reactor. The design was collectively produced by Kristiane Melingen, Christian Rosenkilde, Bjørnar Gjesdal, Espen T. Wefring and Astrid Salvesen.

The reactor has two gas inlets for Cl_2 and CO, respectively, and one gas outlet for $AlCl_3$ and CO_2. As illustrated, the reactor contains a removable tube, where Al_2O_3 will be placed on top of quartz frit (por2). This will prohibit Al_2O_3 from escaping the outlet, while allowing gaseous species to surpass.

The reactor consists of quartz and is placed within a gold furnace. It withstands temperatures as high as 900 °C. Pressure is measured on the inside of the reaction, and alumina is weighed before and after the reaction.

After a few experimental trials some adjustments were made to the set-up. This was due to issues with large pressure buildups, causing clogging from chloride condensation near the outlet. This was somewhat solved by installing a heat gun, creating a "hot-box" at the bottom of the reactor. This way the temperature at the bottom of the reactor is

maintained high enough for chloride not to condensate. Despite the heat gun, clogs were sometimes forming in the sodawash due to NaCl precipitation in the inlet tube. The adjusted set-up is presented in Figure 18 below.

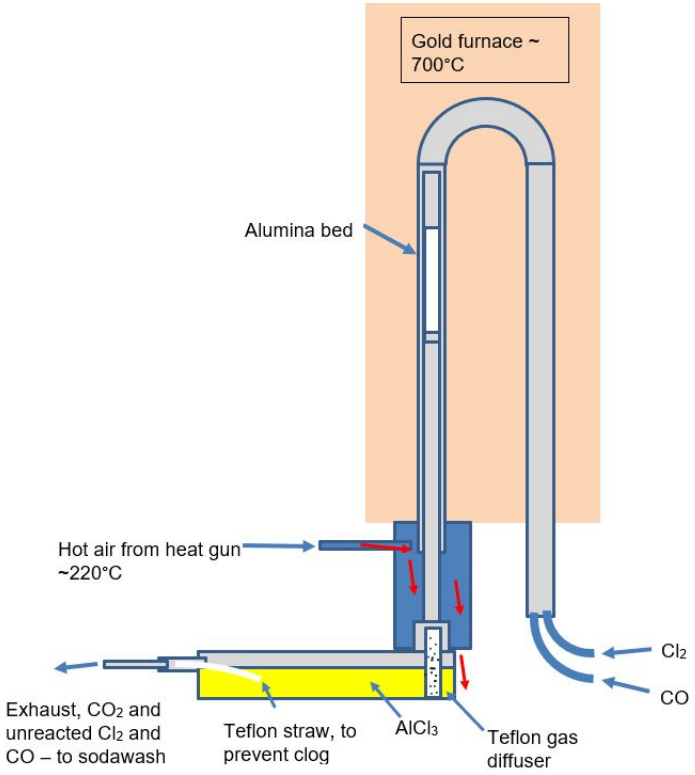

Figure 18: Adjusted set-up for the carbochlorination reactor due to complications with clogging. Figure is constructed by Bjørnar Gjesdal.

3.2.2 Experimental Matrix

Following is an experimental matrix, providing an overview of the experiments conducted in this work. Experiments 1 through 5 vary temperature for the reaction, using the same quality of SMG-alumina. Experiment 6 has adjusted gasflow ratio. Samples used in experiments 7 through 9 use calcined ATH samples, providing $\gamma-, \delta-$ and/or θ-alumina.

Table 8: Experimental matrix for carbochlorination of Alumina.

	Alumina Quality	Amount [g]	Time [hrs]	Temp [°C]	Gas Composition [Cl_2/CO]	Gas Flow [ml/min]
1	SMG	20	5	550	50/50	100
2	SMG	20	5	600	50/50	100
3	SMG	20	5	650	50/50	100
4	SMG	20	5	700	50/50	100
5	SMG	20	5	800	50/50	100
6	SMG	20	5	700	40/60	100
7	γ, δ, θ	20	5	700	50/50	100
8	γ, δ	20	5	700	50/50	100
9	γ	20	5	700	50/50	100

3.2.3 Gas Analysis

The gas analysis experiments in this subchaper were conducted by Bjørnar Gjesdal of Norsk Hydro. The following procedure is based on the theoretical framework presented in Chapter 2.5.2.

The $Na_2S_2O_3$ solution was made from $Na_2S_2O_3 \cdot H_2O$-salt, and weighed out using an analytical balance. The KI-solution was mixed from KI-salt dried overnight at 110 ° C. The concentration of the $Na_2S_2O_3$ and KI solutions were 0.1089 M and 17 g/L, respectively.

The starch indicator consisted of potato starch. 1 g of starch was mixed with 10 ml, producing a paste. Followingly, this was added to 100 ml of boiling water, while stirring. To acidify the solution glacial acetic acid was added.

To obtain an aliqout of the lye sample, 10 ml of sample was dilluted to 250 ml in a volumetric flask. Furthermore, 10 ml of the aliqout was transferred to a small flask for titration. Followingly, 25 ml KI solution and approximately 1 ml 100% acetic acid were added to the solution. A stirrer magnet was put in the flask and the sample was titrated against the $Na_2S_2O_3$ solution. When the brown solution turned slightly green/yellow, approximately 2 ml of the starch indicator was added. The titration was the continued until the solution turned clear.[9]

The experimental conversion is then calculated through subtracting moles of Cl_2 absorbed in lye from the moles of Cl_2 sent into the reactor, then diving by 3, giving moles of Al_2O_3 reacted. Followingly, this is multiplied by the molar mass of Al_2O_3, giving mass of Al_2O_3 reacted. Finally, these values are divided by the start weight of Al_2O_3, giving the conversion. This is done for each titration. A regression line is then produced, giving an expression for conversion with respect to time.

3.3 Model Fitting

Prior to conducting the Python script, it was assumed that the reaction would follow the shrinking-core model. Therefore, the script was made following the mathematical model of SCM, presented in Chapter 2.6.1. Though parameters such as composition, temperature, pressure, sample amount, conversion and gas flow are known, others were adjusted to fit the experimental results. These include, reaction rate constant and diffusion coefficient as both were unknown. Though some studies provide suggested values, these would not necessarily fit due to dissimilar reaction conditions. Therefore, these were adjusted to provide a similar plot to the one obtained from the reaction.

Demonstrated below, is the method of calculating the initial concentration profile of Cl_2 along the bed.

At the beginning of each time step, the concentration is calculated using an average particle radius. For the next time step, the concentration is used to calculate the reduction in particle size. This is done for each node along the bed, producing an expression for concentration with respect to distance into bed.

```
#Calculate gas velocity
gasflowT = gasflowCl2*(T0_K)/298 + gasflowCO*(T0_K)/298 #m3/min
gas_v = gasflowT/60/(np.pi*Tube_d**2/4) #m/s
conc_p = rho_bulk/ (4*np.pi*rho_Al2O3*r_0**3/3) #[#/m^3] # Upstream chlorine concentration
conc_Cl2 = 1.1013E5*0.4/R/(T0_K)
c = np.zeros((timesteps,zsteps))   #Concentration, one row for each timestep and one column for
    each z node
c[:,0] = conc_Cl2  #Concentration at top of bed equal to upstream conc. at all times.
for j in range(1,zsteps):
    c[0,j] = (c[0,j-1]/(1+conc_p/gas_v*4*np.pi*rad[0,j]**2*((2+0.6*((gas_v*2*rad[0,j]*rho_Cl2)/Mu
    )**(0.5)*(Nu/D)**(0.33))*D/2/rad[0,j])*dz))
```

As for the particle radius, it is calculated by the same means as presented in Equation 17, with the total reaction constant, k, calculated with respect to both reaction and diffusion. It is also important to note that radius is defined for both time and distance into bed, for the concentration profile of Cl_2. Other values, such as mass, volume and area, are also calculated as illustrated below.

```
for l in range(0, timesteps):
    X[l] = 0
#Loops over all nodes in bed.
    for j in range(0,zsteps):
        if rad[l-1,j] > 0:
            k = 1/(1/((2+0.6*((gas_v*2*rad[l-1,j]*rho_Cl2)/Mu)**(0.5)*(Nu/D)**(0.33))*D/2/rad[l
    -1,j]) + 1/k_r) #combines diffusion and reaction terms
            if j>0 :
                c[l,j] = (c[l,j-1]/(1+conc_p/gas_v*4*np.pi*rad[l-1,j]**2*k*dz))
            rad[l,j] = (rad[l-1,j] -  MW_Al2O3/rho_Al2O3/3*k*c[l,j]*dt)
```

```
        else:
            c[l,j] = conc_Cl2
        A[l,j]=4*np.pi*(rad[l,j]**2)
        X[l] = X[l] + (1 - ((rad[l,j])**3)/r_0**3)/zsteps
        m_Al2O3[l-1,j] = m_Al2O3[0,zsteps-1]*(1-(X[l]))
        n_Al2O3[l,j] = (m_Al2O3[l-1,j])/MW_Al2O3
        V_Al2O3[l,j]=part*((4/3) *( np . pi ) * (rad[l,j]) **3)
        dw_dt[l-1,j] = (m_Al2O3[l-1,j]-m_Al2O3[l,j])/dt
        if rad[l,j] <= 0:
             rad[l,j] == 0
             V_Al2O3[l,j] == 0 # avoids invalid values
    t_step[l] = t_step[l-1] + dt
```

It should also be mentioned that time and distance into bed is defined as follows:

```
#height- and timesteps
dt =0.01       # [s]
zsteps = 20 #
timesteps = 1800000
dz = bed_h/zsteps #[m]
```

This way, time is defined as 1800000 steps, where each step is 0.01 s, providing a time frame of 18000 s (5 hrs). The same method is used for the bed height, only with 20 steps. This enables parameters to be defined with respect to both distance into bed and time. The reasoning behind having so many time steps is to provide high accuracy and enable the mass balance to function properly.

When attempting to match the SCM plot to the experimental results, the conversion is plotted together with a polynomial regression line from the experimental conversion (each regression plot has an R^2-value above 0.98 to ensure a good fit). In fitting the plots, it is important that the plots both begin at the same value for time. If, for example, the experimental plot starts at t = 50 s, it is plotted as X with respect to time-50, and so on. Then, k_r or D is increased or decreased until the plots align. When adjusting for k_r, D is put at an unrealistically high value and vice versa. This way the conversion will only be affected by one or the other, as the combined k-term divides 1 by D and k_r (see Equation 18 or above). When the plots fit, the SCM values for conversion are extracted and plotted with the real experimental points for conversion, as opposed to the regression line (see Chapter 4.2). Before commencing it is important to adjust parameters for temperature, gas flow, initial mass, etc. correctly, as these vary.

Furthermore, in calculating the R^2-value for conversion, it was impossible to include every conversion value from the script as there are 1,800,000 of them, and the amount of values from each source needs to be equal. To simplify the task, around 20 values were used from each respective source, as this matches the amount of titrations. These were provided by extracting every 90,000th value from the script. Followingly, R^2-values are calculated using the Pearson

product moment correlation method. The whole SCM script is presented in Appendix A.

Chapter 4

Results

4.1 Carbochlorination and Model Fitting

Results from the carbochlorination reaction with respective fitted shrinking-core models are presented here. As previously mentioned, the reaction rate constant, k_r, and the diffusion coefficient, D, were the parameters adjusted to fit the SCM to the experimental results. To demonstrate how well the model fits, it is presented in the same plot as the experimental conversion (tables for which can be found in Appendix D). The experimental conversion points are calculated from the titrations performed throughout the carcochlorination experiment, as presented in subchapter 3.2.3. Other generated results from the Python script will also be presented (radius and mass of Al_2O_3, concentration profile of Cl_2, etc.). As mentioned, it should be noted that in plots for experimental conversion, plots are adjusted to commence at time = 0 s. This is because the reaction will not necessarily start the second it is exposed to Cl_2 and CO, as the script will display. This way the plots can overlap. The correct time for when the reaction commences can be seen in plots for absorbed and calculated Cl_2 in Appendix C.
R^2-values were calculated with respect to conversion from the SCM and experimental results.

Table 9: Summary of experimental results.

Exp.	Alumina Quality	Temp [°C]	Gas Composition [Cl_2/CO]	Final Conversion	k_r	R^2	D	R^2
1	SMG	550	50/50	71.9	$2.6 \cdot 10^{-5}$	0.983	$1.3 \cdot 10^{-10}$	0.987
2	SMG	600	50/50	88.4	$4 \cdot 10^{-5}$	0.969	$1.8 \cdot 10^{-10}$	0.985
3	SMG	650	50/50	85.09	$2.4 \cdot 10^{-5}$	0.995	$1 \cdot 10^{-10}$	0.998
4	SMG	700	50/50	56.6	$2.5 \cdot 10^{-5}$	0.989	$9 \cdot 10^{-11}$	0.989
5	SMG	800	50/50	93.4	$4 \cdot 10^{-5}$	0.990	$2.2 \cdot 10^{-10}$	0.993
6	SMG	700	40/60	94.8	$1.2 \cdot 10^{-5}$	0.997	$2.5 \cdot 10^{-10}$	0.999
7	γ, δ, θ	700	50/50	88.7	$3 \cdot 10^{-5}$	0.992	$1.5 \cdot 10^{-10}$	0.996
8	γ, δ	700	50/50	98.1	$3.5 \cdot 10^{-5}$	0.991	$2 \cdot 10^{-10}$	0.993
9	γ	700	50/50	86.9	$3.5 \cdot 10^{-5}$	0.992	$1.5 \cdot 10^{-10}$	0.998

4.1.1 Experiment 1

The following experiment was conducted at 550°C, using SMG Al_2O_3. The flow rates of Cl_2 and CO were equal at 50 ml/min.

Table 10: Results of weighing before and after carbochlorination of SMG Al_2O_3 at 550°C

Start Weight [g]	19.6
Al_2O_3 Consumed [g]	14.1
Final Conversion [%]	71.9

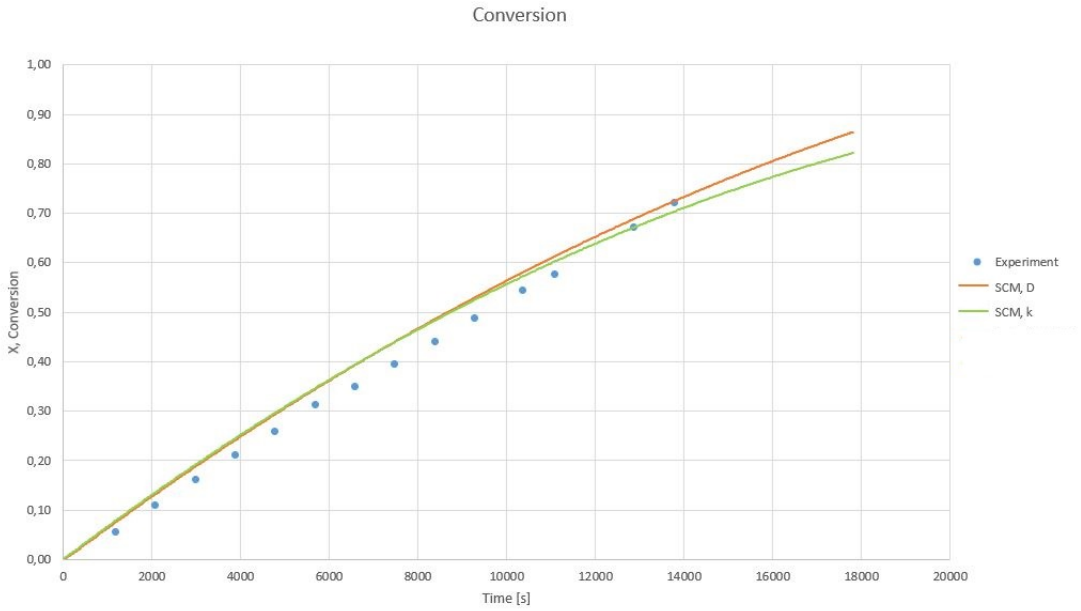

Figure 19: Conversion of SMG Al_2O_3 carbochlorinated at 550°C, together with plots of SCM's adjusted to fit the experiment with respect to k_r and D. The experimental conversion points are calculated from the titrations performed throughout the carcochlorination experiment, as presented in subchapter 3.2.3.

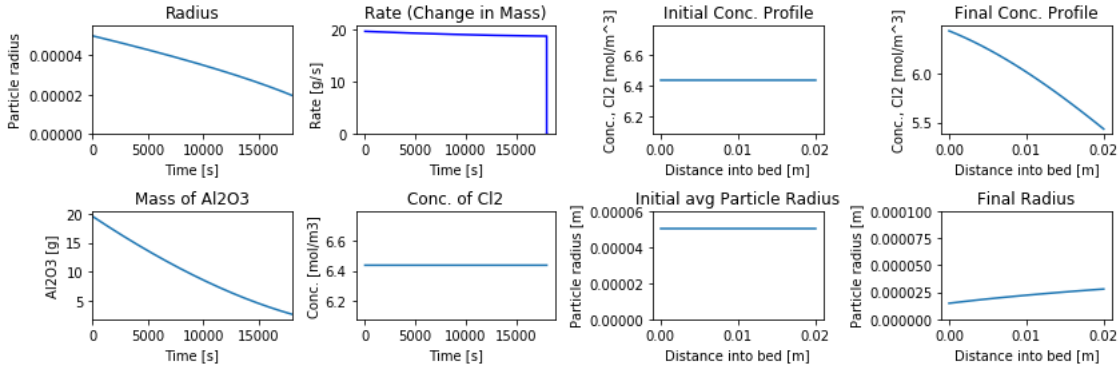

Figure 20: Resulting parameters from the SCM-script for adjusted diffusion coefficient, with respect to time and distance into bed for carbochlorination of SMG-alumina at 550°C.

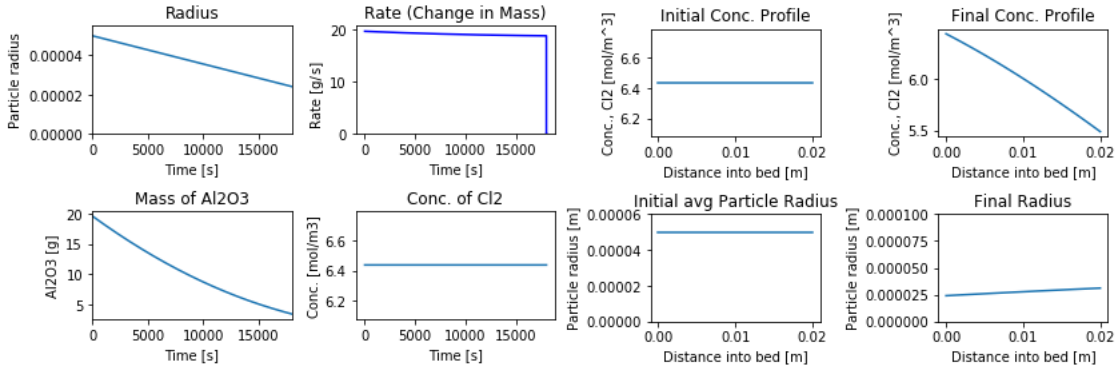

Figure 21: Resulting parameters from the SCM-script for adjusted reaction constant, with respect to time and distance into bed for carbochlorination of SMG-alumina at 550°C.

Table 11: Fitted values for diffusion coefficient and reaction constant for carbochlorination of SMG-alumina at 550°C, with respective R^2-values for SCM model vs. experimental values.

		R^2 [x100]
D $[m^2/s]$	$1.3 \cdot 10^{-}10$	98.7
k $[m/s]$	$2.6 \cdot 10^{-}5$	98.3

4.1.2 Experiment 2

The following experiment was conducted at 600°C, using SMG-Al_2O_3. The flow rates of Cl_2 and CO were equal at 50 ml/min.

Table 12: Results of weighing before and after carbochlorination of SMG-Al_2O_3 at 600°C

Start Weight [g]	16.4
Al_2O_3 Consumed [g]	14.5
Final Conversion [%]	88.4

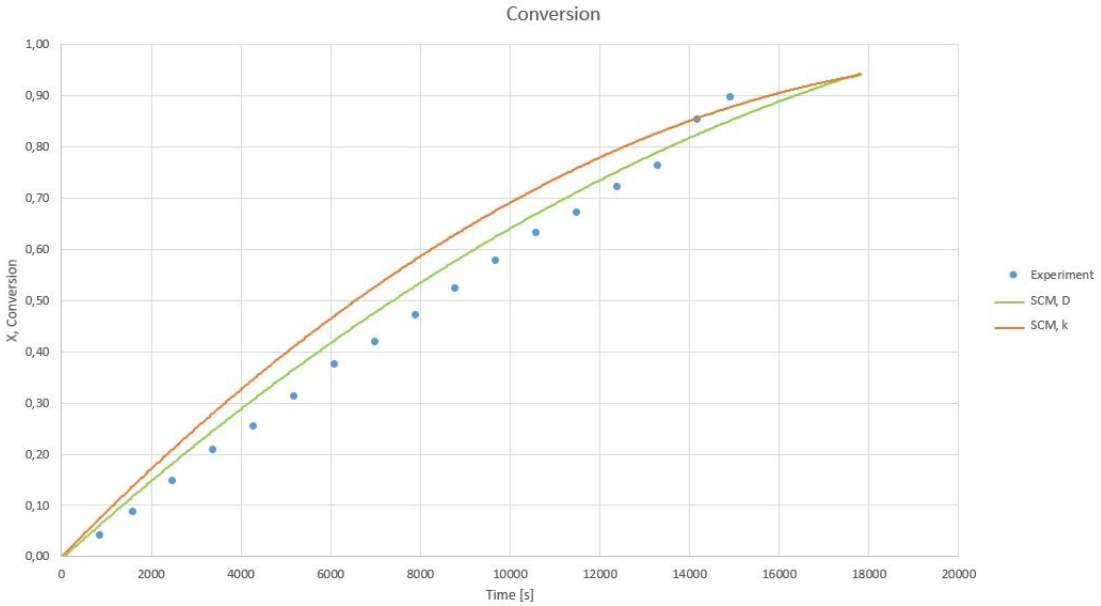

Figure 22: Conversion of SMG Al_2O_3 carbochlorinated at 600°C, together with plots of SCM's adjusted to fit the experiment with respect to k_r and D. The experimental conversion points are calculated from the titrations performed throughout the carcochlorination experiment, as presented in subchapter 3.2.3.

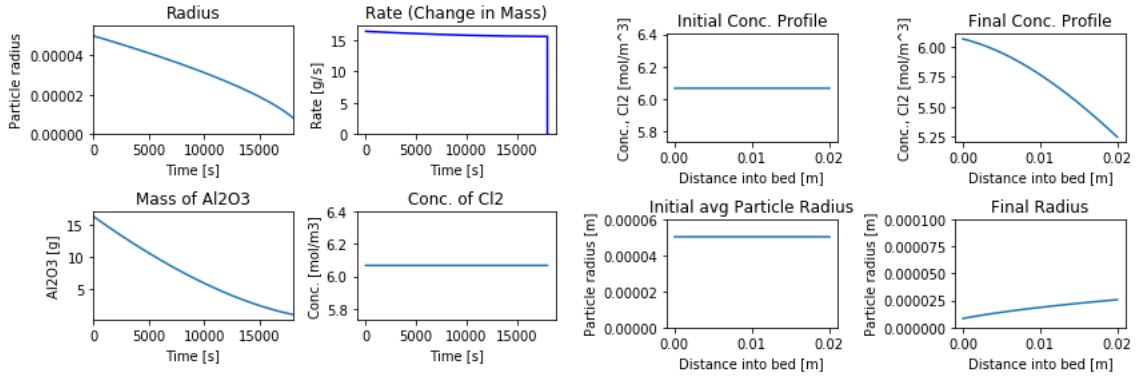

Figure 23: Resulting parameters from the SCM-script for adjusted diffusion coefficient, with respect to time and distance into bed for carbochlorination of SMG-alumina at 600°C.

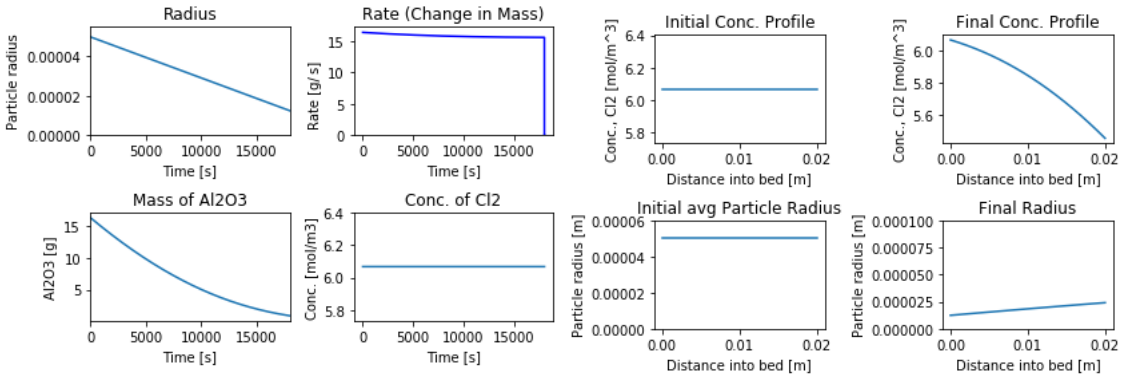

Figure 24: Resulting parameters from the SCM-script for adjusted reaction constant, with respect to time and distance into bed for carbochlorination of SMG-alumina at 600°C.

Table 13: Fitted values for diffusion coefficient and reaction constant for carbochlorination of SMG-alumina at 600°C, with respective R^2-values for SCM model vs. experimental values.

		R^2 [x100]
D $[m^2/s]$	$1.8 \cdot 10^{-}10$	98.5
k $[m/s]$	$4 \cdot 10^{-}5$	96.9

4.1.3 Experiment 3

The following experiment was conducted at 650°C, using SMG Al_2O_3. The flow rates of Cl_2 and CO were equal at 50 ml/min.

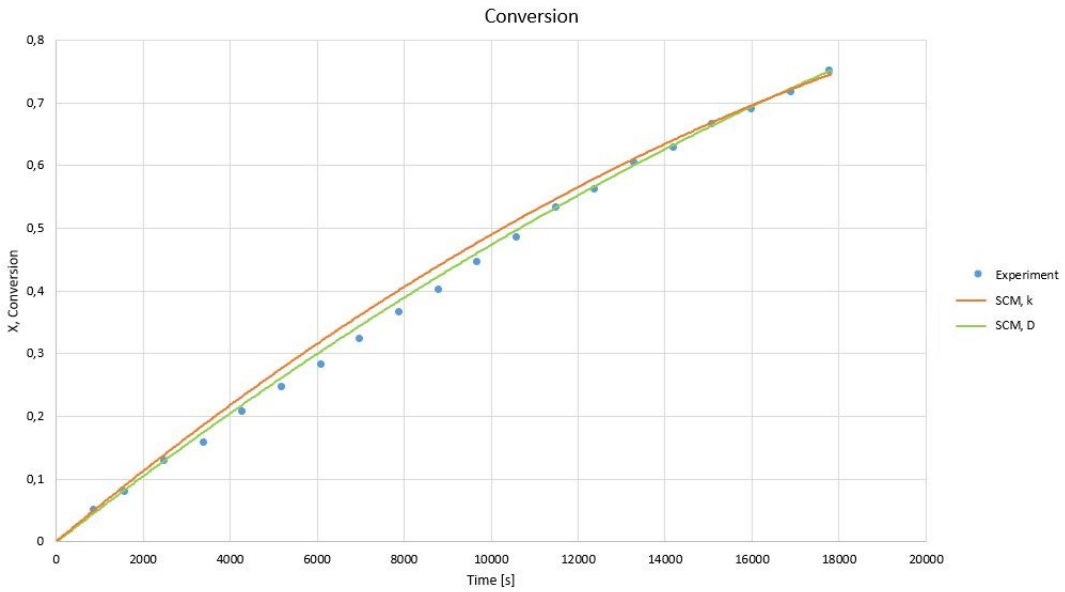

Figure 25: Conversion of SMG Al_2O_3 carbochlorinated at 650°C, together with plots of SCM's adjusted to fit the experiment with respect to k_r and D. The experimental conversion points are calculated from the titrations performed throughout the carcochlorination experiment, as presented in subchapter 3.2.3.

Table 14: Results of weighing before and after carbochlorination of SMG Al_2O_3 at 650°C

Start Weight [g]	22.8
Al_2O_3 Consumed [g]	19.4
Final Conversion [%]	85.09

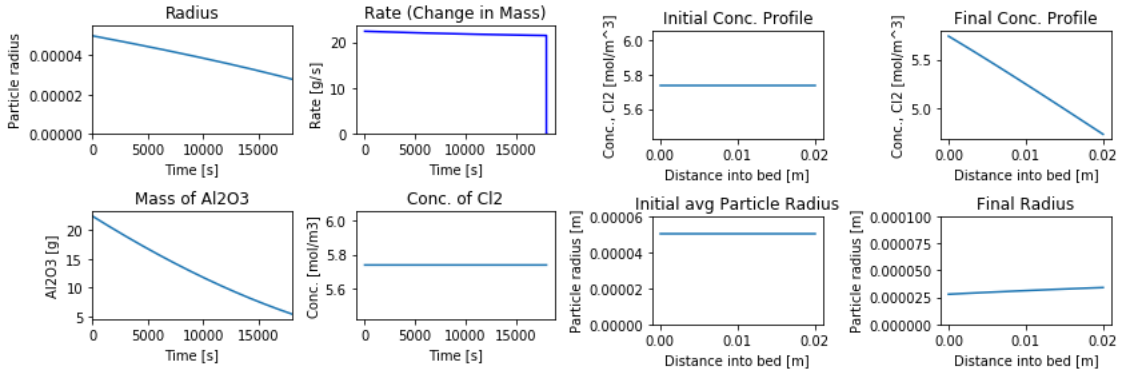

Figure 26: Resulting parameters from the SCM-script for adjusted diffusion coefficient, with respect to time and distance into bed for carbochlorination of SMG-alumina at 650°C.

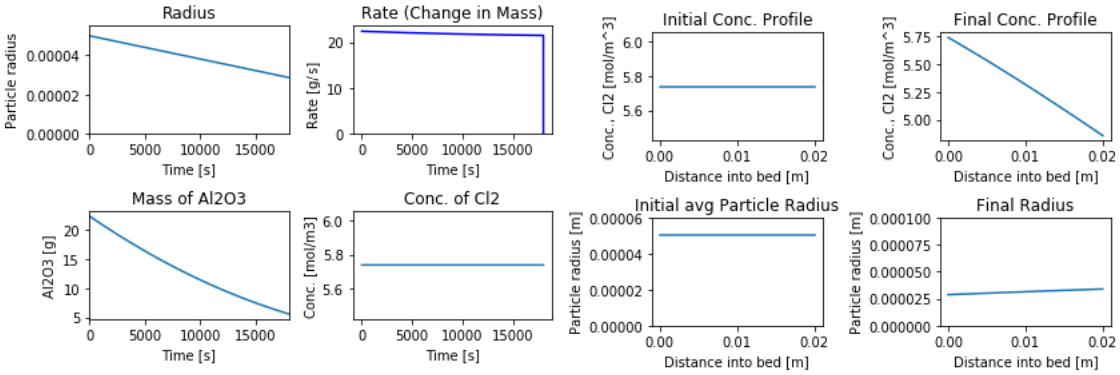

Figure 27: Resulting parameters from the SCM-script for adjusted reaction constant, with respect to time and distance into bed for carbochlorination of SMG-alumina at 650°C.

Table 15: Fitted values for diffusion coefficient and reaction constant for carbochlorination of SMG-alumina at 650°C, with respective R^2-values for SCM model vs. experimental values.

		R^2 [x100]
D $[m^2/s]$	$1 \cdot 10^-10$	99.8
k $[m/s]$	$2.4 \cdot 10^-5$	99.5

4.1.4 Experiment 4

The following experiment was conducted at 700°C, using SMG Al_2O_3. The flow rates of Cl_2 and CO were equal at 50 ml/min

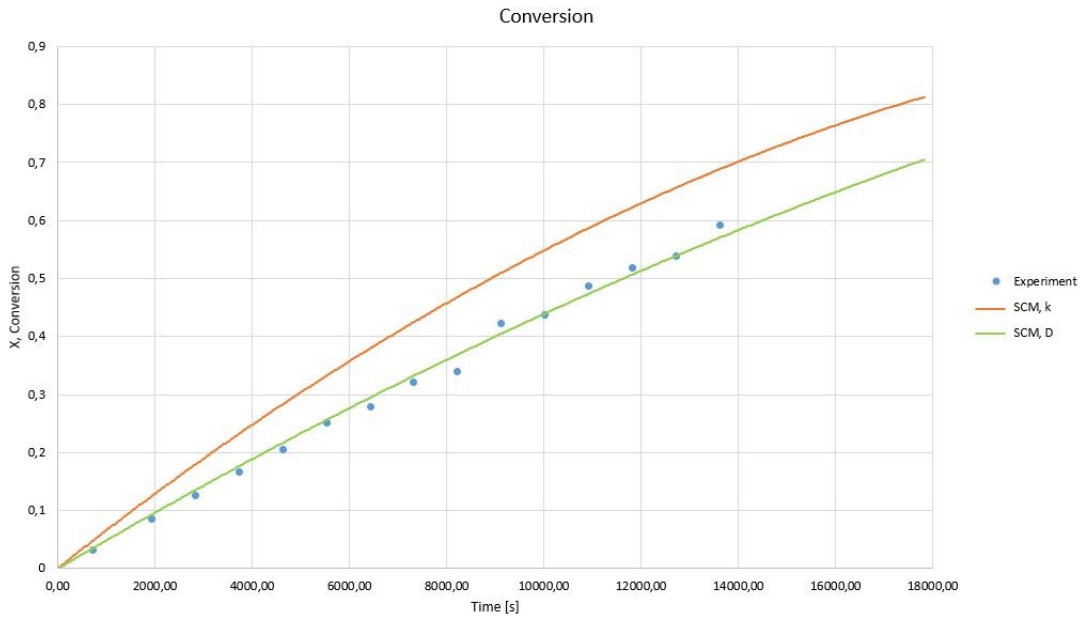

Figure 28: Conversion of SMG Al_2O_3 carbochlorinated at 700°C, together with plots of SCM's adjusted to fit the experiment with respect to k_r and D. The experimental conversion points are calculated from the titrations performed throughout the carcochlorination experiment, as presented in subchapter 3.2.3.

Table 16: Results of weighing before and after carbochlorination of SMG Al_2O_3 at 700°C

Start Weight [g]	24.2
Al_2O_3 Consumed [g]	13.7
Final Conversion [%]	56.6

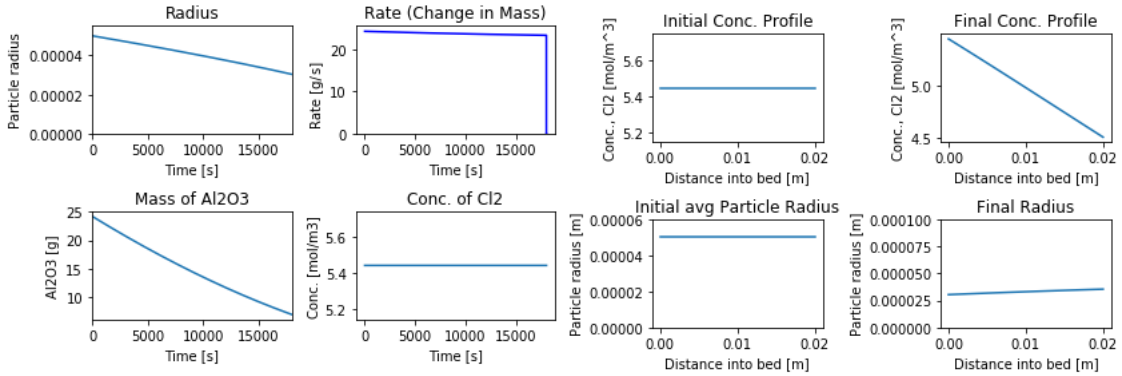

Figure 29: Resulting parameters from the SCM-script for adjusted diffusion coefficient, with respect to time and distance into bed for carbochlorination of SMG-alumina at 700°C.

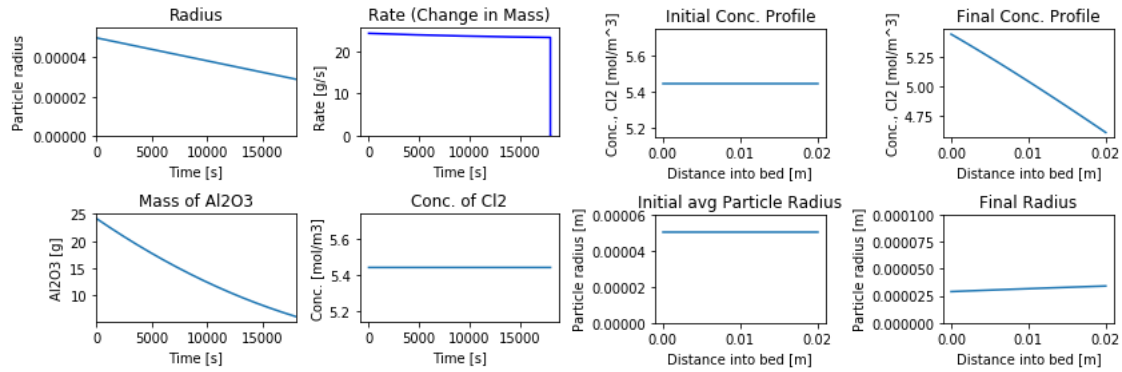

Figure 30: Resulting parameters from the SCM-script for adjusted reaction constant, with respect to time and distance into bed for carbochlorination of SMG-alumina at 700°C.

Table 17: Fitted values for diffusion coefficient and reaction constant for carbochlorination of SMG-alumina at 700°C, with respective R^2-values for SCM model vs. experimental values.

		R^2 [x100]
D $[m^2/s]$	$9 \cdot 10^{-}11$	99.6
k $[m/s]$	$2.5 \cdot 10^{-}5$	98.9

4.1.5 Experiment 5

The following experiment was conducted at 800°C, using SMG Al_2O_3. The flow rates of Cl_2 and CO were equal at 50 ml/min

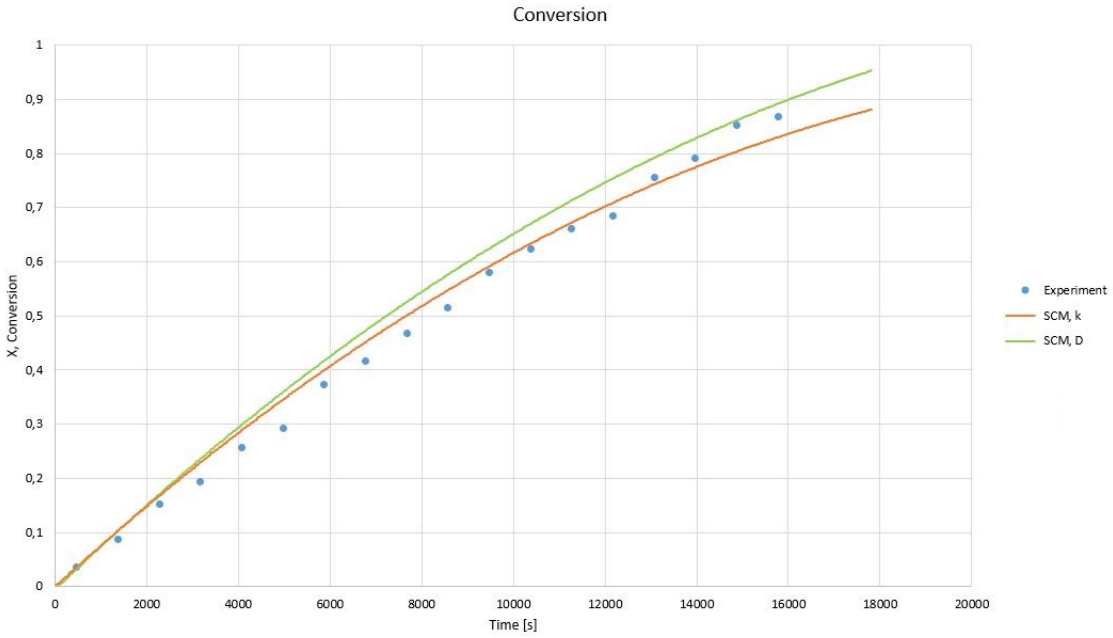

Figure 31: Conversion of SMG Al_2O_3 carbochlorinated at 800°C, together with plots of SCM's adjusted to fit the experiment with respect to k_r and D. The experimental conversion points are calculated from the titrations performed throughout the carcochlorination experiment, as presented in subchapter 3.2.3.

Table 18: Results of weighing before and after carbochlorination of SMG Al_2O_3 at 800°C

Start Weight [g]	16.6
Al_2O_3 Consumed [g]	15.5
Final Conversion [%]	93.4

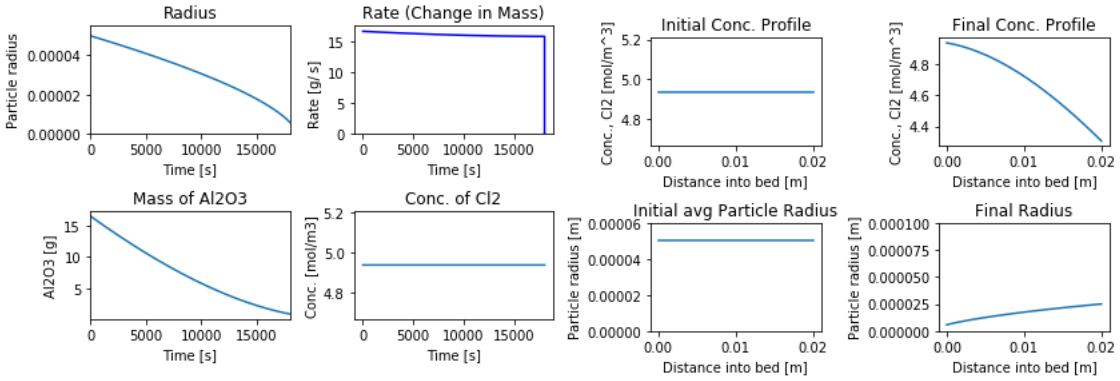

Figure 32: Resulting parameters from the SCM-script for adjusted diffusion coefficient, with respect to time and distance into bed for carbochlorination of SMG-alumina at 800°C.

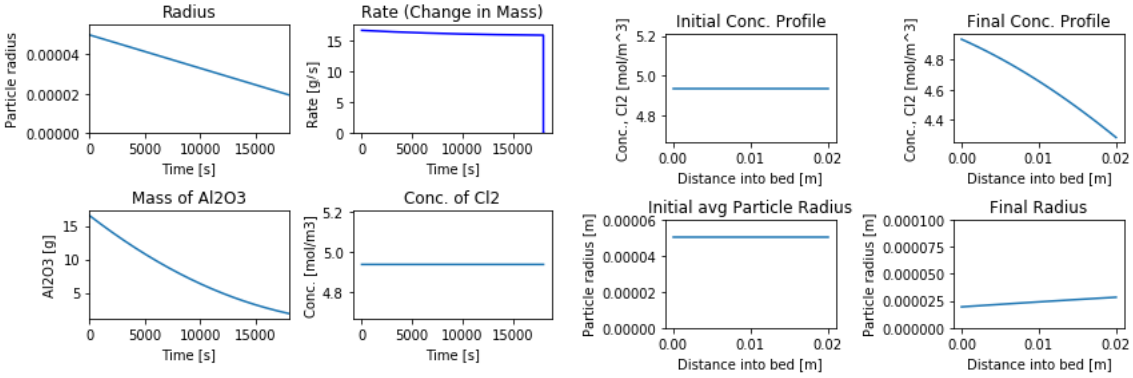

Figure 33: Resulting parameters from the SCM-script for adjusted reaction constant, with respect to time and distance into bed for carbochlorination of SMG-alumina at 800°C.

Table 19: Fitted values for diffusion coefficient and reaction constant for carbochlorination of SMG-alumina at 800°C, with respective R^2-values for SCM model vs. experimental values.

		R^2 [x100]
D $[m^2/s]$	$2.2 \cdot 10^{-}10$	99.3
k $[m/s]$	$4 \cdot 10^{-}5$	99.0

4.1.6 Experiment 6

The following experiment was conducted at 700°C, using SMG Al_2O_3. The flow rates of Cl_2 and CO were 40 and 60 ml/min, respectively.

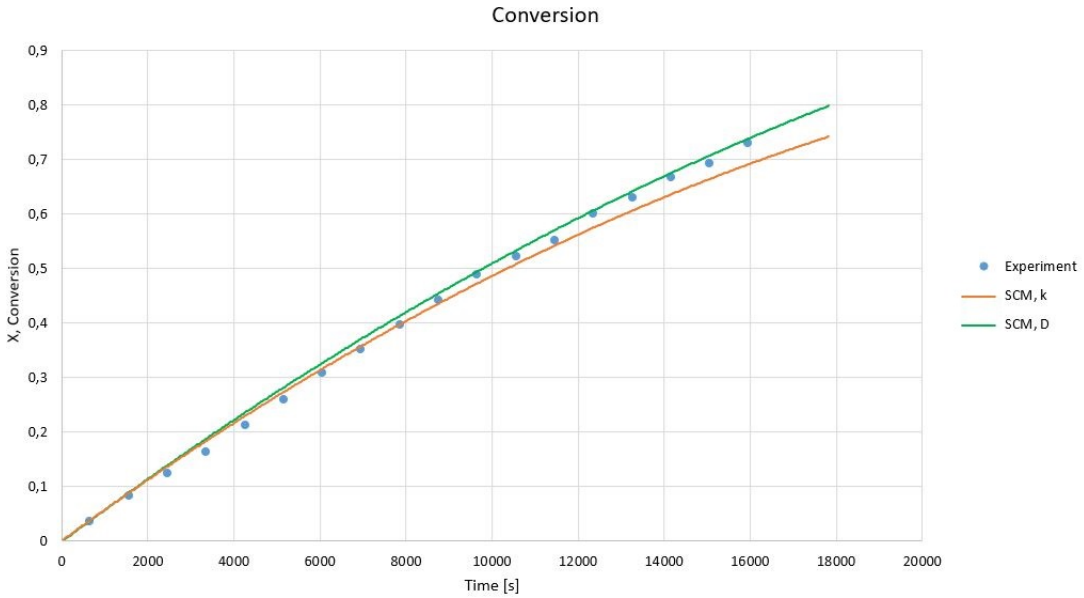

Figure 34: Conversion of SMG Al_2O_3 carbochlorinated at 700°C, with gas flows of 40 and 60 ml/min of Cl_2 and CO, respectively. Plotted together with plots of SCM's adjusted to fit the experiment with respect to k_r and D. The experimental conversion points are calculated from the titrations performed throughout the carcochlorination experiment, as presented in subchapter 3.2.3.

Table 20: Results of weighing before and after carbochlorination of SMG Al_2O_3 at 700°C. The flow rates of Cl_2 and CO were 40 and 60 ml/min, respectively.

Start Weight [g]	19.1
Al_2O_3 Consumed [g]	18.1
Final Conversion [%]	94.8

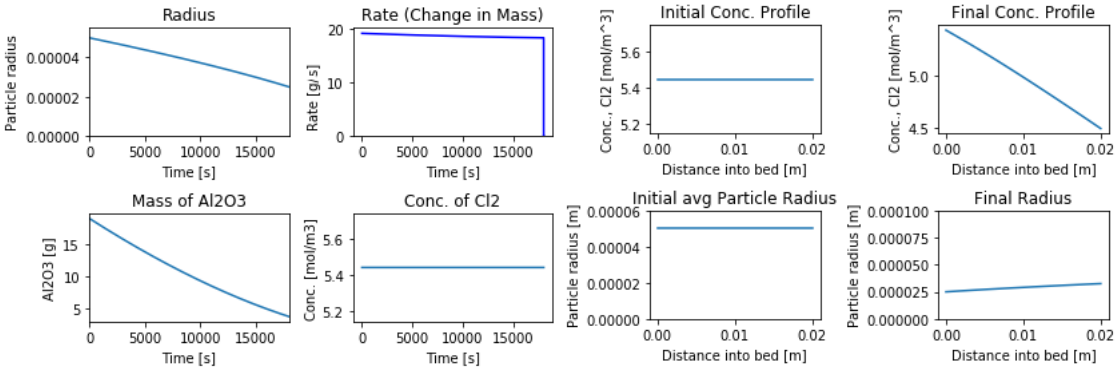

Figure 35: Resulting parameters from the SCM-script for adjusted diffusion coefficient, with respect to time and distance into bed for carbochlorination of SMG-alumina at 700°C.

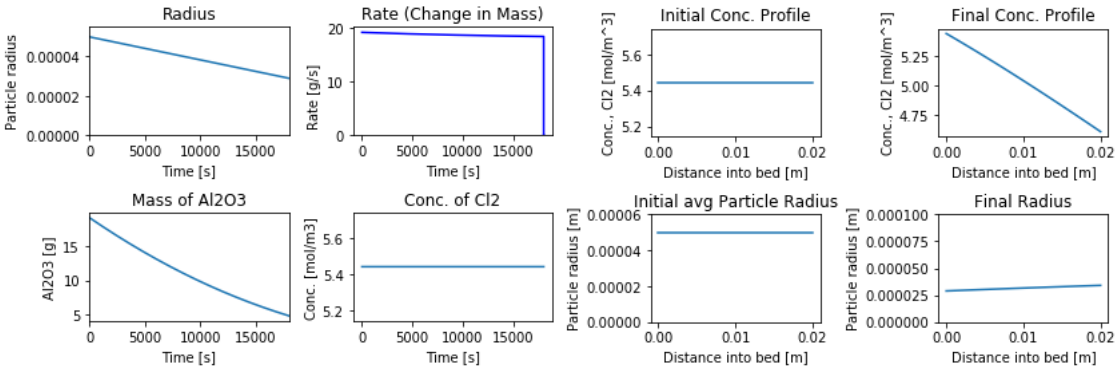

Figure 36: Resulting parameters from the SCM-script for adjusted reaction constant, with respect to time and distance into bed for carbochlorination of SMG-alumina at 700°C.

Table 21: Fitted values for diffusion coefficient and reaction constant for carbochlorination of SMG-alumina at 700°C, with respective R^2-values for SCM model vs. experimental values.

		R^2 [x100]
D $[m^2/s]$	$1.2 \cdot 10^{-}10$	99.9
k $[m/s]$	$2.5 \cdot 10^{-}5$	99.7

4.1.7 Experiment 7

The following experiment was conducted at 700°C, using Al_2O_3 calcined at 1000°C. The sample contains a mixture of $\gamma-, \delta-$ and $\theta-Al_3O_3$. The flow rates of Cl_2 and CO were equal at 50 ml/min.

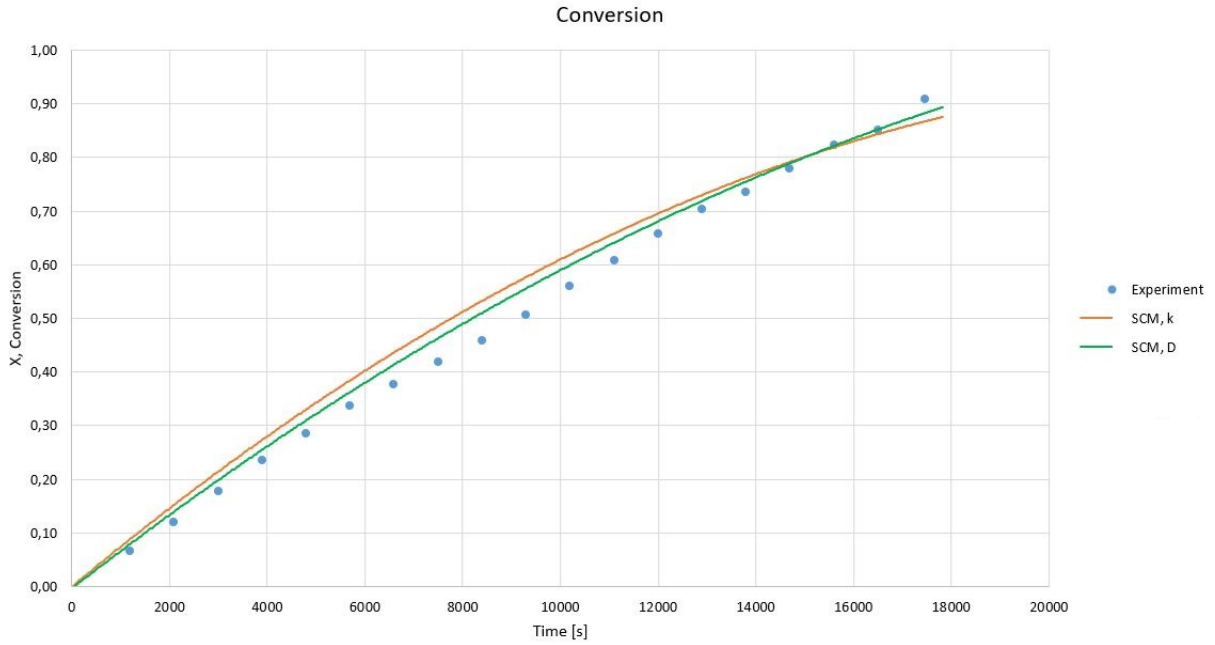

Figure 37: Conversion of $\gamma-, \delta-$ and $\theta-Al_3O_3$ carbochlorinated at 700°C, together with plots of SCM's adjusted to fit the experiment with respect to k_r and D. The experimental conversion points are calculated from the titrations performed throughout the carcochlorination experiment, as presented in subchapter 3.2.3.

Table 22: Results of weighing before and after carbochlorination of $\gamma-, \delta-$ and $\theta-Al_3O_3$ at 700°C

Start Weight [g]	16.8
Al_2O_3 Consumed [g]	14.9
Final Conversion [%]	88.7

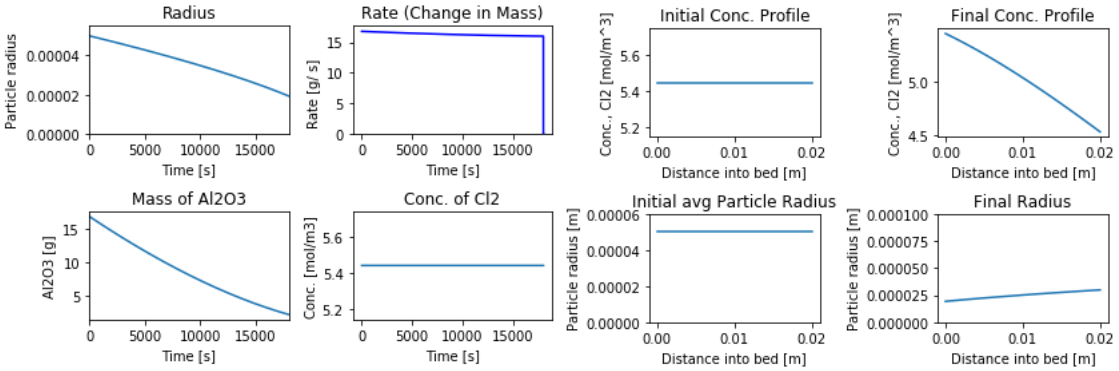

Figure 38: Resulting parameters from the SCM-script for adjusted diffusion coefficient, with respect to time and distance into bed for carbochlorination of 1000°C-calcined alumina at 700°C.

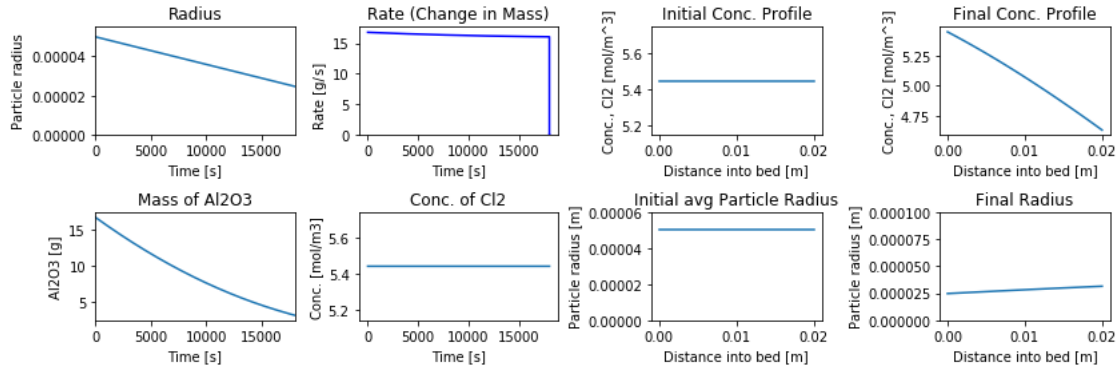

Figure 39: Resulting parameters from the SCM-script for adjusted reaction constant, with respect to time and distance into bed for carbochlorination of 1000°C-calcined alumina at 700°C.

Table 23: Fitted values for diffusion coefficient and reaction constant for carbochlorination of 1000°C-calcined alumina at 700°C, with respective R^2-values for SCM model vs. experimental values.

		R^2 [x100]
D $[m^2/s]$	$1.5 \cdot 10^{-}10$	99.6
k $[m/s]$	$3 \cdot 10^{-}5$	99.2

4.1.8 Experiment 8

The following experiment was conducted at 700°C, using Al_2O_3 calcined at 900°C. The sample contains a mixture of $\gamma-$ and $\delta-$-Al_3O_3. The flow rates of Cl_2 and CO were equal at 50 ml/min.

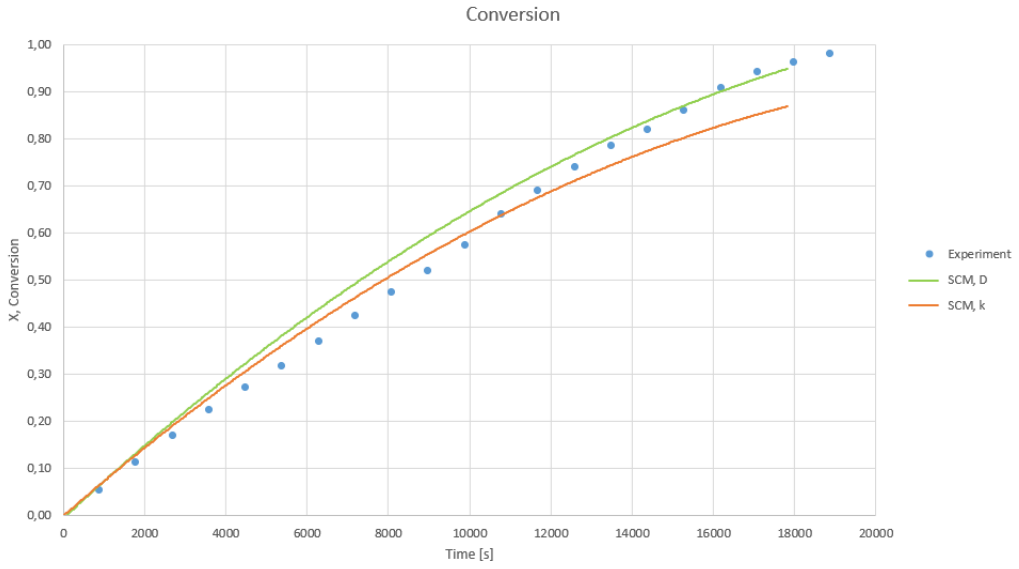

Figure 40: Conversion of $\gamma-$ and $\delta-$-Al_3O_3 carbochlorinated at 700°C, together with plots of SCM's adjusted to fit the experiment with respect to k_r and D. The experimental conversion points are calculated from the titrations performed throughout the carcochlorination experiment, as presented in subchapter 3.2.3.

Table 24: Results of weighing before and after carbochlorination of $\gamma-$ and $\delta-$-Al_3O_3 at 700°C.

Start Weight [g]	15.9
Al_2O_3 Consumed [g]	15.6
Final Conversion [%]	98.1

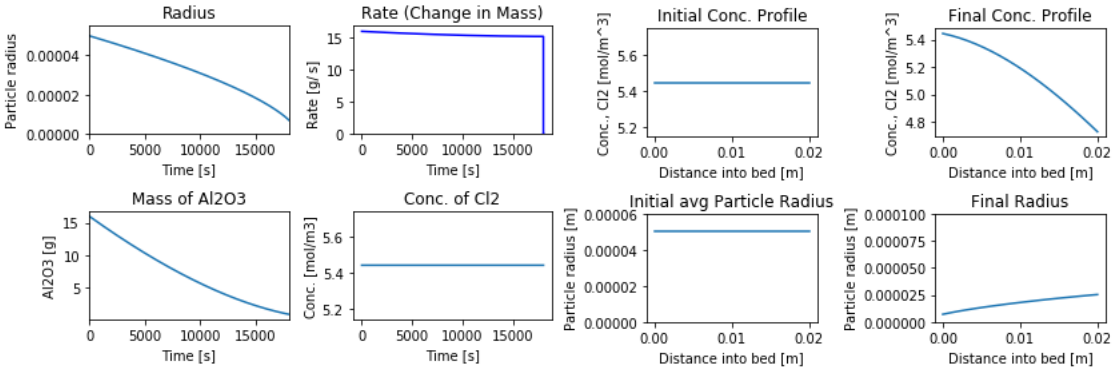

Figure 41: Resulting parameters from the SCM-script for adjusted diffusion coefficient, with respect to time and distance into bed for carbochlorination of 900°C-calcined alumina at 700°C.

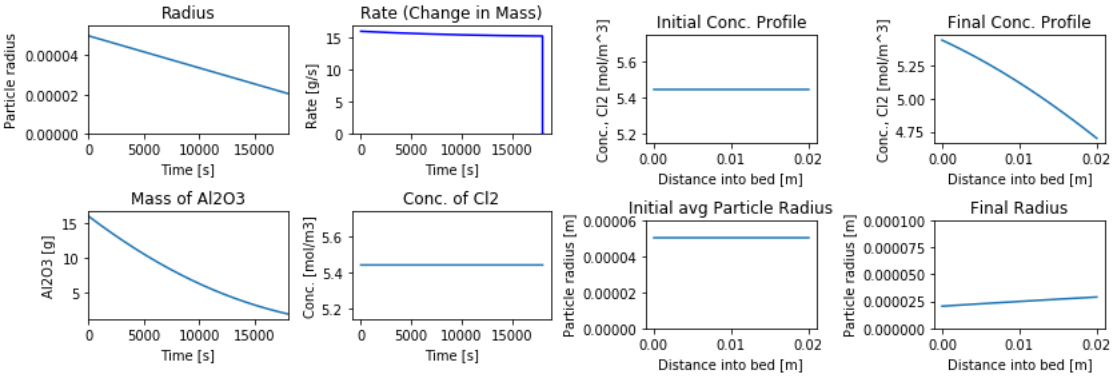

Figure 42: Resulting parameters from the SCM-script for adjusted reaction constant, with respect to time and distance into bed for carbochlorination of 900°C-calcined alumina at 700°C.

Table 25: Fitted values for diffusion coefficient and reaction constant for carbochlorination of 900°C-calcined alumina at 700°C, with respective R^2-values for SCM model vs. experimental values.

		R^2[x100]
D $[m^2/s]$	$2 \cdot 10^{-}10$	99.3
k $[m/s]$	$3.5 \cdot 10^{-}5$	99.1

4.1.9 Experiment 9

The following experiment was conducted at 700°C, using Al_2O_3 calcined at 800°C. The sample contains $\gamma-$-Al_3O_3. The flow rates of Cl_2 and CO were equal at 50 ml/min.

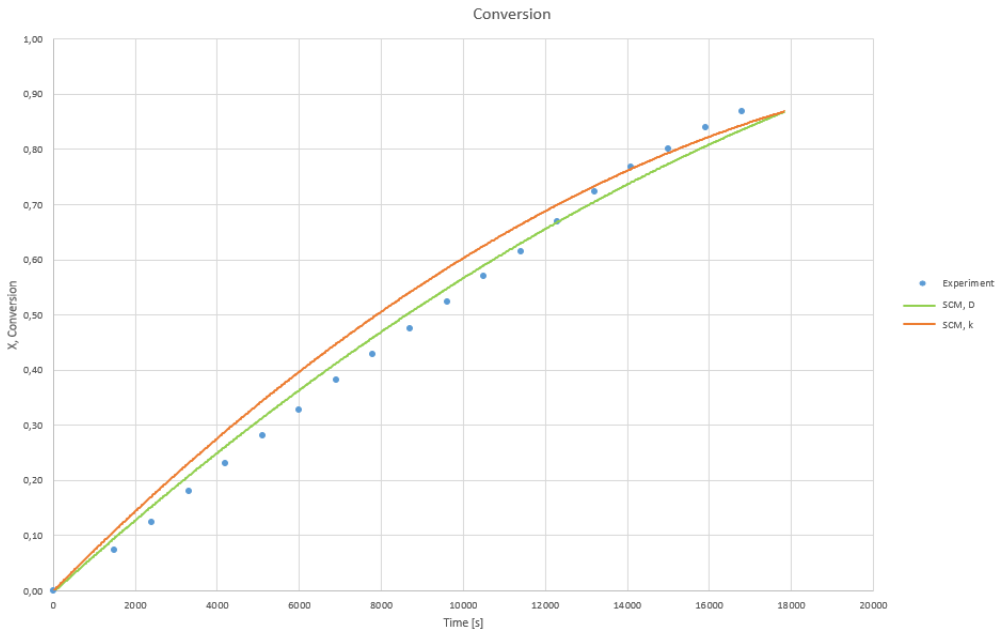

Figure 43: Conversion of $\gamma-$-Al_3O_3 carbochlorinated at 700°C, together with plots of SCM's adjusted to fit the experiment with respect to k_r and D. The experimental conversion points are calculated from the titrations performed throughout the carcochlorination experiment, as presented in subchapter 3.2.3.

Table 26: Results of weighing before and after carbochlorination of $\gamma-$-Al_3O_3 at 700°C.

Start Weight [g]	17.5
Al_2O_3 Consumed [g]	15.2
Final Conversion [%]	86.9

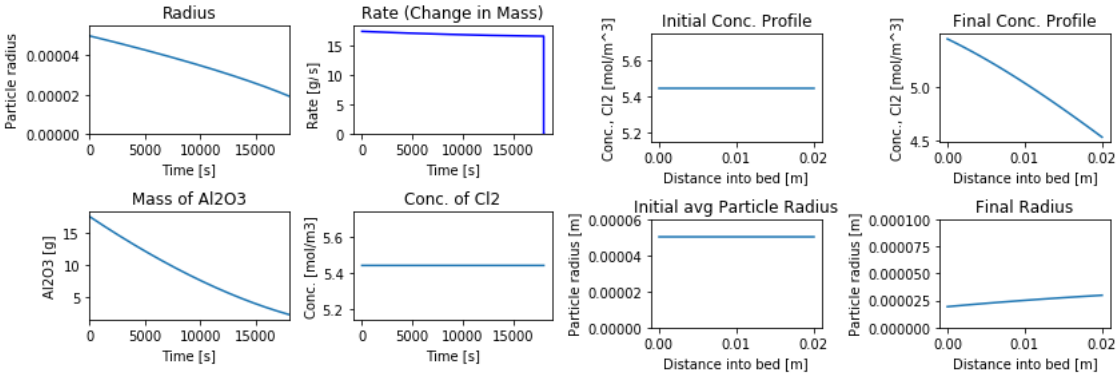

Figure 44: Resulting parameters from the SCM-script for adjusted diffusion coefficient, with respect to time and distance into bed for carbochlorination of 800°C-calcined alumina at 700°C.

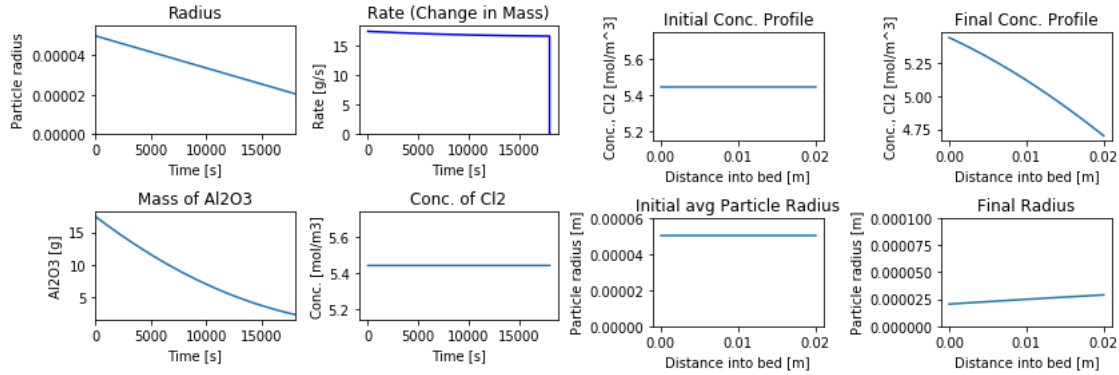

Figure 45: Resulting parameters from the SCM-script for adjusted reaction constant, with respect to time and distance into bed for carbochlorination of 800°C-calcined alumina at 700°C.

Table 27: Fitted values for diffusion coefficient and reaction constant for carbochlorination of 800°C-calcined alumina at 700°C, with respective R^2-values for SCM model vs. experimental values.

		R^2[x100]
D $[m^2/s]$	$1.5 \cdot 10^{-}10$	99.8
k $[m/s]$	$3.5 \cdot 10^{-}5$	99.2

4.1.10 Arrhenius Plot

The Arrhenius plots for Experiments 1 through 5 are presented below. These are presented to display the reaction's variation with respect to temperature, and to observe if there is diffusion- and/or reaction control. The two plots are produced as functions of k_r and D, respectively. Followingly, these values can be used in quantification of the SCM.

Table 28: Values used to produce Arrhenius plot.

T [°C]	1/T [1/K]	k_r	ln(k_r)	D	ln(D)
550	0.00122	0.000026	-10.56	1.3·10−10	-22.76
600	0.00115	0.00004	-10.13	1.8·10−10	-22.44
650	0.00108	0.000024	-10.64	1.0·10−10	-23.03
700	0.00103	0.000025	-10.60	9.0·10−11	-23.13
800	0.00093	0.00004	-10.13	2.2·10−10	-22.24

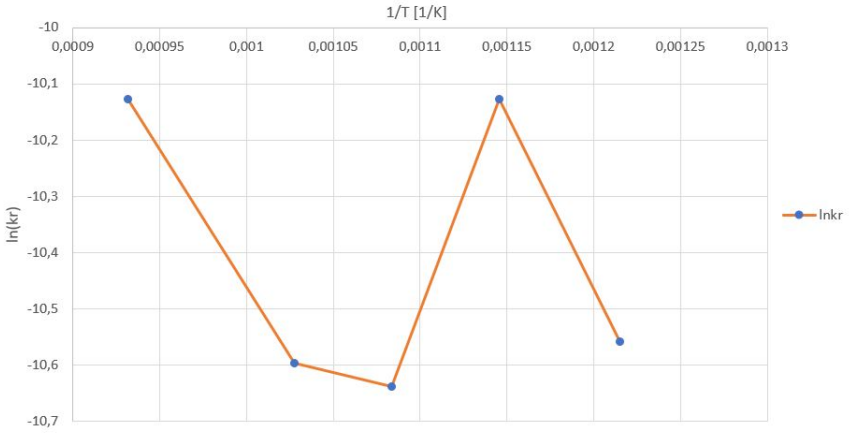

Figure 46: Arrhenius plot for respective values of k_r

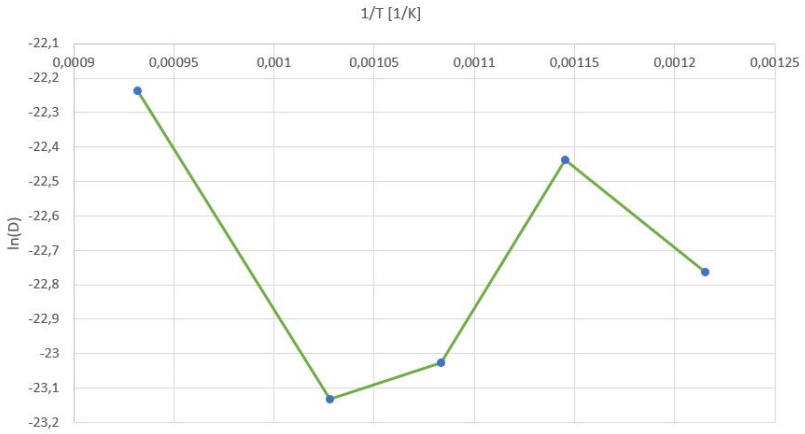

Figure 47: Arrhenius plot for respective values of D

Though ln(k_r) and ln(D) do not demonstrate systematic change with temperature and may not be applicable to separate between diffusion- and reaction control, two separate temperature regions somewhat display increase in ln(k_r) and ln(D) with respect to temperature. Assuming the range 650 - 800 °C accounts for diffusion control, as diffusion control generally occurs at higher temperatures and D's values are quite similar at 650 and 700 °C. The range 550 - 600 °C was assumed to account for reaction control, expressions for the Arrhenius equation may be produced. Using a regression line in the Arrhenius plot for D, for temperatures 650 - 800 °C gave an expression for D as a function of temperature:

$$ln(D) = -5838.1\frac{1}{T} - 16.10 \tag{36}$$

The same was done for k_r within the temperature range 550 - 600 °C:

$$ln(k_r) = -6190.2\frac{1}{T} - 3.04 \tag{37}$$

This gives:

Table 29: Values for reaction coefficient at various temperatures, k_r, and diffusion coefficient, D, calculated from the Arrhenius equations.

T	k_r	D
550	$2.6{\cdot}10^{-5}$	
600	$4{\cdot}10^{-5}$	
650		$1.8{\cdot}10^{-10}$
700		$2.5{\cdot}10^{-10}$
750		$3.4{\cdot}10^{-10}$
800		$4.4{\cdot}10^{-10}$

This way, these values can be used during quantification of the model. Though there is hardly reason to believe the assumptions above, concerning rate control, are valid, this way deviation due to experimental error is avoided in quantification.

4.1.11 Quantification

Following are plots produced from the SCM script, where respective parameters have been quantified to look at their effects on conversion. This is done by adjusting specific parameters for an otherwise equal experiment. For example, increasing and decreasing the particle radius of Al_2O_3 by 50%, at 700 °C and equimolar gas flow. The parameters that are studied are temperature, radius, gas flow ratio and D.

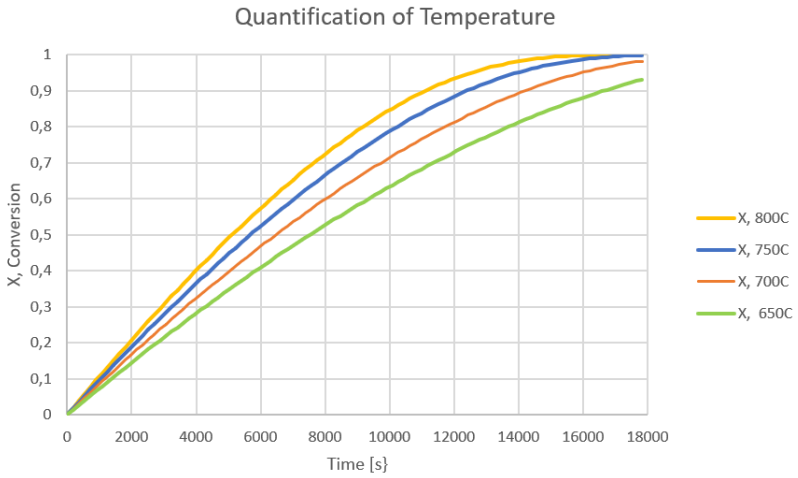

Figure 48: Comparison of conversion with respect to temperature. Here, the plots have been produced with estimated D-values for their respective temperature, from the Arrhenius equation regression line for D (Equation 36

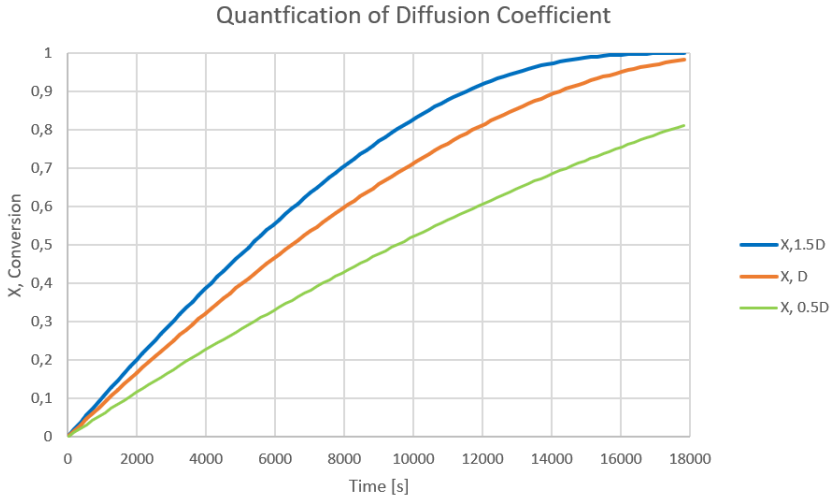

Figure 49: Comparison of conversion with respect to diffusion coefficient. Here, the basis D is $2.53{\cdot}10^{-10}$, as this is the Arrhenius value at T = 700 °C (Table 29), and it is increased/decreased by 50%.

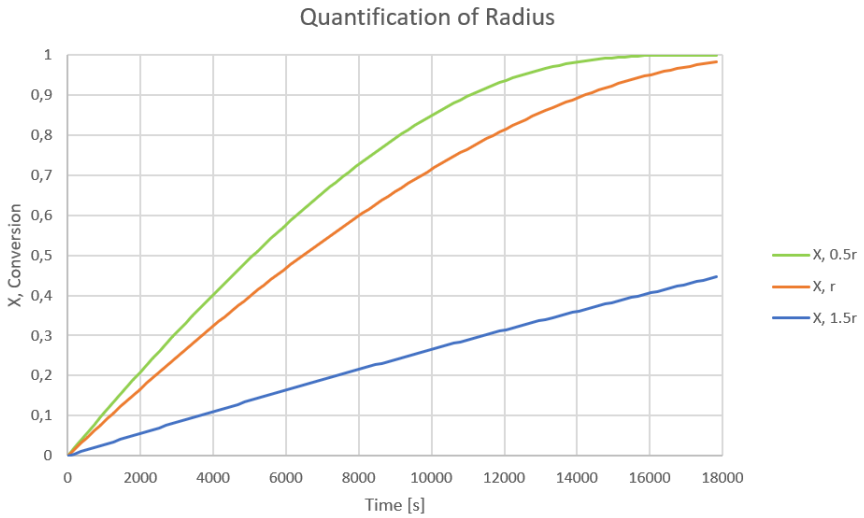

Figure 50: Comparison of conversion with respect to radius. Here, the basis radius is 50 μm and it is increased/decreased by 50%.

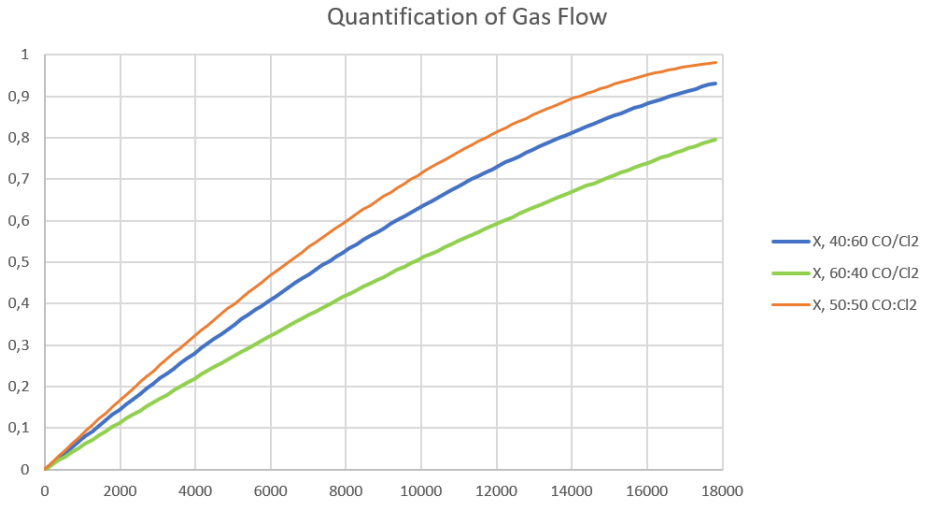

Figure 51: Comparison of conversion with respect to gas flow. The green plot is from the SCM script, adjusted to Experiment 6, whereas the blue plot is from the SCM script at 700 °C with adjusted gasflow and D adjusted for the diffusion of Cl_2 as shown in Equation 35. The orange plot is also from the script, with D = $2.53 \cdot 10^{-10}$. The plots are modelled at T = 700 °C.

Chapter 5

Discussion

5.1 Gas Analysis

A limitation that follows the gas analysis, is that there may have been uncertainties with the titrations, causing inaccurate convertion. As a small amount of titrant was used during titration, the accuracy is quite likely to have been affected. This could have been solved by diluting 1:10 or higher, instead of 1:25. In addition, due to reduced access to equipment, time pressure became a challenge. There were too few volumetric flasks to place samples in. This could have been solved by having an automatic pipette and dispenser for the KI-solution. In addition, the KI-solution should have been acidified to remove a step from the process. However, calculated Cl_2 data (Appendix C) showed that inaccuracy was mostly due to the transition from N_2 to Cl_2 in the pipe from the chlorine flask to the soda wash, as N_2 is passed by the soda wash prior to Cl_2. Furthermore, the concentration profile of Cl_2 shows a kink, and this is caused by the system being blocked by a steel end-piece in the teflon tube, leading to the soda wash (see Figure 17). It was expected that this may corrode, however, not to complete blockage. The gas flow was restarted by cutting the end of the teflon tube.[9]

5.2 Kinetics

As previously mentioned, clogging was a reoccuring issue with the reactor, and was caused by condensation of chloride. The condensation occurred due to the high temperature drop at the gas outlet. Though the clogging occurred less frequently after installing a heat gun, creating a "hot-box", it was not until the calcined Al_2O_3-samples at 800, 900 and 1000 °C were used, an experiment went by without any clogging or leaks. This was because the reaction occurred slower for these samples, than for the SMG-alumina. There could be several factors affecting this result. For instance, this could be due to presence of α-alumina as this reacts slower or not at all. However, the XRD-results do not show α-alumina to be present in these samples. Yet, it is the thermodynamically favorable state of alumina, and though it would be unlikely at room temperature, it may have accumulated over time. Still, it has been confirmed that the SMG-alumina does contain some α-alumina and had a higher reaction rate. This implies that presence of α-alumina is hardly the cause. The slower reaction rate is more likely to be caused by larger particle sizes. As seen from the BET results, the calcined samples at 900 and 1000 °C have smaller surface areas than the SMG-alumina. Assuming uniform particle size distribution, this may imply the particle size is larger for the calcined samples. Thus, slowing down the reaction, as there is less contact between solid and gas. However, large surface areas also imply porous material, meaning that the calcined samples are less porous, thus reacting slower, also due to less interaction with the gas. On the other hand, the sample calcined at 800 °C had a larger surface area than SMG-alumina (Table 1)

and still reacted slower. This was unexpected as it was anticipated that the samples with larger surface areas would result in higher reaction rate. This gives reason to believe that the distribution of particle size is of greater interest than predicted, and should not be assumed uniform. Though high reaction rate is desired, it proved to be beneficial to have it slowed down as this avoided complications with the reactor.

As for the produced $AlCl_3$, it had a yellow color, which implies contamination of $FeCl_3$. Though contaminants are generally undesirable, traces of $FeCl_3$ may not be an issue in this case, as it were $NaAlCl_4$ and $LiAlCl_4$ that proved to be the major sources of solidified impurities found in the Alcoa reactor. This gives reason to believe that some $FeCl_3$ contamination is of less concern than other impurities, but was the only confirmed contaminant in this work. On the other hand, it may be a problem during electrolysis. From Table 5, it appears Fe_2O_3 contamination is present in all samples. However, there may be reason to believe the calcined samples produced during the specialization project do not contain as many impurities. Though, SMG-alumina is also calcined during production, it is calcined at a higher temperature for a short time, compared to the other samples used in this work. Thus, the long calcination process may have affected some of the contaminants. The TGA results may imply that contaminants leave the samples at temperatures above 300 °C, however, this may just be remaining water. For future reference, the produced $AlCl_3$ should be examined for contaminants.

Former studies have proven k to follow the Arrhenius equation for this reaction, and it is evident that both k_r and D are dependent on temperature, which was as expected.[19] [20] However, Experiments 1 through 5, where temperature is increased, k_r and D do not increase for all scenarios. They increase from 550 to 600 °C, have similar respective values for 650 and 700 °C, and increase again for 800 °C. This results in a dip in the Arrhenius plot. A possible explanation for this could be that CO and Cl_2 have formed some phosgene, $COCl_2$, which will decompose above 600 °C. Using phosgene, as opposed to mixed CO and Cl_2, has proven to increase carbochlorination, however, the decomposition will eliminate this effect.[19] Another proposition could be traces of alumina trihydrate transitioning to γ-phase, which is seen in the TGA results for SMG-alumina around 130 min (Figure 14). However, the dip is more likely to be caused by experimental error.

Furthermore, R^2-values for k_r and D appear to be quite similar in some cases, yet D's R^2-value is closer to 1 in every experiment, meaning it fits the experimental results better. Given the model is representative for the reaction, this may mean diffusion is more influential than the reaction at the conditions experiments have been conducted at as the plots adjusted with respect to D fit better with the experiments. On the other hand, k_r may be more influential at lower temperatures, as initially presumed. If k_r were approximated in a similar way to how k_m was, as a function of radius, dynamic viscosity, density, etc., it may have fit better.

The values of k_r ranged from $1.2 \cdot 10^{-5}$ to $4 \cdot 10^{-5} m/s$, whereas D ranged from $9 \cdot 10^{-11}$ to $2.5 \cdot 10^{-10} m^2/s$. These values are not consistent with the reaction constant values presented by Toth, which range from 0.14 to 0.18 s^-1 for the same temperatures.[20] However, Toth approached the mathematical model differently. His reaction constants

have different units, which comes from Toth assuming a different reaction mechanism, the Langmuir-Hinshelwood mechanism. This mechanism differs from the SCM by focusing mainly on the rate at which a gas will adsorb to a surface, whereas the SCM will focus on the rate at which Al_2O_3 shrinks, which would explain the deviation in the reaction constants.[19] However, whether the resulting values for D and k_r are factual remains undetermined, but considering the SCM and the mathematical approach in this work, they fit quite well. Followingly, it is important to determine whether the reaction or diffusion is rate determining. According to both Toth and Landsberg the region of chemical control is at 400 °C and below, and in the temperature range 502 - 605 °C Toth stated pore diffusion and chemical reaction are rate determining, and for 647 °C and above, external mass tranfer is rate controlling. This would explain why D's R^2 values were closer to 1 in experiments conducted at 650 °C and higher.[20] [12] Furthermore, this means that Experiments 1 and 2 (550 and 600 °C, respectively) may have experienced mixed rate control, which could explain why these experiments did not fit as well as the others, as the model adjusted for D and k_r separately.
In observing the conversion plots, it appears that the plots approximated with respect to k_r are more curved than those for D. This would explain why D has the R^2-values closest to 1, as the experimental conversion progresses quite linearly. It would also give reason to believe that diffusion is the rate determining factor for these temperatures. The experimental plots may have displayed a more curved form if titrations were performed more frequently throughout the experiments or if k_r were approached differently, as mentioned. However, the results and literature indicate that diffusion is, in fact, the rate-controlling factor for experiments conducted at 650 °C and above, and that there is mixed control for temperatures below.

Furthermore, it was observed that the conversion was affected by the gas flow. As seen in Experiment 6, where the gas consisted of a 40:60 ratio for Cl_2 and CO, respectively. This experiment provided high conversion, especially in comparison to Experiment 4, which was conducted at the same temperature, but with equimolar gas flow of Cl_2 and CO. With that in mind, there is reason to believe that Experiment 4 should have provided higher conversion than it did. This allegation is based on literature on the same reaction and the fact that this was one of the first experiments that was conducted and was, therefore, exposed to more complications with the reactor and arguably terminated prematurely.[12] [20] With that said, Experiment 6 does have a higher rate, giving reason to believe that gas flow ratio does, indeed, affect the kinetics of the reaction. However, with doubts surrounding Experiment 4 it is difficult to draw any conclusions. In looking at the SCM results, however, it appears an excess of Cl_2 is more favourable to an excess of CO (Figure 51). This result is also presented by Toth.[20] This is most likely due to the diffusion of Cl_2 having a larger impact on the reactivity than CO, as Cl_2 is a heavier gas and will therefore have more difficulty accessing and diffusing through the material. In addition, the carbochlorination reaction requires equal amounts of both molecules, and as Cl_2 has more trouble reaching the site of reaction, it is beneficial to have an excess of Cl_2. Though such an experiment was not conducted in this work, it is recommended to conduct for future reference.

All in all, most experiments were quite successful in regards to conversion. The worst outcome was Experiment 4

with equimolar ratio of Cl_2 and CO at 700°, resulting in a conversion of 53%. As mentioned, there is reason to believe the low conversion is mainly caused by this being one of the first experiments conducted, and that if the same experiment was re-done the conversion would be higher. With this in mind, Experiment 4's values for k_r and D should be higher, which explains why the Arrhenius plot for ln(D) does not steadily increase from 650 to 800 °C. However, the Arrhenius plots do not demonstrate the systematic change in k_r or D with respect to temperature that was expected for other experiments as well. This outcome is unfortunate, as these plots will not be adequate in supporting the claims separating between diffusion- and reaction controlled rate. The lack of systematic change in the plots could be caused by faulty values for k_r and D, as assumed for Experiment 4, or it may be the reaction does not follow apparent Arrhenius behavior. Conclusions regarding rate control are, therefore, based on how well the SCM fits the experimental results when adjusted for k_r or D, and literature on the reaction.

5.3 Model Fitting

All in all, the SCM curves proved to fit well with the experiments, with R^2-values ranging from 0.968 to 0.999. However, the experimental conversions had a, generally, more linear progression than the SCM. In some cases, for example Experiment 8 in Figure 42, among others, the model fits well for the most part, but at high conversion the SCM plot starts to curve more, whereas the experimental plot keeps steadily increasing. As the model assumes spherical particles and conversion is defined with respect to volume, the conversion is a function of r^3, curving the plot. This means that assuming spherical particles may be far-fetched for some cases. Furthermore, the model also assumes equal bulk density throughout the experiment, which is inaccurate as the bed should become more porous with time. Another factor that may affect the accuracy of the model is a gas channels forming. It should also be noted that the R^2-values are only calculated from around 20 points, equal to the amount of titrations, and could, therefore, be more accurate if more titrations were performed.

It should also be noted that for Experiment 4, the experimental final conversion largely deviates from the SCM. This is because the model fit well throughout the reaction, and there is reason to believe the experiment was prematurely terminated, as mentioned above. If the reaction was kept running for longer, the final conversions may have been similar.

As the SCM is a merely a mathematical prediction of how the reaction progresses and does not account for experimental mistakes, such as the reactor clogging or leaking, some variance was expected. The more unexpected outcome was the dip in the Arrhenius plot, as it was initially believed that k would increase with temperature. However, that is given the model fits. This result may imply that the SCM is not the case for the carbochlorination reaction. This could mean that if the dip in the Arrhenius plot is not caused by something else, like phosgene disassociating and/or transitioning to γ-alumina, the SCM may not be a representative model for the carbochlorination of alumina. That being said, the experiments that the model was the least suitable for were Experiments 1 and 2, and the dip is most

likely caused by experimental complication. As these were the "outliers" in the Arrhenius plot, there is reason to believe that the reaction does follow the SCM, but at temperatures above 600 °C, or, more likely, the rate control is mixed. Another explanation could be the fact that k_r was not calculated the same way k_m was, as mentioned above. It should also be mentioned that conversion is generally quite high, which may be a contributing factor in making it difficult to accurately adjust D and k_r, thus producing an unexpected Arrhenius plot. Furthermore, the model also assumes uniform particle size, which will affect how well it fits with the experiments, as there will be variations in particle size within a sample.

Furthermore, the resulting SCM plots for mass and radius with respect to time appear to reduce in well accordance with the conversion. As for the radius change with respect to distance into bed, there appears to be some flaws with the model. As seen in Figure 24, for example, the bed height should fall more throughout the experiment, and the figure shows that there are particles present in the whole bed. This may have been solved by using smaller time steps as this increases the accuracy of the mass balance. However, that will cause quite a long run-time for the script. Furthermore, the initial concentration profiles generally demonstrate that the whole bed is filled with Cl_2, which is not realistic. The reason for this result is most likely because the model assumes no Cl_2 has reacted at this point. It should also be mentioned that the bed height is larger than 2 cm in reality, which it is defined as in the script. This height will naturally vary with respect to starting mass of alumina. The bed height is defined this way as a simplification with regard to varying mass and the demonstration of the reaction outcome, by only focusing on the first 2 cm. Apart from these flaws, the model appears to demonstrate the reaction outcome quite well, and there is reason to believe that the carbochlorination reaction of Al_2O_3 does follow the shrinking-core model.

5.4 Quantification

In the quantification plots in subchapter 4.1.11, the model's sensitivity to changes in temperature, gas flow, D and radius was studied. It appears that changes in particle radius is especially effective in the SCM. Through increasing radius by 50% the final conversion also decreased by 50%, approximately. By decreasing the radius by 50% the conversion is also quite altered, though not to the same extent. Given the model fits, this means the reaction is highly sensitive to large particle sizes, and these should be avoided for high reaction rate. Furthermore, by adjusting the gas flow ratio it appears an excess of Cl_2 is superior to an excess of CO in regards to reaction rate, which is in accordance with previous studies on the same reaction.[20] However, the model demonstrates that an excess of Cl_2 does not lead to higher conversion than with an equimolar ratio. Whether this is factual is difficult to determine without having conducted an experiment with excess of Cl_2, but gives reason to attempt such an experiment. According to Toth, the maximum reaction rate is provided by excess of Cl_2 and is justified by the difference in diffusivities of these gases.[20] As for the model's sensitivity to temperature, the reaction rate increases with temperature, as mentioned, and provides similar final conversions for 700 °C and higher. As for sensitivity to D, 50%-adjustments are quite

influential, considering a 50% decrease caused a nearly 20% drop in conversion. All in all, the quantification results demonstrate that in order to maximize the conversion and reaction rate, particle radius should be optimized. Whereas temperature has been studied in this work, gas flow adjustments will also be significant in optimization of rate and conversion, and should be further studied.

Chapter 6

Conclusion and Recommendations

All in all, the results provide reason to believe the reaction does, indeed, follow the SCM. This is based on the fact that the experimental conversion fit quite well for most experiments. However, for future reference the model should be adjusted to account for particle size distribution, which should be experimentally determined prior to carbochlorination. As the model demonstrated, the reaction is highly sensitive to particle size of Al_2O_3, making it a priority to optimize this parameter in the future.

It also believed that the reaction rate is controlled by diffusion within the temperature range 650 - 800 °C, based on previous publications on the same reaction, and the fact that the model fit better when adjusted with respect to the diffusion coefficient. Furthermore, it is assumed the reaction rate is controlled by diffusion and reaction within the temperature range 550 - 600 °C. As for the mixed control regime, this is also justified by the literature, and the fact that the model did not fit as well for these experiments when adjusted for k_r and D alone. For future reference, this should be studied further, as the reaction did not demonstrate systematic change with respect to temperature for the Arrhenius plots. This could be due to experimental errors, or the reaction may not experience Arrhenius behavior. In the future, k_r and D should be attempted to be expressed differently, i.e. not with the Arrhenius equation, as this may provide different results.

As for alumina quality, it may be recommended to use calcined ATH, as opposed to SMG-alumina. This is due to the supposition of less α-alumina content. These samples also have larger particle sizes and fewer impurities, decreasing complications with the reactor. Considering the fate of Alcoa's reactor, this should be a priority. Not only will it be safer, but it will also aid in keeping the process running without interruptions. On the other hand, the reasoning behind the lack of complications with the reactor come from decreasing the reaction rate. As high reaction rate is desirable, SMG-alumina is beneficial in this regard. Therefore, another proposition is to use SMG-alumina for high reaction rate and re-evaluate the reactor design. Furthermore, the reactor design will differ on a larger scale, meaning the complications with the reactor that occurred in this work may not be of concern. All in all, which sample to use will depend on the design of the potential large-scale reactor, and if it is more sensitive to presence of α-Al_2O_3 or reaction rate. This leads to the conclusion that for the system used in this work, calcined ATH is the recommended Al-source, but SMG-Al_2O_3 may be superior in a different set-up due to its higher reaction rate.

Gas composition is also believed to have an affect on the reactivity, and that an excess of CO may be beneficial as it

resulted in high conversion of Al_2O_3 (94.9%). In the future, it is recommended to conduct experiments with Cl_2 in excess as well, as previous publications state that this provides the highest conversion of Al_2O_3.[19]

Furthermore, in the future a second model, considering a second order reaction should be considered to confirm whether the reaction is of first order or not. To verify ranges of temperature where reaction and/or diffusion is rate-controlling, the reaction is recommended to be tested with a catalyst and, as mentioned above, adjustments to pressure.

References

[1] Gahan Blackman. *SI Chemical Data, 7th Edition*. Wiley, 2014.

[2] M. E. Brown. *Introduction to Thermal Analysis: Techniques and Application, Second Edition*. Springer, 2007.

[3] C. Vinod Chandran. Alumina: discriminative analysis using 3D correlation of solid-state NMR parameters. *Royal Society of Chemistry*, 48:134–149, 2019.

[4] Raymond Chang and Kenneth A. Goldsby. *General Chemistry, The Essential Concepts, 7th Edition*. McGraw Hill, 2014.

[5] H. Wayne Cotten. *The Alcoa Smelting Process at Anderson County Texas*. 2018.

[6] Element. *ICP Analysis Laboratories– ICP-MS, ICP-AES, ICP-OES*, 2019. `https://www.element.com/materials-testing-services/chemical-analysis-labs/icp-analysis-laboratories\%E2\%80\%93-icp-ms,-icp-aes,-icp-oes` (accessed 06.12.2019).

[7] B. L. Dutrow. et al. *X-ray Powder Diffraction (XRD)*, 2019. `https://serc.carleton.edu/research_education/geochemsheets/techniques/XRD.html` (accessed 06.12.2019).

[8] H. Scott Fogler. *Elements of Chemical Reaction Engineering, 5th Edition*. Pearson, 2016.

[9] Bjørnar Gjesdal. Memo - Chlorine Adsorption in Lye. 2020.

[10] Nina Hwang and Andrew R. Barron. *Physical Methods in Chemistry and Nano Science*. Pavan M. V. Raja, Andrew R. Barron, 2009.

[11] C. Misra K. Wefers. Oxides and Hydroxides of Aluminium Alcoa Technical Paper N19. *Aluminium Company of America Pittsburgh, PA*, 1987.

[12] A. Landsberg. Chlorination Kinetics of Aluminum Bearing Minerals. *Metallurgical Transactions B*, 6B, 1975.

[13] Octave Levenspiel. *Chemical Reaction Engineering, 2nd Edition*. Prentice Hall, 2017.

[14] I. Levin and D. Brandon. Metastable Alumina Polymorphs: Crystal Structures and Transition Sequences. *Journal of the American Ceramic Society*, 81:1995–2012, 1998.

[15] Kristiane Melingen. Literature Study on the Carbochlorination of Alumina. *NTNU: Department of Materials Science and Engineering*, 2019.

[16] Kristiane Melingen. Specialization Project: Characterization of Alumina for a Carbochlorination Process. 2019.

[17] Microsoft. *RSQ function*, 2020. https://support.microsoft.com/en-us/office/rsq-function-d7161715-250d-4a01-b80d-a8364f2be08f (accessed 02.07.2020).

[18] Christian Rosenkilde. Is Revisiting the Alcoa Chloride Process Worthwile? *Hydro*, 2019.

[19] A. Toth. Kinetics of gamma-Alumina Chlorination by Phosgene. *Budapest: Research Laboratory for Inorganic Chemistry of the Hungarian Academy of Sciences*, 1980.

[20] A. Toth. Kinetics of Gamma-Alumina Chlorination by Carbon Monoxide and Chlorine. *Budapest: Research Laboratory for Inorganic Chemistry of the Hungarian Academy of Sciences*, 1981.

[21] Raboud University. *ICP-MS*, 2019. https://www.ru.nl/science/gi/facilities-activities/elemental-analysis/icp-ms/ (accessed 16.12.2019).

[22] et. al. V. Safari, G. Arzpeyma. A shrinking Particle—Shrinking Core Model for Leaching of a Zinc Ore Containing Silica. *Elsevier*, 2009.

[23] Bjarte Øye. Carbochlorination routes in production of Al. *FME HighEFF*, 2018.

Appendix

A: SCM Script

```
import time
import numpy as np
import matplotlib.pyplot as plt
start = time.time ()
"""
Input :
"""
#shrinking core model
T0 = 700 #C  bulk gas temperature
T0_K = T0 + 273.15 #K, temp conversion
P_CO_atm_b = 0.5 #atm  bulk partial pressure of O2-->CO
P_Cl_atm_c = 0.5 #atm  bulk partial pressure of O2--> Cl2
D = 100000 #m^2/ s diffusion coefficient of the binary pair CO-Cl2, adjusted to fit
r_0 = 0.00005 #m initial particle radius
MW_Cl2 = 70.9 # molar mass of Cl2 [g/mol]
MW_CO = 28 #molar mass of CO [g/mol]
MW_gas = (MW_Cl2*P_Cl_atm_c) + (MW_CO*P_CO_atm_b) #molar weight of bulk gas [g/mol]

#height model parameters
gasflowCl2 = 50*(10**-6)  # gas flow of Cl2 [m3/min] @ 298K
gasflowCO  = 50*(10**-6)  # gas flow of CO [m3/min] @ 298K
Tube_d = 0.02        # tube diameter [m]
bed_h  = 0.02       # height of bed [m]

# constants :
R = 8.3145 # universal gas constant [m3*Pa/K/ mol]
phi_Al2O3 = 9807.77 # molar density of Al2O3 [mol/m3]
MW_Al2O3 = 101.96 # molar mass of Al2O3 g/ mol
rho_Al2O3 = 3950000    # density of Al2O3 [g/m^3]
rho_bulk  = 1000000        # density of bulk [g/m^3]
# Physical properties
Mu  = 2.75E-4                 # Dynamic viscosity [Pa s]
rho_Cl2 = 0.890E3            # Density of Cl2 [g/m^3]
Nu  = Mu/rho_Cl2              # Kinematic Viscosity [m^2/s]

# Al2O3 + 3CO + 3Cl2 = 2AlCl3 + 3CO2:
```

```
37
38 #rate constant parameter
39 k_r = 0.000025 #reaction constant [m/s], adjusted to fit
40
41 #height- and time steps
42 dt = 0.01       # [s]
43 zsteps = 20 #
44 timesteps = 1800000
45 dz = bed_h/zsteps #[m]
46
47 #conversion vectors
48 m_Al2O3 = np.zeros((timesteps,zsteps))  #mass Al2O3 [g]
49 m_Al2O3[0,0]= 20
50 n_Al2O3= np.zeros((timesteps,zsteps)) #moles Al2O3
51 n_Al2O3[0,:] = (m_Al2O3[0]/MW_Al2O3)
52 V_Al2O3 = np.zeros((timesteps,zsteps)) #Volume [m3]
53 dw_dt = np.zeros((timesteps,zsteps))  #rate [g/s]
54 A = np.zeros((timesteps,zsteps))#[None for i in range (t+1)]
55 A[0,:] = 4*np.pi*(r_0**2) #surface area of sphere
56 n_part = ((4/3) *( np . pi ) * r_0 **3)*phi_Al2O3  #moles per particle
57 part = n_Al2O3[0,0]/n_part #amount of particles
58 V_Al2O3[0,:] = part*((4/3) *( np . pi ) * r_0 **3)
59 X = np.zeros((timesteps)) #Conversion
60
61 #Calculate gas velocity
62 gasflowT = gasflowCl2*(T0_K)/298 + gasflowCO*(T0_K)/298 #m3/min
63 gas_v    = gasflowT/60/(np.pi*Tube_d**2./4) #m/s
64
65 # Numerical solution of differential equations.
66 # For each timestep the concentration profile is calculated using average particle radius at
       begining of timestep.
67 # The concentration is then used to calculate the reduction in particle size in each node along
       the bed.
68
69 #particle concentration, bulk density/particle weight
70 conc_p = rho_bulk/ (4*np.pi*rho_Al2O3*r_0**3/3) #[#/m^3]
71 # Upstream chlorine concentration
72 conc_Cl2 = 1.1013E5*0.4/R/(T0_K)
73
74 c = np.zeros((timesteps,zsteps))   #Concentration, one row for each timestep and one column for
       each z node
75 rad = np.zeros((timesteps,zsteps))   #Radius, one row for each timestep and one column for each z
```

```
     node
t_step = np.zeros(timesteps)            #Timesteps
z = np.linspace(0,bed_h,zsteps)
rad[0,:] = r_0                         #Put radius equal to r0 at time = 0 along the whole bed.
c[:,0] = conc_Cl2                   #Concentration at top of bed equal to upstream conc. at all
    times.



#Calculates initial conc. profile along the bed. t = 0
for j in range(1,zsteps):
    c[0,j] = (c[0,j-1]/(1+conc_p/gas_v*4*np.pi*rad[0,j]**2*((2+0.6*((gas_v*2*rad[0,j]*rho_Cl2)/Mu
    )**(0.5)*(Nu/D)**(0.33))*D/2/rad[0,j])*dz))
for l in range(0, timesteps):
    X[l] = 0
#Loops over all nodes in bed.
    for j in range(0,zsteps):
        if rad[l-1,j] > 0: #
            k = 1/(1/((2+0.6*((gas_v*2*rad[l-1,j]*rho_Cl2)/Mu)**(0.5)*(Nu/D)**(0.33))*D/2/rad[l
    -1,j]) + 1/k_r)
            if j>0 :
                c[l,j] = (c[l,j-1]/(1+conc_p/gas_v*4*np.pi*rad[l-1,j]**2*k*dz))
            rad[l,j] = (rad[l-1,j] -  MW_Al2O3/rho_Al2O3/3*k*c[l,j]*dt)
        else:
            c[l,j] = conc_Cl2
        A[l,j]=4*np.pi*(rad[l,j]**2)
        X[l] = X[l] + (1 - ((rad[l,j])**3)/r_0**3)/zsteps
        m_Al2O3[l-1,j] = m_Al2O3[0,0]*(1-(X[l]))
        n_Al2O3[l,j] = (m_Al2O3[l-1,j])/MW_Al2O3
        V_Al2O3[l,j]=part*((4/3) *( np . pi ) * (rad[l,j]) **3)
        dw_dt[l-1,j] = (m_Al2O3[l-1,j]-m_Al2O3[l,j])/dt
        if dw_dt[l-1,j] < 0:
            dw_dt[l-1,j] ==0
        if rad[l,j] <= 0:
             rad[l,j] == 0
             V_Al2O3[l,j] == 0 # avoids invalid values
    t_step[l] = t_step[l-1] + dt



fig,b =  plt.subplots(2,2)
plt.subplots_adjust( wspace=0.5, hspace=0.5)
```

```
114
115 b[0][0].plot(t_step, rad[:,0])
116 b[0][0].set_title('Radius')
117 b[0][0].set_ylabel('Particle radius')
118 b[0][0].set_xlabel('Time [s]')
119 b[0][0].set( ylim=(0, 0.000055))
120 b[0][0].set( xlim=(0,timesteps*dt))
121
122
123 b[0][1].plot( t_step, np.array(dw_dt[:,0]) , 'b')
124 b[0][1].set_title('Rate (Change in Mass)')
125 b[0][1].set_ylabel('Rate [g/0.001s]')
126 b[0][1].set_xlabel('Time [s]')
127 b[0][1].set(ylim=0)
128
129 b[1][0].plot( t_step, m_Al2O3[:,zsteps-1])
130 b[1][0].set_title('Mass of Al2O3')
131 b[1][0].set_ylabel('Al2O3 [g]')
132 b[1][0].set_xlabel('Time [s]')
133 b[1][0].set( xlim=(0, timesteps*dt-1))
134
135
136 b[1][1].plot( t_step , c[:,0])
137 b[1][1].set_title('Conc. of Cl2')
138 b[1][1].set_ylabel('Conc. [mol/m3]')
139 b[1][1].set_xlabel('Time [s]')
140
141 #experimental regression plots, with respective start-values for time
142 ex1 = -2*(10**-10)*t_step**2 + 5.5*(10**-5)*t_step - 0.0055 #t_step-90
143 ex2 = -1*(10**-10)*t_step**2 + 6.1*(10**-5)*t_step - 0.018 #t_step-200
144 ex3 =-4*(10**-10)*t_step**2 + 5.1*(10**-5)*t_step - 0.0573 #t_step-1100
145 ex4 = -2*(10**-10)*t_step**2 + (4.6*10**-5)*t_step - 0.0253 #t_step-450
146 ex5 = -7*(10**-10)*t_step**2 + (6.7*10**-5)*t_step - 0.0313 #t_step-400
147 ex6 = -6*(10**-10)*t_step**2 + 6.3*(10**-5)*t_step - 0.3179 #t_step-5200
148 ex7 = -5*(10**-10)*t_step**2 + 6*(10**-5)*t_step + 0.001
149 ex8 = -7*(10**-10)*t_step**2 + 7*(10**-5)*t_step + 0.0124 #t_step-1800
150 ex9 = -4*(10**-10)*t_step**2 + 6*(10**-5)*t_step -0.0112 #t_step-100
151
152 ex = ex1 #insert which experimental conversion to plot here, for example ex1 for experiment 1
153
154 X_2 = X[0::18000] #list of every 18000th value for X
155
```

```
with open('doc.txt', 'w') as f: #prints out X_2 in a .txt file
    for item in X_2:
        f.write("%s\n" % item)



plt.tight_layout()
plt.show()

fig = plt.figure()
plt.plot(t_step , X[:], 'b', label = 'SCM')
plt.plot(t_step, ex, 'g', label='Experiment')
plt.xlabel('Time [s]') #time (s)
plt.ylabel('Conversion, X')
plt.title('Conversion wrt time')
plt.ylim(0,1)
plt.xlim(0)
plt.legend(loc='best')
P = format(( time.time() - start ) )



fig,a =  plt.subplots(2,2)
plt.subplots_adjust( wspace=0.5, hspace=0.5)

a[0][0].plot(z,c[0,:])
a[0][0].set_title('Initial Conc. Profile')
a[0][0].set_ylabel('Conc., Cl2 [mol/m^3]')
a[0][0].set_xlabel('Distance into bed [m]')


a[0][1].plot(z,c[timesteps-1,:])
a[0][1].set_title('Final Conc. Profile')
a[0][1].set_ylabel('Conc., Cl2 [mol/m^3]')
a[0][1].set_xlabel('Distance into bed [m]')


a[1][0].plot(z,rad[0,:])
a[1][0].set_title('Initial avg Particle Radius')
a[1][0].set_ylabel('Particle radius [m]')
a[1][0].set_xlabel('Distance into bed [m]')
a[1][0].set( ylim=(0, 0.00006))
```

```
198
199
200 a[1][1].plot(z,rad[timesteps-1,:])
201 a[1][1].set_title('Final Radius')
202 a[1][1].set_ylabel('Particle radius [m]')
203 a[1][1].set_xlabel('Distance into bed [m]')
204 a[1][1].set( ylim=(0, 0.0001))
205 plt.tight_layout()
206 plt.show()
```

B: XRD

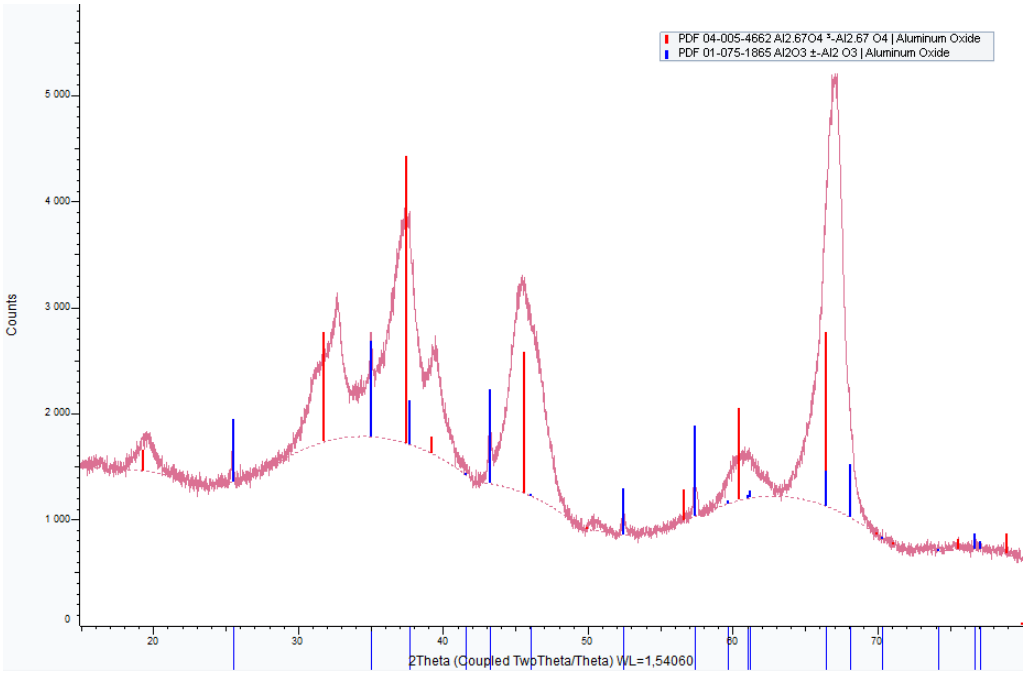

Figure 52: Diffractogram of SMG-alumia. Blue corresponds to alpha and red corresponds to gamma.

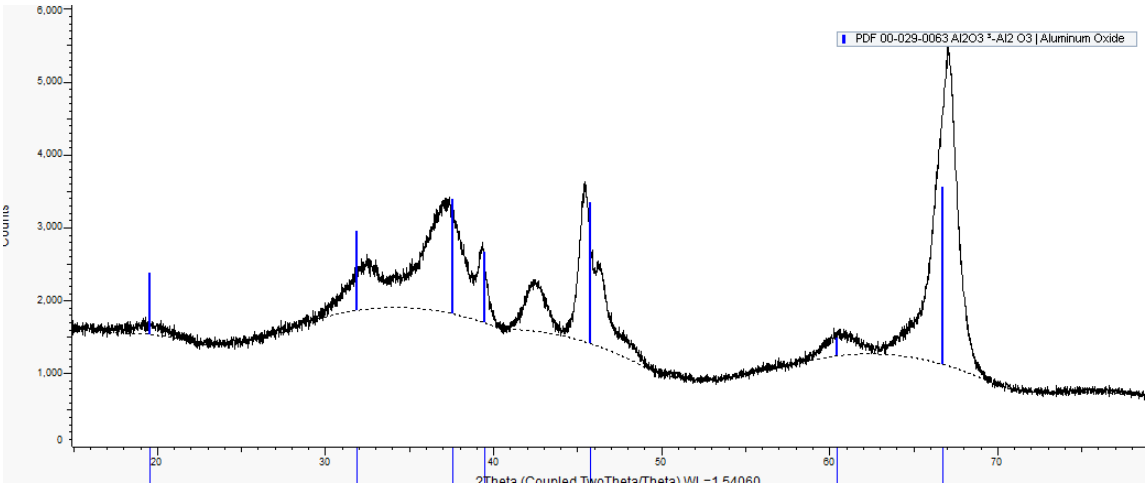

Figure 53: Diffractogram of sample 800. Blue corresponds to gamma.

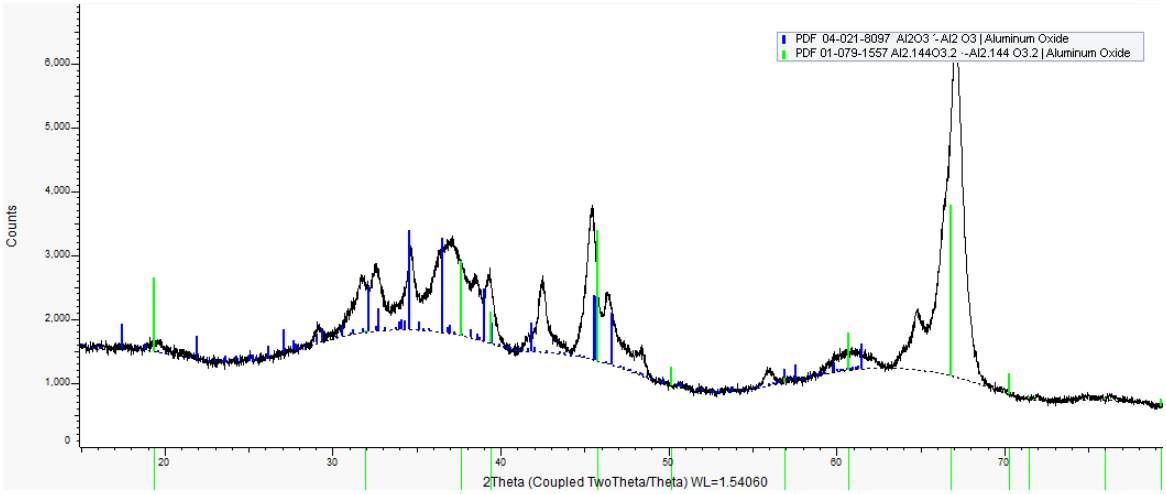

Figure 54: Diffractogram of sample 900. Blue corresponds to delta and green corresponds to gamma.

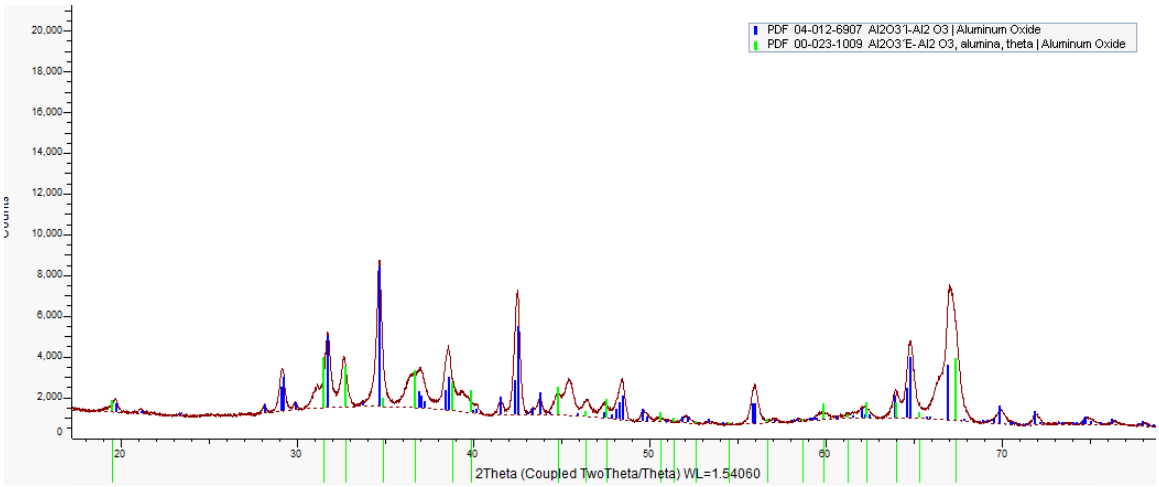

Figure 55: Diffractogram of sample 1000. Blue corresponds to delta and green corresponds to theta.

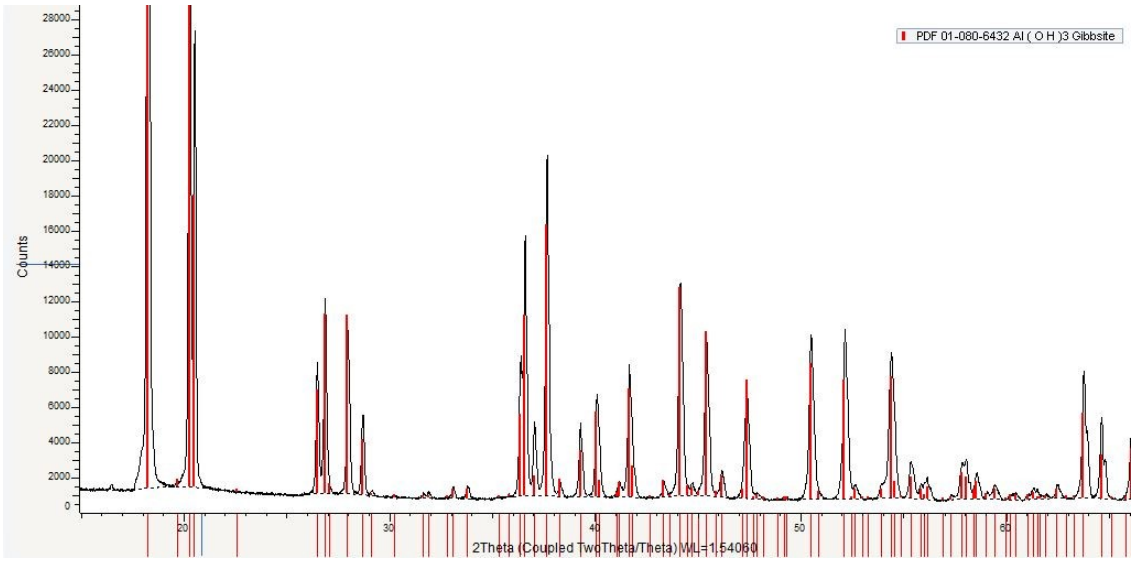

Figure 56: Diffractogram of sample ATH. Red corresponds gibbsite.

C: Chlorine, Pressure and Flow Plots

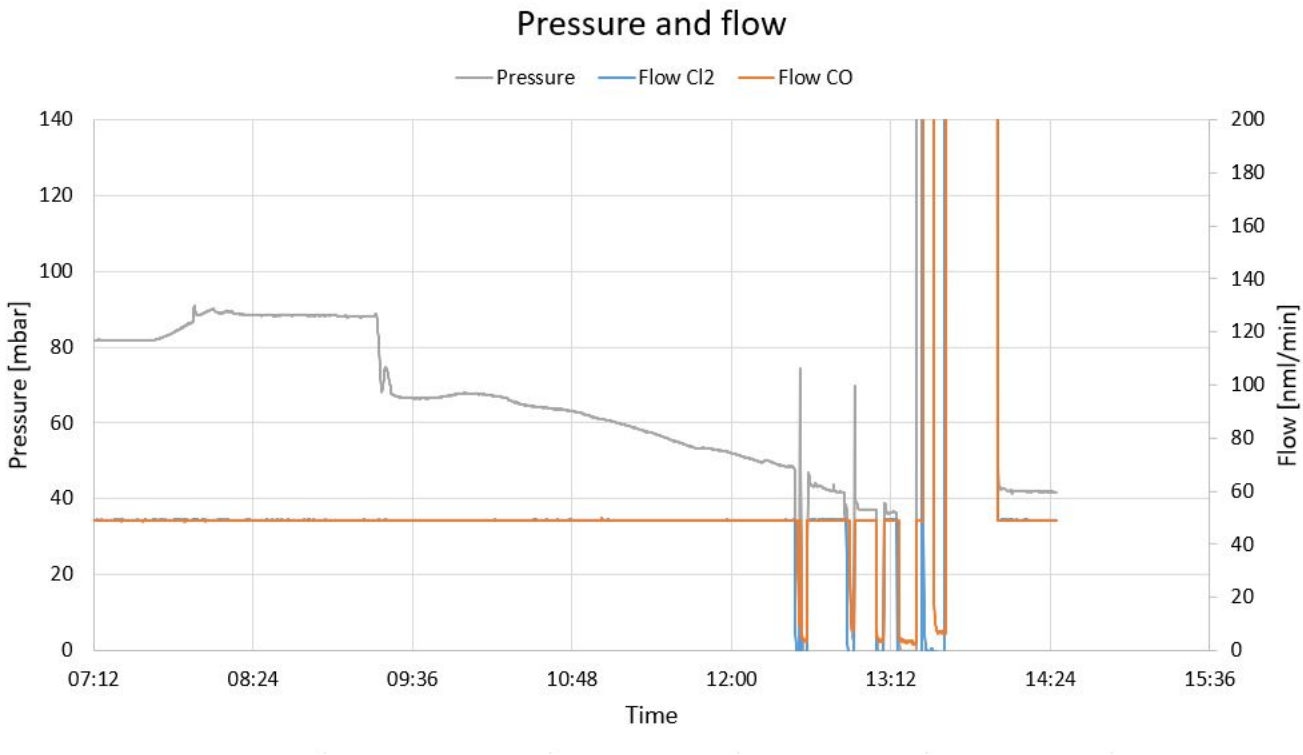

Figure 57: Pressure and flow plot for Experiment 1.

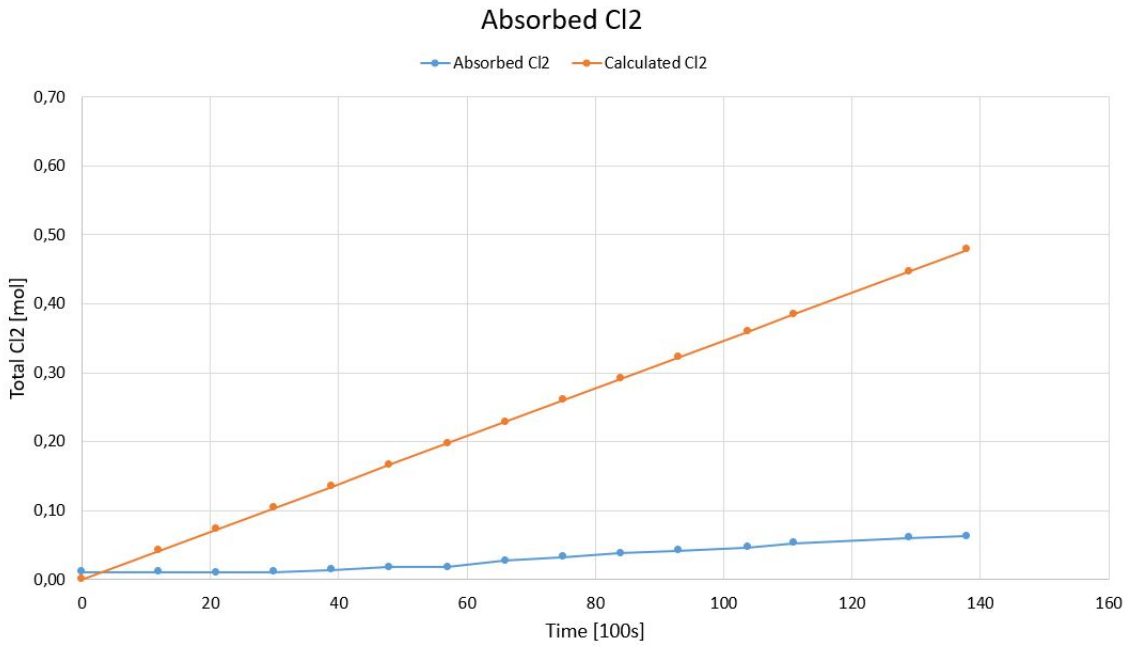

Figure 58: Cl_2 levels during carbochlorination of SMG Al_2O_3 at 550°C. Calculated Cl_2 is the total amount of Cl_2 that enters the inlet, whereas the absorbed Cl_2 is the Cl_2 that exits the outlet and has not reacted with Al_2O_3.

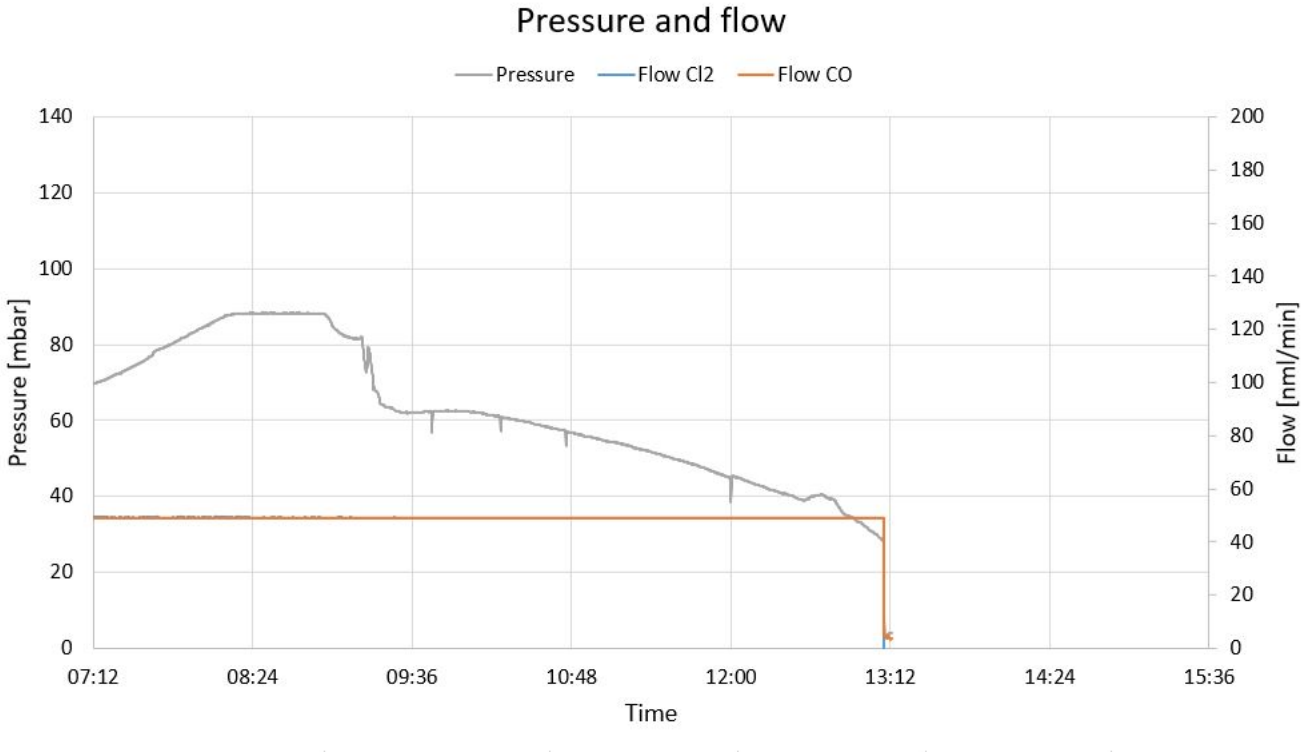

Figure 59: Pressure and flow plot for Experiment 2.

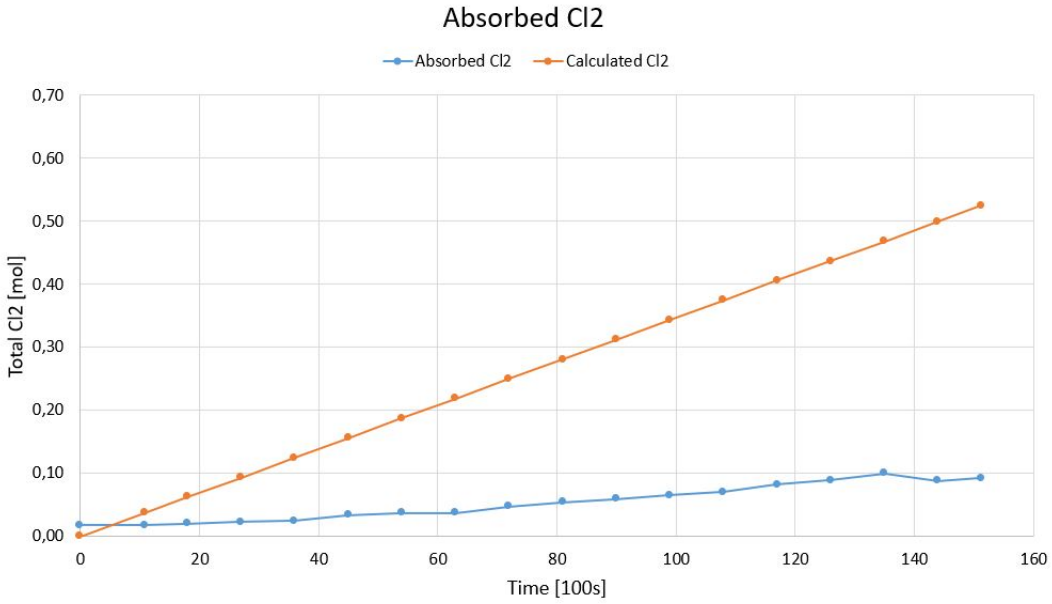

Figure 60: Cl_2 levels during carbochlorination of SMG Al_2O_3 at 600°C. Calculated Cl_2 is the total amount of Cl_2 that enters the inlet, whereas the absorbed Cl_2 is the Cl_2 that exits the outlet and has not reacted with Al_2O_3.

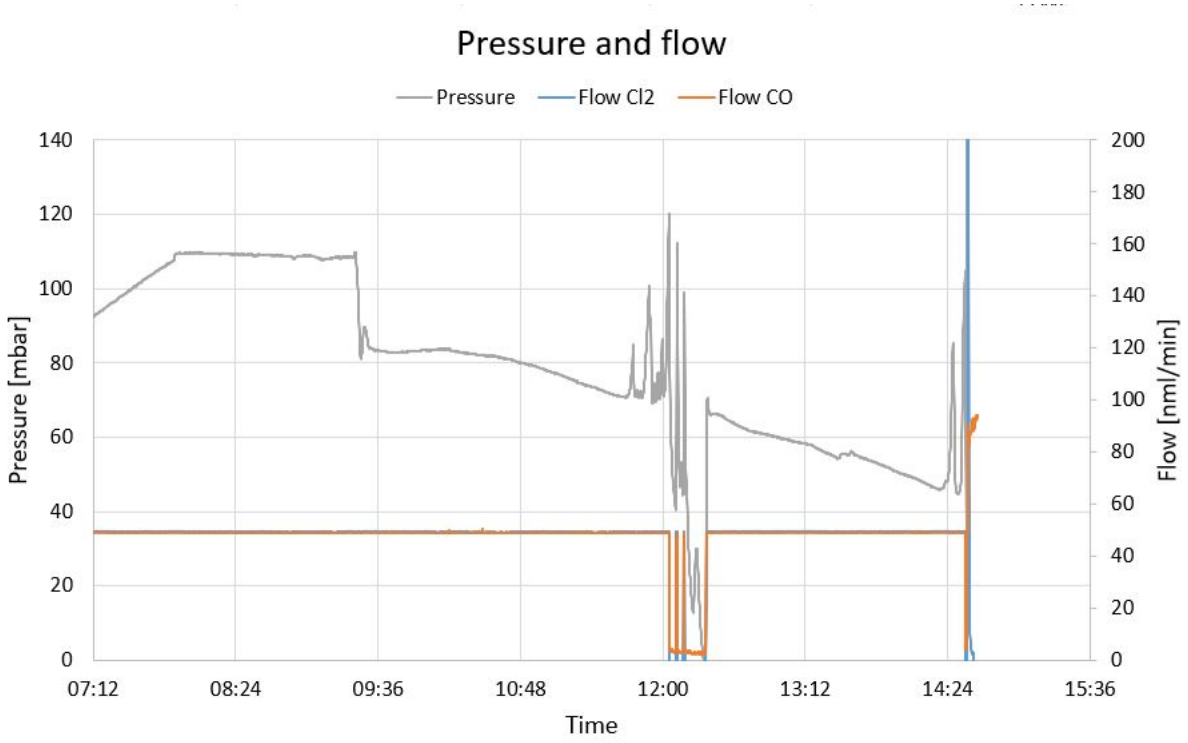

Figure 61: Pressure and flow plot for Experiment 3.

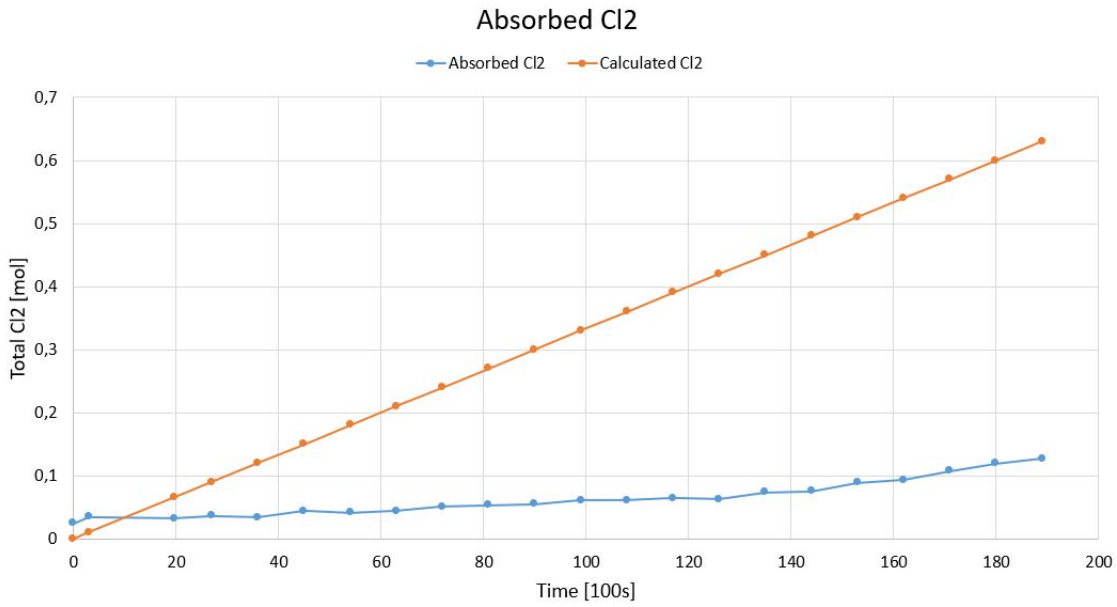

Figure 62: Cl_2 levels during carbochlorination of SMG Al_2O_3 at 650°C. Calculated Cl_2 is the total amount of Cl_2 that enters the inlet, whereas the absorbed Cl_2 is the Cl_2 that exits the outlet and has not reacted with Al_2O_3.

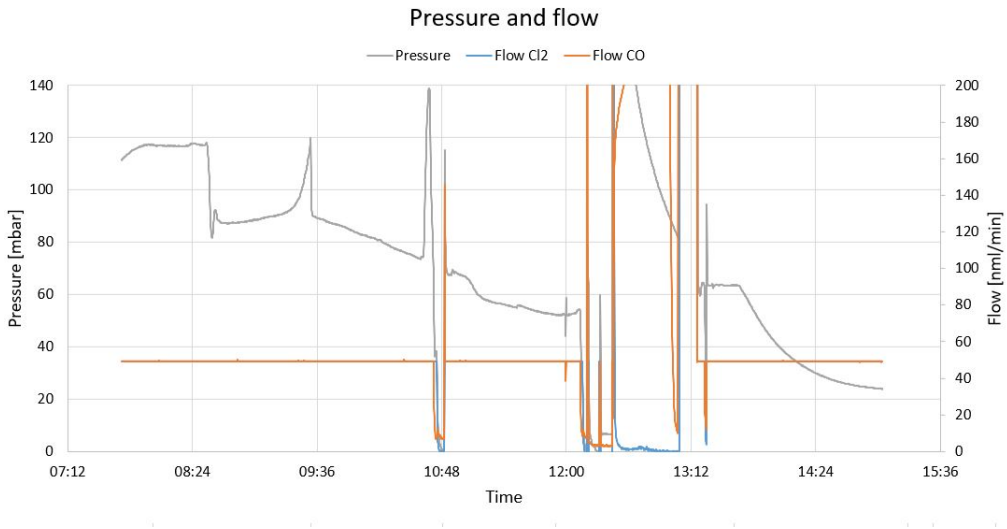

Figure 63: Pressure and flow plot for Experiment 4.

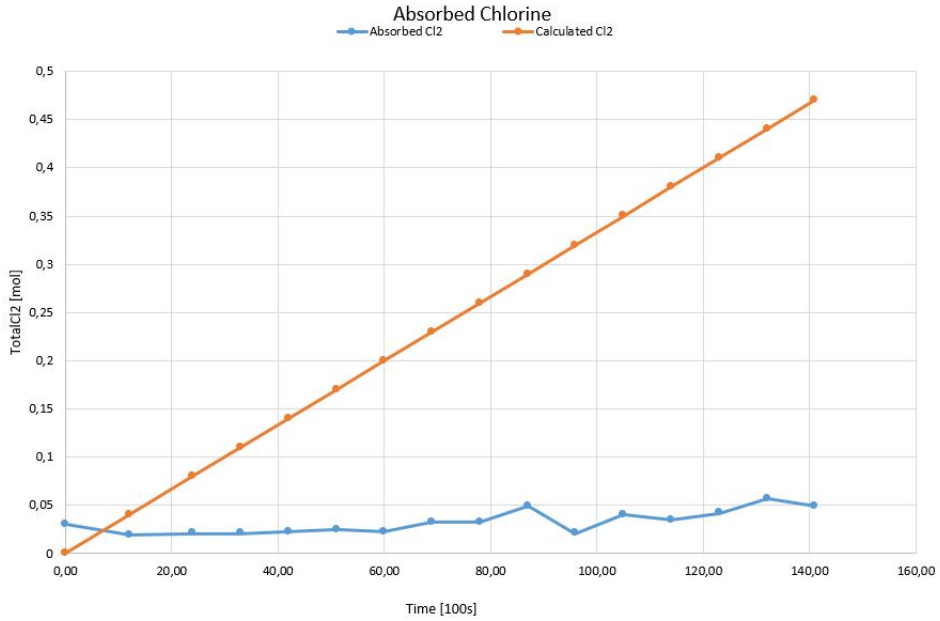

Figure 64: Cl_2 levels during carbochlorination of SMG Al_2O_3 at 700°C. Calculated Cl_2 is the total amount of Cl_2 that enters the inlet, whereas the absorbed Cl_2 is the Cl_2 that exits the outlet and has not reacted with Al_2O_3.

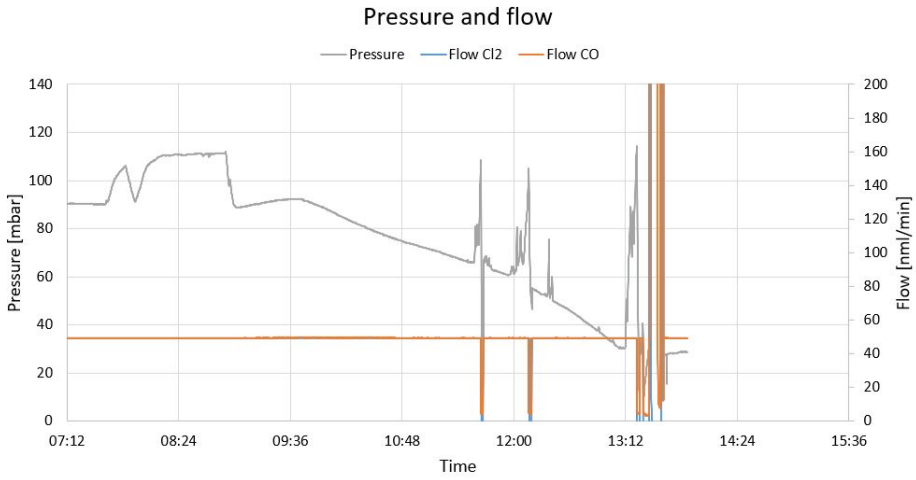

Figure 65: Pressure and flow plot for Experiment 5.

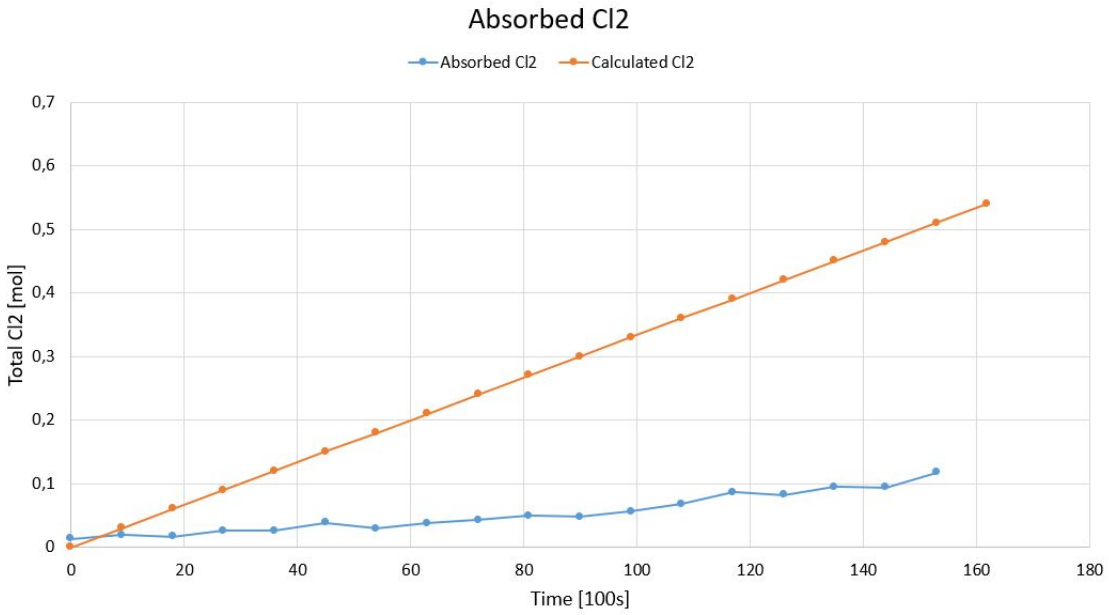

Figure 66: Cl_2 levels during carbochlorination of SMG Al_2O_3 at 800°C. Calculated Cl_2 is the total amount of Cl_2 that enters the inlet, whereas the absorbed Cl_2 is the Cl_2 that exits the outlet and has not reacted with Al_2O_3.

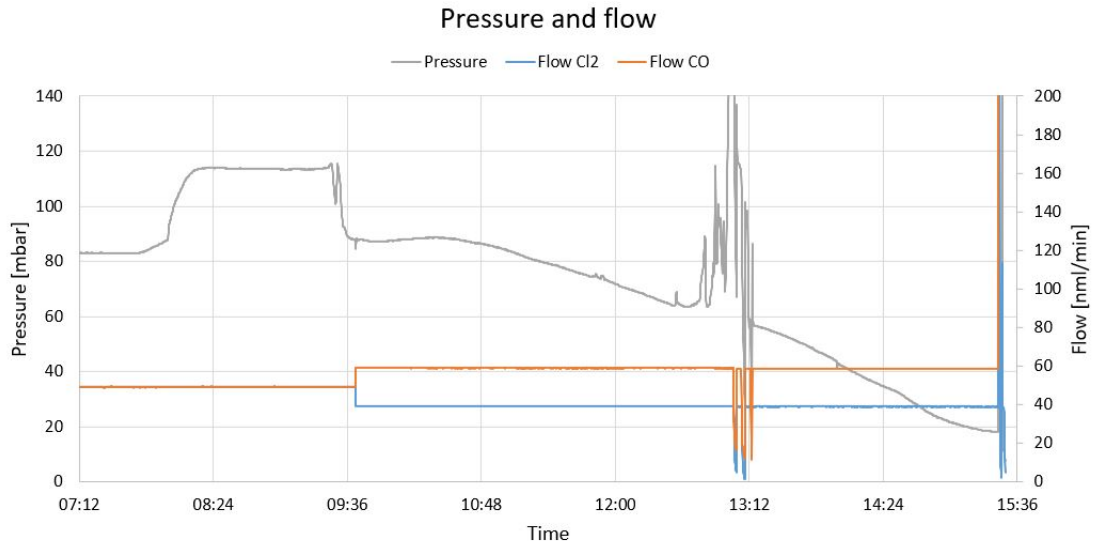

Figure 67: Pressure and flow plot for Experiment 6.

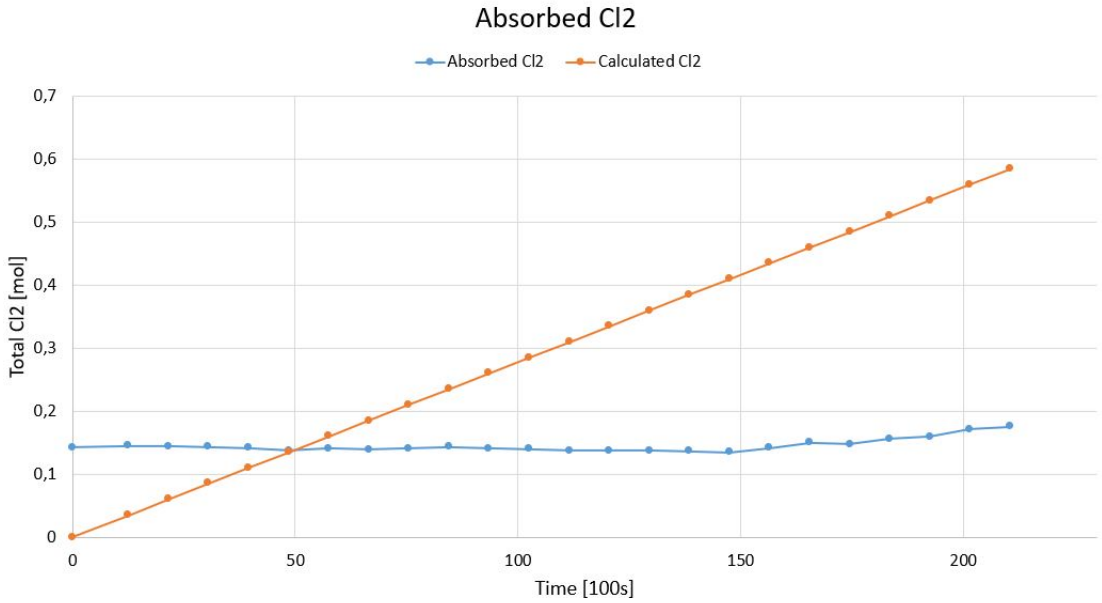

Figure 68: Cl_2 levels during carbochlorination of SMG Al_2O_3 at 700°C, with gas flows of 40 and 60 ml/min of Cl_2 and CO, respectively.. Calculated Cl_2 is the total amount of Cl_2 that enters the inlet, whereas the absorbed Cl_2 is the Cl_2 that exits the outlet and has not reacted with Al_2O_3.

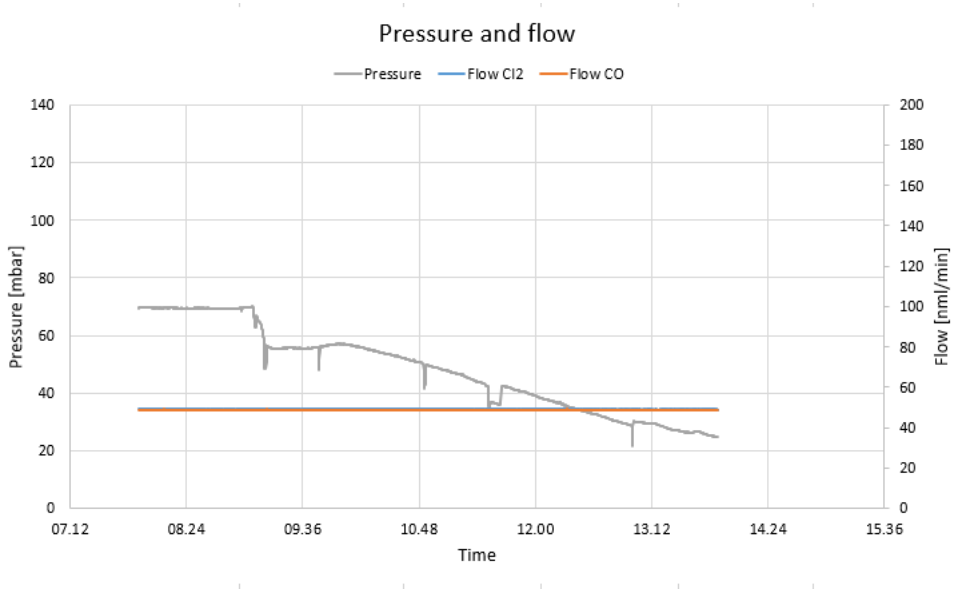

Figure 69: Pressure and flow plot for Experiment 7.

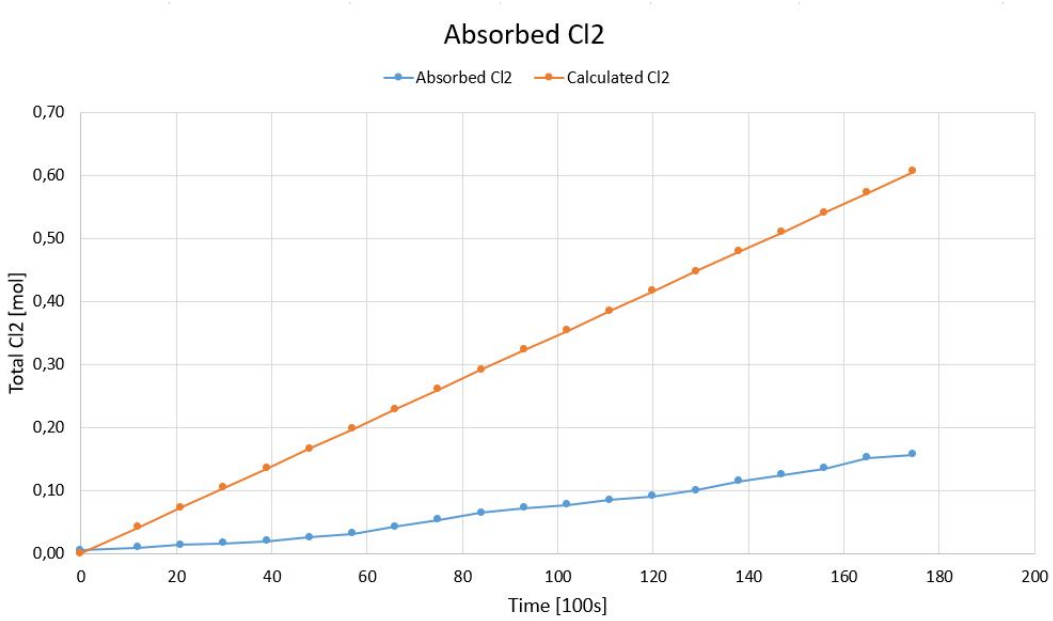

Figure 70: Cl_2 levels during carbochlorination of $\gamma-, \delta-$ and $\theta-Al_3O_3$ at 700°C. Calculated Cl_2 is the total amount of Cl_2 that enters the inlet, whereas the absorbed Cl_2 is the Cl_2 that exits the outlet and has not reacted with Al_2O_3.

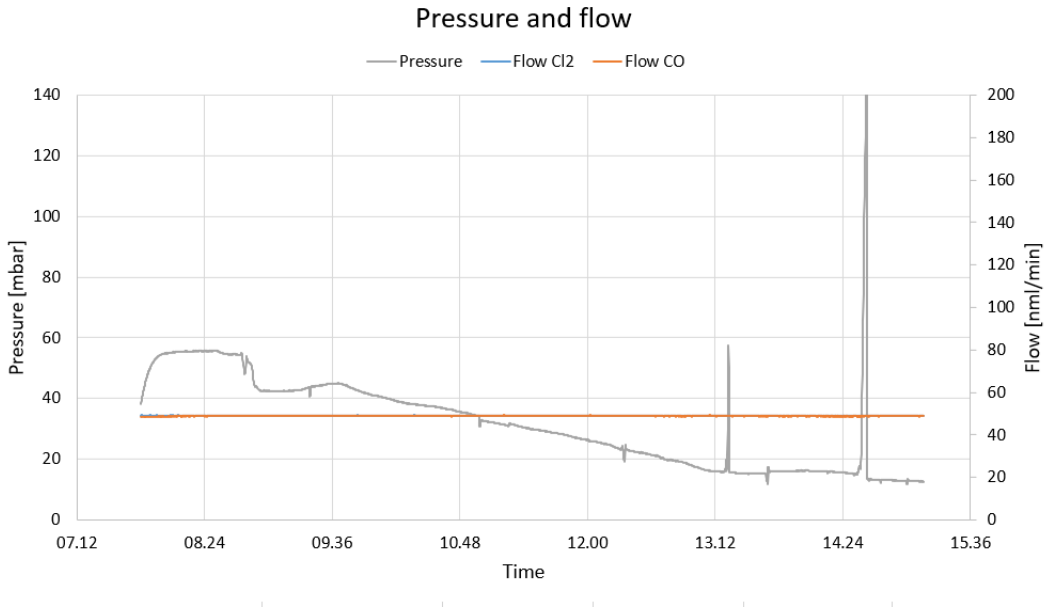

Figure 71: Pressure and flow plot for Experiment 8.

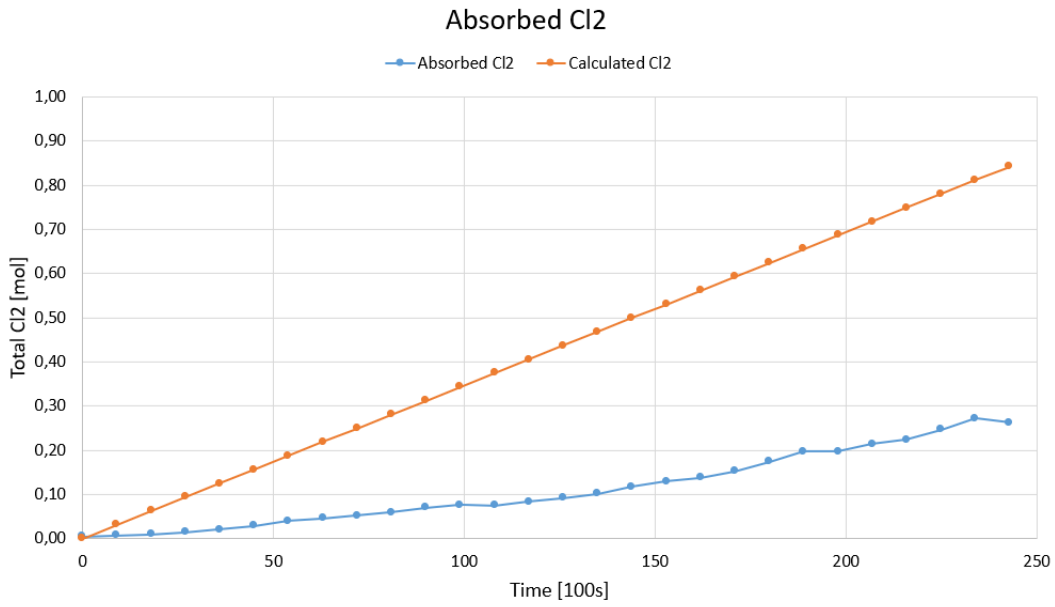

Figure 72: Cl_2 levels during carbochlorination of $\gamma-$ and $\delta-$-Al_3O_3 at 700°C. Calculated Cl_2 is the total amount of Cl_2 that enters the inlet, whereas the absorbed Cl_2 is the Cl_2 that exits the outlet and has not reacted with Al_2O_3.

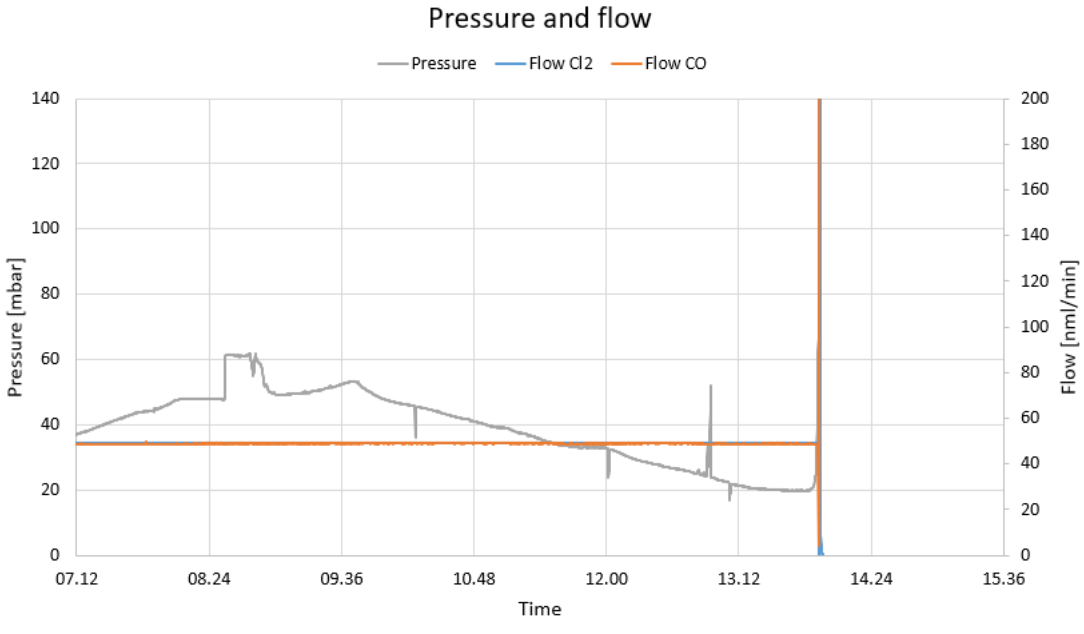

Figure 73: Pressure and flow plot for Experiment 9.

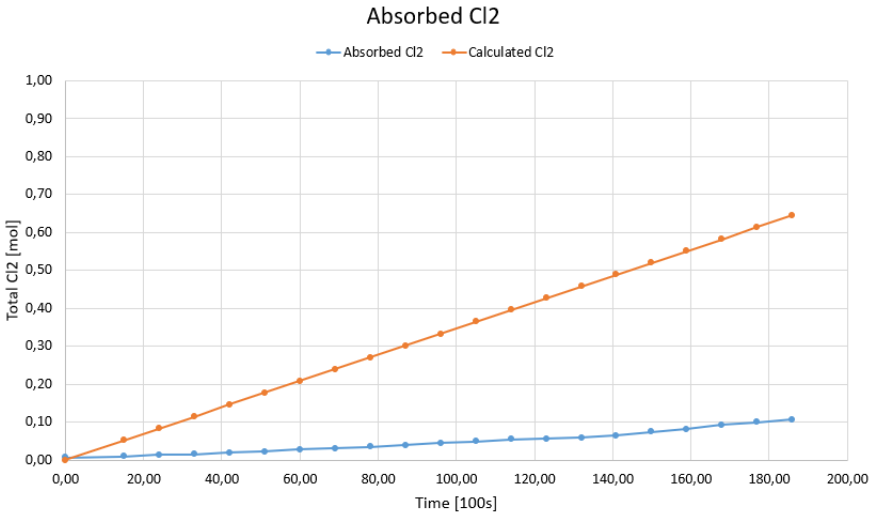

Figure 74: Cl_2 levels during carbochlorination of $\gamma-$-Al_3O_3 at 700°C. Calculated Cl_2 is the total amount of Cl_2 that enters the inlet, whereas the absorbed Cl_2 is the Cl_2 that exits the outlet and has not reacted with Al_2O_3.

D: Experimental Conversion Values

X,1	X, 2	X, 3	X, 4	X, 5	X, 6	X, 7	X, 8	X, 9
0	0	0	0	0	0	0	0	0
0,0537427	0,04098285	0,050474	0,02930911	0,03436976	0,03439722	0,06534421	0,06534421	0,0530306
0,10870517	0,08721035	0,07940537	0,0827987	0,08445889	0,08219842	0,1201774	0,1201774	0,11231664
0,1607595	0,14739587	0,12868738	0,12493093	0,14995403	0,12282829	0,17790722	0,17790722	0,16875685
0,20997203	0,20764647	0,1574372	0,16437644	0,1926796	0,16213054	0,23479219	0,23479219	0,22390839
0,25712232	0,25390659	0,2067192	0,20382195	0,25446685	0,21139551	0,28536301	0,28536301	0,27195882
0,31146004	0,31159335	0,24687579	0,24864091	0,2901161	0,25782372	0,33611168	0,33611168	0,31600899
0,34894599	0,37492836	0,28246967	0,27733954	0,37062558	0,30702061	0,37711598	0,37711598	0,36767038
0,39366361	0,41810406	0,32262626	0,31947177	0,41405617	0,35068013	0,41843789	0,41843789	0,42318436
0,43853604	0,47070219	0,3650642	0,33742352	0,46505921	0,39574669	0,45829878	0,45829878	0,47328861
0,48561998	0,52348252	0,40065808	0,41985655	0,51258937	0,44083594	0,50556641	0,50556641	0,51884223
0,5429644	0,57644505	0,44537738	0,43512159	0,57834564	0,4886258	0,55921173	0,55921173	0,5717386
0,57543117	0,63048127	0,48553397	0,48531398	0,6225857	0,5217893	0,60691767	0,60691767	0,63930703
0,67099231	0,670527	0,53253462	0,51669933	0,65998444	0,54991471	0,65832063	0,65832063	0,68926361
0,72064162	0,72061335	0,56128443	0,5373378	0,68364833	0,59923641	0,70219615	0,70219615	0,73891145
	0,7622143	0,60372238	0,59021691	0,7533736	0,62910927	0,73531093	0,73531093	0,78361939
	0,85264531	0,62790948		0,7882656	0,66697045	0,779034	0,779034	0,8169709
	0,89542399	0,66578471		0,85114955	0,69101092	0,82223618	0,82223618	0,85755776
		0,68997182		0,86614429	0,72805511	0,85079003	0,85079003	0,9064673
		0,71644027				0,90805828	0,90805828	0,94050342
		0,7497528						0,9614112
								0,97837241

Figure 75: Conversion values from titration for each carbochlorination experiment.